Molecular basis for the control of motor-based transport of MHC class II compartments

Rocha, N.

Molecular basis for the control of motor-based transport of MHC class II compartments

Nuno Rocha

Molecular basis for the control of motor-based transport of MHC class II compartments

Proefschrift

ter verkrijging van
de graad van Doctor aan de Universiteit Leiden,
op gezag van Rector Magnificus prof.mr. P.F. van der Heijden,
volgens besluit van het College voor Promoties
te verdedigen op woensdag 8 oktober 2008
klokke 13.45 uur

door

Nuno Rocha

geboren te Lissabon, Portugal
in 1976

Promotiecommissie

Promotor:	Prof. Dr. J.J. Neefjes
Referent:	Prof. Dr. W.H. Moolenaar
Overige leden:	Prof. Dr. J. Borst Universiteit van Amsterdam
	Prof. Dr. E.J. Wiertz
	Dr. N. Savage
	Dr. E. Roos Het Nederlands Kanker Instituut, Amsterdam
	Prof. Dr. F. Koning

The work described in this thesis was performed at the Division of Tumor Biology of the Netherlands Cancer Institute, Amsterdam, The Netherlands, and supported by grants from the Netherlands Organization for Scientific Research (NWO), the Dutch Cancer Society (KWF), and a personal doctoral grant from the Portuguese Foundation for Science and Technology (FCT)/ Fundo Social Europeu (FSE)/ Programa Operacional Ciencia e Inovacao (POCI) 2010.

The publication of this thesis was financially supported by the Dutch Cancer Society (KWF), the Netherlands Organization for Scientific Research (NWO), and the Portuguese Ministry of Science, Technology and Higher Education/ Fundo Social Europeu (FSE)/ Programa Operacional Ciência e Inovação (POCI) 2010.

Para os meus pais

Contents

The following figures may contain relevant information in color and are presented in full-color mode in **Appendix A** (page 127):

Figures 1 and 2 from Chapter 1;
Figures 2, 3, 5, 6, 7, and 8 from Chapter 2;
Figures 1, 3, 4, 5, 6, 7, and S2 from Chapter 3;
Figures 2, 3, and 5 from Chapter 4;
Figures 1, 5, and 6 from Chapter 5.

Chapter 1

Introduction:

Scope of the thesis

MHC class II molecules on the move for successful antigen presentation
Adapted from EMBO J. 2008. 27:1-5

Scope of the thesis

Antigen presentation by major histocompatibility complex class II (MHC II) molecules to $CD4^+$ T-cells is crucial for the adaptive immune system to mount defensive reactions against pathogens. In addition, it is also implicated in the control of cytotoxic T-cell activation, maintenance of self-tolerance, autoimmune responses and other immune responses to pathogens or the environment.

MHC II molecules en route to the cell surface intersect the endocytic pathway where they acquire, in a notably unique and complex series of reactions, immunogenic peptides derived from internalized exogenous proteins. The primary site for antigen loading of MHC II molecules is the specialized lysosomal-related organelle (LRO) known as MHC II-containing compartment or MIIC. Ultimately, the MHC II-peptide complexes are transported for display at the cell surface.

Despite our advanced understanding of many of the mechanisms involved in the control of MHC II antigen presentation, some are still poorly understood. Studying the cell biology of antigen presentation is of crucial importance to reveal novel modes for the manipulation of MHC II-restricted immune responses, particularly those implicated in the pathogenesis of autoimmune diseases. This thesis focuses on the study of the mechanisms governing intracellular transport of MHC II-containing compartments.

Chapter 1 serves as a general introduction on the role of MHC II antigen presentation in the immune system and on the cell biology of antigen presentation by MHC class II molecules, with an emphasis on the control of intracellular motor-based transport of MIICs.

In **Chapter 2**, we propose a model that aims at explaining how a molecular switch, such as the late endosomal small GTPase Rab7 lies at the heart of the control of microtubular transport of MIICs, late endosomes, lysosomes and LROs, such as early melanosomes, cytolytic granules, and phagosomes. A cascade of linked events, initiated by the activation of Rab7, leads to the assembly of a tripartite specific receptor for the minus end-directed dynein-dynactin motor on the cytosolic face of LROs. Upon activation, Rab7 becomes membrane-associated and recruits its effectors Rab7-interacting lysosomal protein (RILP) and OSBP-related protein 1L (ORP1L) to form the Rab7-RILP-ORP1L tripartite complex. We show that by interacting directly and simultaneously with GTP-Rab7 and a subunit of the dynein-dynactin motor ($p150^{Glued}$), RILP establishes the molecular link between the small GTPase and the dynein motor. However, this appears to not suffice for active transport of LROs toward the minus end of microtubules. Instead, full activation of minus end-directed transport requires the parallel activity of a second receptor for the dynein-dynactin motor on the surface of LROs—βIII spectrin. In this way, the concerted action of two receptors on the surface of LROs is used to achieve control of minus end-directed transport: firstly, Rab7-RILP acts to specify the target membrane for dynein-dynactin recruitment; subsequently, in a process dependent on ORP1L, βIII spectrin functions as a general receptor for the dynein motor.

Whereas this model explains how the small GTPase Rab7 controls minus end-directed transport, it does not suffice to explain the characteristic pattern of motility exhibited by LROs. These subcellular compartments move bidirectionally along microtubules by the alternating actions of kinesin and dynein motor proteins. In **Chapter 3**, we propose that the observed swift mechanism operating as directional switch in microtubular transport of LROs is, surprisingly, not based on the GTPase state of Rab7. Instead, we show that the cholesterol content of LROs determines the conformation of ORP1L which acts as a switch that controls binding of dynein-

dynactin to its receptor Rab7-RILP. This mechanism regulates the direction of transport and late endosomal positioning. In addition, it may explain how cholesterol accumulation leads to lysosomal clustering at the minus end of microtubules, as observed in Niemann-Pick type C disease.

Chapter 4 describes the identification and characterization of a naturally occurring splice variant of RILP (RILPsv). RILPsv lacks 27 amino acid residues encoded by exon VII and, although it binds to active GTP-bound Rab7 slowing down its GTPase activity and induces clustering of late endosomal compartments, unlike RILP, it does this independently of efficient direct dynein-dynactin recruitment.

In **Chapter 5**, we look at how the tripartite Rab7-RILP-ORP1L may constitute the mechanistic link that integrates the spatio-temporal control of transport and docking/tethering of LROs, two consecutive processes within the endocytic pathway.

Chapter 7 summarizes the findings described in this thesis as well as their possible implications.

MHC class II molecules on the move for successful antigen presentation

Nuno Rocha and Jacques Neefjes*

Division of Tumor Biology, The Netherlands Cancer Institute, Amsterdam, The Netherlands

Major histocompatibility complex class II molecules (MHC II) are targeted to endocytic compartments, known as MIIC, by the invariant chain (Ii) that is degraded upon arrival in these compartments. MHC II acquire antigenic fragments from endocytosed proteins for presentation at the cell surface. In a unique and complex series of reactions, MHC II succeed in exchanging a remaining fragment of Ii for other protein fragments in subdomains of MIIC before transport to the cell surface. Here, the mechanisms regulating loading and intracellular trafficking of MHC II are discussed.

Role of MHC II in the immune system

Major histocompatibility complex class II molecules (MHC II) are expressed by immune cells like B cells, dendritic cells (DC), and monocytes/macrophages and designed to stably bind and present fragments from exogenous proteins to the immune system. MHC II present antigens to $CD4^+$ T helper cells and then control differentiation of B cells in antibody-producing B cell blasts. Patients or mice failing to produce proper MHC II-peptide complexes will not produce efficient antibody-responses to infection (Viville et al., 1993). MHC II are also important to control cytotoxic T cell activation, autoimmune responses and other responses to pathogens or the environment.

MHC II are polymorphic and various MHC II alleles show linkage disequilibrium to a variety of autoimmune diseases. These cannot be linked entirely to the MHC II allele implying further involvement of genetic and/or environmental factors. For example, 95% of patients with Celiac Disease express an MHC II molecule, HLA-DQ2, present in 25% of the population. The gliadin peptide (a gluten fragment) is selectively presented by HLA-DQ2, which, in addition to unknown factors, causes this disorder (www.enabling.org/ia/celiac). Studying the cell biology of antigen presentation by MHC II is of crucial importance to identify these factors or reveal modes for controlling MHC II antigen presentation.

How MHC II acquire peptides in the endocytic route?

Antigen loading of MHC II occurs in the endocytic pathway at a site that is commonly known as MIIC (for 'MHC class II-containing compartment') (Neefjes et al., 1990). MHC II assemble as heterodimers in the endoplasmic reticulum (ER) to form a peptide-binding groove (Brown et al., 1993). Efficient ER egress of MHC II is assisted by the invariant chain (Ii) (Bikoff et al., 1993; Viville et al., 1993). An

* Corresponding author. Division of Tumor Biology, The Netherlands Cancer Institute, Plesmanlaan 121, Amsterdam 1066 CX, The Netherlands. Tel.: + 31 20 5122012; Fax: + 31 20 5122029; E-mail: J.NEEFJES@NKI.NL

Ii region called CLIP occupies the peptide-binding groove, thereby preventing premature peptide binding (Roche and Cresswell, 1990). Ii also contains a cytosolic di-leucine targeting motif that directs MHC II complexes into the endocytic pathway, either directly from the trans-Golgi network or—if this fails—via rapid internalization (Bakke and Dobberstein, 1990; Roche et al., 1993). After having guided MHC II to MIIC, Ii is degraded by various late endosomal proteases, including cathepsin S and L, to prepare MHC II for peptide loading. Inhibition of these proteases will prevent MHC II antigen presentation, immune responses (Riese and Chapman, 2000) but also cell surface expression (Neefjes and Ploegh, 1992). Consequently, inhibitors for cathepsin S are currently developed for the treatment of autoimmune diseases (Vasiljeva et al., 2007). The proteases degrade Ii in a stepwise fashion leaving the CLIP fragment occupying the peptide-binding groove. The resulting MHC II complex does not contain relevant antigenic information for the immune system. Exchange of CLIP for such antigenic fragments is facilitated by low pH, proteolytic trimming of the CLIP peptide, and by a unique chaperone called HLA-DM, which is surprisingly an MHC II look-alike (Mosyak et al., 1998). HLA-DM is a dedicated chaperone (only target known: MHC II) in a compartment where other proteins are usually degraded. HLA-DM stabilizes MHC II devoid of peptides, preventing aggregation and supporting peptide exchange until a high-affinity-binding peptide is acquired (Denzin et al., 1996; Sloan et al., 1995). HLA-DM is thus editing the MHC II peptide repertoire (Kropshofer et al., 1996). But the reaction is more complicated. The interaction between MHC II and HLA-DM occurs in subdomains of the MIIC (the intraluminal vesicles) and not at the limiting membrane as determined by FRET studies (Zwart et al., 2005). Consequently, MHC II fails to acquire antigenic peptides in phagosomes containing intracellular bacteria as these lack intraluminal vesicles (Zwart et al., 2005). Possibly, microdomains like those formed by members of the tetraspanin family of proteins (the tetraspanin web) residing in the intraluminal vesicles of the MIIC and interacting with MHC II, HLA-DM, and other proteins (Hammond et al., 1998) play an additional role in efficient peptide loading of MHC II.

Whether loading of MHC II with high-affinity peptides is a prerequisite for transport from MIIC to the plasma membrane is unlikely. Endosomes may not have a sophisticated 'quality control system' like the ER that allows the egress of properly folded proteins only, since CLIP exchange by HLA-DM is not required for cell surface expression of MHC II (Fung-Leung et al., 1996; Martin et al., 1996). Proper expression levels of HLA-DM, transport of MHC II and HLA-DM to internal vesicles in MVB, transit time of MHC II through the MIIC, proteolysis of antigen and Ii, and delivery of antigenic fragments (by diffusion?) to MHC II probably ensure that the system suffices to efficiently load MHC II in transit through the MIIC.

Definition of the MIIC

The exact definition of THE MIIC as the site of MHC II peptide loading has been a matter of debate. Originally, the MIIC was defined based on immuno-electronmicroscopy studies as a late endosome (LE) with multilamellar morphology containing MHC II (Peters et al., 1991). MHC II was subsequently found in many different compartments with distinct morphologies and its expression in HEK 293 cells even induced the multilamellar morphology (Calafat et al., 1994). Thus, neither morphology nor the presence of MHC II can define THE MIIC. Other factors required for efficient loading of MHC II include acidic pH (Ziegler and Unanue, 1982), HLA-DM and proteases like cathepsin S and L (Honey and

Rudensky, 2003). Electronmicroscopy showed that these locate in LEs that label for the conventional markers Lamp-1 and CD63.

Is the MIIC then a unique compartment or a LE expressing additional proteins for MHC II antigen presentation? Eliminating MHC II, cathepsin S or HLA-DM still shows LEs labeling for the conventional markers, indicating that MHC II-related proteins are not critical in this compartment. In addition, LEs lacking MHC II are difficult to detect in cells expressing MHC II. MIIC appears to be a LE with the components for efficient MHC II loading. Still, loading of MHC II at nearly every location of the endocytic route is reported. Since HLA-DM is transported in the MIIC to the plasma membrane along with MHC II (Wubbolts et al., 1996), loading may even be supported by HLA-DM at the plasma membrane (Moss et al., 2007), albeit at neutral pH and without proteases for antigen preparation. Moreover, HLA-DM contains a classical tyrosine-based internalization motif and will be internalized, thus entering early endosomal compartments in transit to MIIC. In principle, HLA-DM support in MHC II loading can occur whenever protein fragments are present, although the late endosomal MIIC likely is the primary site for antigen loading of MHC II, since it congregates all known components for efficient peptide loading.

Further control of MHC II antigen presentation

The complex process of MHC II antigen presentation is further complicated by additional factors. Immature B cells express an HLA-DM homologue called HLA-DO (Liljedahl et al., 1996). This non-polymorphic MHC II-like molecule stably interacts with HLA-DM and acts as a pH sensor to preferentially stimulate presentation of antigens entering the more acidic LEs at the cost of normal HLA-DM functioning, paradoxically resulting in MHC II-CLIP complexes and reduced immune responses (Denzin et al., 1997; van Ham et al., 1997). Other factors involved in MHC II presentation are more related to the control of protein targeting to MIIC or the control of proteolysis. Antibody-bound proteins can be recognized by Fc receptors for uptake, transfer to MIIC and degradation. Analogously, surface Ig receptors on B cells can specifically recognize and target antigens to LEs for degradation, which also affects the specificity of antigen proteolysis (Davidson and Watts, 1989). Alterations in proteolytic conditions contribute to the success of MHC II antigen presentation as well. In classic experiments, neutralization of acidic compartments inhibited MHC II antigen presentation, implying lysosomal proteases in antigen presentation (Ziegler and Unanue, 1982).

Some late endosomal proteases are critical in MHC II antigen presentation. Cathepsin-S- and -L-deficient mice have reduced Ii degradation and antigen presentation (Nakagawa et al., 1998; Shi et al., 1999). To complicate matters, naturally occurring inhibitors of lysosomal proteases, called cystatins, can also exert a regulatory role. Overexpression of cystatin C inhibits the activity of cathepsin S, and consequently, Ii degradation and MHC II cell surface expression in DC (Pierre and Mellman, 1998).

Finally, control of MHC II antigen presentation by interleukins and Toll-like receptors (Blander and Medzhitov, 2006) occurs in particular cell types. The 'immunosuppressive' interleukin IL-10 prevents MHC II cell surface expression in human monocytes (Koppelman et al., 1997) whereas interferon-γ enhances MHC II expression and presentation.

Proteases, protease inhibitors, protease conditions and substrate delivery are all factors contributing to the efficiency and specificity of MHC II antigen presentation and therefore represent attractive targets for manipulating immune responses. In addition, motor proteins, kinases, GTPases and possibly other

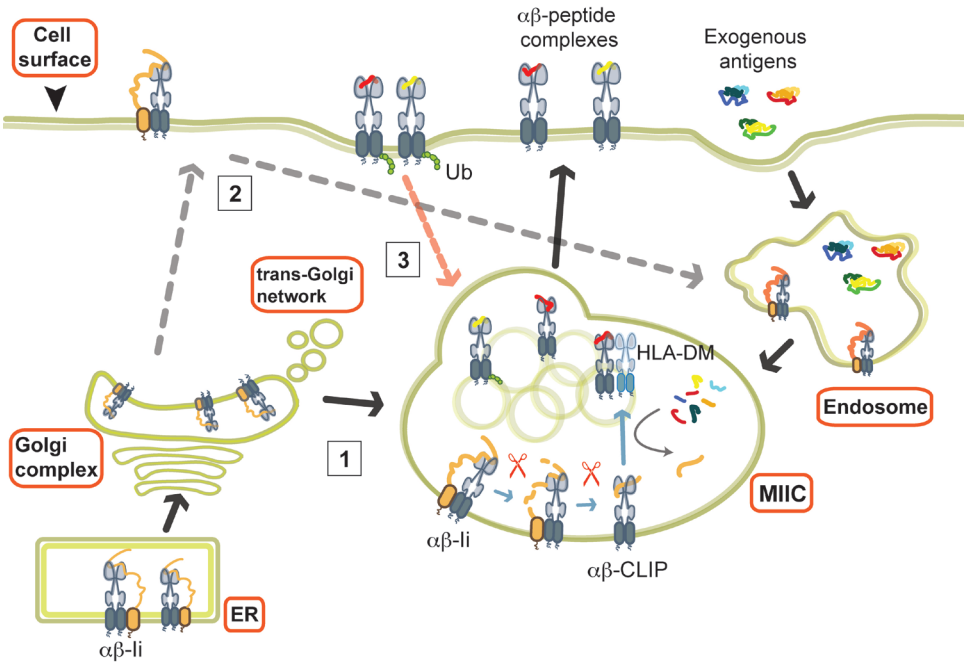

Figure 1. The cell biology of antigen presentation by MHC II. MHC II αβ heterodimers are assembled in the endoplasmic reticulum (ER) and form a peptide-binding groove that is occupied by Ii. Ii chaperones MHC II often directly (route 1; black solid arrows) and sometimes indirectly after internalization from the cell surface (route 2; grey dashed arrows) into MIIC where Ii is degraded by a series of endosomal proteases with the CLIP fragment remaining (orange). HLA-DM assists exchange of CLIP for relevant exogenous antigenic fragments (red or yellow) in subdomains of MIIC (the internal vesicles) prior to transport for stable integration in the plasma membrane (blue arrows in MIIC) unless internalization is induced by processes like ubiquitination (Ub) of the MHC II β-chain cytoplasmic tail (route 3; pink dashed arrow).

signaling systems control MHC II presentation. These include the actin-based motor protein myosin II that interacts with Ii following B cell receptor activation and is essential for antigen presentation (Vascotto et al., 2007), and GTPases of the families Rab and Rho (Ghittoni et al., 2006). We are only beginning to grasp the complexity of regulating MHC II antigen presentation.

How to move MHC II to the plasma membrane?

Trafficking of late endosomal proteins, including MHC II, to the plasma membrane is poorly understood. LEs may not have the machinery for the selective sorting of molecules and the appearance at the plasma membrane of many late endosomal proteins is followed by efficient internalization and transport back to LEs. Ii contains the targeting motif for MHC II. Since degradation of this motif occurs in the MIIC, MHC II remains stable at the plasma membrane upon delivery, unless internalization is supported for example by its ubiquitination (Shin et al., 2006; van Niel et al., 2006).

Transport of GFP-tagged MHC II has been studied in tissue culture cells (Wubbolts et al., 1996) B cells and mouse DC (Boes et al., 2002; Chow et al., 2002). We visualized MIIC with GFP-

tagged MHC II exhibiting the canonical motility of LEs. These two similar compartments move in a so-called bidirectional manner and in a stop-and-go fashion along microtubules to the plasma membrane (Wubbolts et al., 1996). This required the activities of oppositely directed motor proteins; dynein (powers transport to the microtubule-organizing center) and kinesin (powers outward transport) (Wubbolts et al., 1999). Ultimately, MIIC fuses to the plasma membrane (Raposo et al., 1996; Wubbolts et al., 1996).

An additional route for the transport of MHC II to the plasma membrane has been observed in activated DC. Upon activation, DC upregulate surface expression of MHC II from intracellular storages and tubular structures emanating from the MIIC and containing MHC II are formed (Boes et al., 2002; Chow et al., 2002; Kleijmeer et al., 2001). Live-imaging revealed that these tubules exhibit dynamics similar to MIIC, including bidirectional microtubule-based movement in a stop-and-go fashion (Vyas et al., 2007). Since immature DC, B cells and melanoma do not show these tubules but do express MHC II at the plasma membrane, tubules may be an activated DC-selective route for the transport of MHC II to the cell surface.

How MIIC (and possibly tubules) fuse to the plasma membrane is unclear. It probably requires the activities of Rab GTPases, actin-based motor proteins and actin depolymerizing factors, analogously to the situation for other specialized lysosome-related organelles such as cytolytic granules and melanosomes (Jordens et al., 2006; Raposo et al., 2007).

Two collaborating receptors for one or more motor proteins on MIIC

Rab7 is a small Rab GTPase decorating membranes of MIIC and other late endocytic structures (Chavrier et al., 1990; Meresse et al., 1995; Wubbolts et al., 1996). Activated Rab7 specifies the target membrane for dynein recruitment through an interaction of its effector Rab7-interacting lysosomal protein (RILP) with the $p150^{Glued}$ subunit of dynactin, a critical component of the dynein motor complex (Johansson et al., 2007). RILP expression promotes inward-directed dynein-mediated transport of MIIC/LEs to the microtubule minus-end (Jordens et al., 2001).

The Rab7-RILP complex interacts with a second effector protein—OSBP-related protein 1L (ORP1L)—to form a tripartite complex on lysosomal membranes. ORP1L is required to transfer the dynein/dynactin motor complex from the specific lysosomal receptor Rab7-RILP to a general receptor termed βIII spectrin (Johansson et al., 2007). βIII spectrin is located on the cytosolic side of multiple compartments and can interact, via its actin-binding domain (ABD), with actin-related protein 1 (Arp1) at the base of dynactin (Karki and Holzbaur, 1999). The dynein motor only becomes active after consecutive interactions with these two membrane-associated receptors: the LE-specific receptor Rab7-RILP and the general receptor βIII spectrin (Johansson et al., 2007) (Figure 2).

The bidirectional nature of vesicle movement implies that, in addition to the inward-directed dynein motor, at least one outward-directed motor is involved. Two members of the kinesin superfamily of motors may be involved in outward-directed motility of LEs along microtubules. Kinesin-1 (conventional kinesin or KIF5) but also kinesin-2 (heterotrimeric kinesin or KIF3) have been implicated (Hollenbeck and Swanson, 1990; Wubbolts et al., 1999).

How do motors of opposite polarity cooperate to achieve bidirectional motility? They may be reciprocally coordinated and not act simultaneously on one individual vesicle. *Xenopus* melanophores as well as *Drosophila* fast axonal cargoes and lipid droplets use dynactin (or its subunit $p150^{Glued}$) to interact with dynein

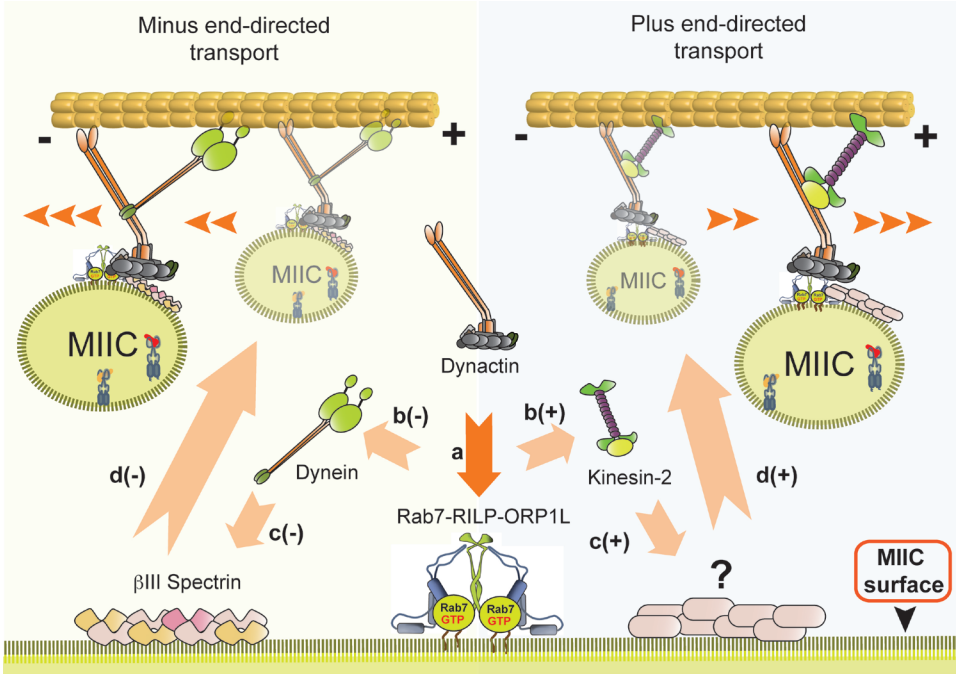

Figure 2. Reciprocal coordination of motor proteins for bidirectional microtubule-based MIIC transport. Left: control of inward transport of MIIC toward the microtubule minus-end. Right: control of plus end-directed transport of MIIC to the cell periphery. Activation of Rab7 precedes formation of the tripartite Rab7-RILP-ORP1L complex. RILP interacts with the dynactin subunit p150Glued (a). Dynactin then interacts either with dynein [b(-)] or kinesin-2 (KIF3) [b(+)] motor proteins, specifying the direction of vesicle transport. Motor activity requires binding to a second LE membrane receptor, βIII spectrin [c(-)]. Full activation of kinesin-2 may require a similar interaction with a general receptor on MIIC [c(+)]. In this model, the $p150^{Glued}$-associated type of motor specifies the direction of MIIC transport (d).

and KIF3 motors in a mutually exclusive manner (Deacon et al., 2003). Furthermore, disruption of the dynactin complex by overexpressing $p50^{dynamitin}$ (Burkhardt et al., 1997) inhibits both minus- and plus-end motility (Deacon et al., 2003). The dynactin subunit $p150^{Glued}$ may be the adaptor for KIF3 and dynein on LEs (Brown et al., 2005; Deacon et al., 2003). Thus, the bidirectionallity of MIIC movement may be accomplished by alternating interactions of $p150^{Glued}$-dynein and $p150^{Glued}$-KIF3 motor complexes with a single Rab7-RILP receptor on MIIC that likely employs βIII spectrin in both cases (Figure 2). The interaction of Rab7-RILP with $p150^{Glued}$ (the common motor adaptor for dynein and kinesin) would then be at the heart of the bidirectionallity of MIIC motility.

The control of motor activities and motor-receptor binding may involve kinases, lipids, the Rab7 GTPase cycle, IL-10 signaling, JNK-interacting proteins (JIPs), and undoubtedly many other factors. How these factors control the motility of MIIC and how these factors are subsequently controlled remains to be determined.

Antigen presentation by MHC II incorporates activities like late endosomal proteolysis of Ii and antigen, regulation of late endosomal morphology and pH, and intracellular transport. Further identification

of molecules involved in controlling these processes should provide targets for further manipulation of MHC II-restricted immune responses, particularly those resulting in autoimmune responses.

Acknowledgements

Nuno Rocha was supported by a grant from the Portuguese Foundation for Science and Technology FCT/ FSE/ POCI 2010. This work was supported by grants from the Dutch Cancer Society KWF and the Chemical Sciences Section of NWO. We thank Helen Pickersgill for critically reading the manuscript.

References

Bakke, O. and Dobberstein, B. (1990) MHC class II-associated invariant chain contains a sorting signal for endosomal compartments. Cell, 63, 707-716.

Bikoff, E.K., Huang, L.Y., Episkopou, V., van Meerwijk, J., Germain, R.N. and Robertson, E.J. (1993) Defective major histocompatibility complex class II assembly, transport, peptide acquisition, and CD4+ T cell selection in mice lacking invariant chain expression. J Exp Med, 177, 1699-1712.

Blander, J.M. and Medzhitov, R. (2006) Toll-dependent selection of microbial antigens for presentation by dendritic cells. Nature, 440, 808-812.

Boes, M., Cerny, J., Massol, R., Op den Brouw, M., Kirchhausen, T., Chen, J. and Ploegh, H.L. (2002) T-cell engagement of dendritic cells rapidly rearranges MHC class II transport. Nature, 418, 983-988.

Brown, C.L., Maier, K.C., Stauber, T., Ginkel, L.M., Wordeman, L., Vernos, I. and Schroer, T.A. (2005) Kinesin-2 is a motor for late endosomes and lysosomes. Traffic, 6, 1114-1124.

Brown, J.H., Jardetzky, T.S., Gorga, J.C., Stern, L.J., Urban, R.G., Strominger, J.L. and Wiley, D.C. (1993) Three-dimensional structure of the human class II histocompatibility antigen HLA-DR1. Nature, 364, 33-39.

Burkhardt, J.K., Echeverri, C.J., Nilsson, T. and Vallee, R.B. (1997) Overexpression of the dynamitin (p50) subunit of the dynactin complex disrupts dynein-dependent maintenance of membrane organelle distribution. J Cell Biol, 139, 469-484.

Calafat, J., Nijenhuis, M., Janssen, H., Tulp, A., Dusseljee, S., Wubbolts, R. and Neefjes, J. (1994) Major histocompatibility complex class II molecules induce the formation of endocytic MIIC-like structures. J Cell Biol, 126, 967-977.

Chavrier, P., Parton, R.G., Hauri, H.P., Simons, K. and Zerial, M. (1990) Localization of low molecular weight GTP binding proteins to exocytic and endocytic compartments. Cell, 62, 317-329.

Chow, A., Toomre, D., Garrett, W. and Mellman, I. (2002) Dendritic cell maturation triggers retrograde MHC class II transport from lysosomes to the plasma membrane. Nature, 418, 988-994.

Davidson, H.W. and Watts, C. (1989) Epitope-directed processing of specific antigen by B lymphocytes. J Cell Biol, 109, 85-92.

Deacon, S.W., Serpinskaya, A.S., Vaughan, P.S., Lopez Fanarraga, M., Vernos, I., Vaughan, K.T. and Gelfand, V.I. (2003) Dynactin is required for bidirectional organelle transport. J Cell Biol, 160, 297-301.

Denzin, L.K., Sant'Angelo, D.B., Hammond, C., Surman, M.J. and Cresswell, P. (1997) Negative regulation by HLA-DO of MHC class II-restricted antigen processing. Science, 278, 106-109.

Denzin, L.K., Hammond, C. and Cresswell, P. (1996) HLA-DM interactions with intermediates in HLA-DR maturation and a role for HLA-DM in stabilizing empty HLA-DR molecules. J Exp Med, 184, 2153-2165.

Fung-Leung, W.P., Surh, C.D., Liljedahl, M., Pang, J., Leturcq, D., Peterson, P.A., Webb, S.R. and Karlsson, L. (1996) Antigen presentation and T cell development in H2-M-deficient

mice. Science, 271, 1278-1281.

Ghittoni, R., Napolitani, G., Benati, D., Ulivieri, C., Patrussi, L., Laghi Pasini, F., Lanzavecchia, A. and Baldari, C.T. (2006) Simvastatin inhibits the MHC class II pathway of antigen presentation by impairing Ras superfamily GTPases. Eur J Immunol, 36, 2885-2893.

Hammond, C., Denzin, L.K., Pan, M., Griffith, J.M., Geuze, H.J. and Cresswell, P. (1998) The tetraspan protein CD82 is a resident of MHC class II compartments where it associates with HLA-DR, -DM, and -DO molecules. J Immunol, 161, 3282-3291.

Hollenbeck, P.J. and Swanson, J.A. (1990) Radial extension of macrophage tubular lysosomes supported by kinesin. Nature, 346, 864-866.

Honey, K. and Rudensky, A.Y. (2003) Lysosomal cysteine proteases regulate antigen presentation. Nat Rev Immunol, 3, 472-482.

Johansson, M., Rocha, N., Zwart, W., Jordens, I., Janssen, L., Kuijl, C., Olkkonen, V.M. and Neefjes, J. (2007) Activation of endosomal dynein motors by stepwise assembly of Rab7-RILP-p150Glued, ORP1L, and the receptor betalll spectrin. J Cell Biol, 176, 459-471.

Jordens, I., Westbroek, W., Marsman, M., Rocha, N., Mommaas, M., Huizing, M., Lambert, J., Naeyaert, J.M. and Neefjes, J. (2006) Rab7 and Rab27a control two motor protein activities involved in melanosomal transport. Pigment Cell Res, 19, 412-423.

Jordens, I., Fernandez-Borja, M., Marsman, M., Dusseljee, S., Janssen, L., Calafat, J., Janssen, H., Wubbolts, R. and Neefjes, J. (2001) The Rab7 effector protein RILP controls lysosomal transport by inducing the recruitment of dynein-dynactin motors. Curr Biol, 11, 1680-1685.

Karki, S. and Holzbaur, E.L. (1999) Cytoplasmic dynein and dynactin in cell division and intracellular transport. Curr Opin Cell Biol, 11, 45-53.

Kleijmeer, M., Ramm, G., Schuurhuis, D., Griffith, J., Rescigno, M., Ricciardi-Castagnoli, P., Rudensky, A.Y., Ossendorp, F., Melief, C.J., Stoorvogel, W. and Geuze, H.J. (2001) Reorganization of multivesicular bodies regulates MHC class II antigen presentation by dendritic cells. J Cell Biol, 155, 53-63.

Koppelman, B., Neefjes, J.J., de Vries, J.E. and de Waal Malefyt, R. (1997) Interleukin-10 down-regulates MHC class II alphabeta peptide complexes at the plasma membrane of monocytes by affecting arrival and recycling. Immunity, 7, 861-871.

Kropshofer, H., Vogt, A.B., Moldenhauer, G., Hammer, J., Blum, J.S. and Hammerling, G.J. (1996) Editing of the HLA-DR-peptide repertoire by HLA-DM. Embo J, 15, 6144-6154.

Liljedahl, M., Kuwana, T., Fung-Leung, W.P., Jackson, M.R., Peterson, P.A. and Karlsson, L. (1996) HLA-DO is a lysosomal resident which requires association with HLA-DM for efficient intracellular transport. Embo J, 15, 4817-4824.

Martin, W.D., Hicks, G.G., Mendiratta, S.K., Leva, H.I., Ruley, H.E. and Van Kaer, L. (1996) H2-M mutant mice are defective in the peptide loading of class II molecules, antigen presentation, and T cell repertoire selection. Cell, 84, 543-550.

Meresse, S., Gorvel, J.P. and Chavrier, P. (1995) The rab7 GTPase resides on a vesicular compartment connected to lysosomes. J Cell Sci, 108 (Pt 11), 3349-3358.

Moss, C.X., Tree, T.I. and Watts, C. (2007) Reconstruction of a pathway of antigen processing and class II MHC peptide capture. Embo J, 26, 2137-2147.

Mosyak, L., Zaller, D.M. and Wiley, D.C. (1998) The structure of HLA-DM, the peptide exchange catalyst that loads antigen onto class II MHC molecules during antigen presentation. Immunity, 9, 377-383.

Nakagawa, T., Roth, W., Wong, P., Nelson, A., Farr, A., Deussing, J., Villadangos, J.A., Ploegh, H., Peters, C. and Rudensky, A.Y. (1998) Cathepsin L: critical role in Ii degradation and CD4 T cell selection in the thymus. Science,

280, 450-453.

Neefjes, J.J. and Ploegh, H.L. (1992) Inhibition of endosomal proteolytic activity by leupeptin blocks surface expression of MHC class II molecules and their conversion to SDS resistance alpha beta heterodimers in endosomes. Embo J, 11, 411-416.

Neefjes, J.J., Stollorz, V., Peters, P.J., Geuze, H.J. and Ploegh, H.L. (1990) The biosynthetic pathway of MHC class II but not class I molecules intersects the endocytic route. Cell, 61, 171-183.

Peters, P.J., Neefjes, J.J., Oorschot, V., Ploegh, H.L. and Geuze, H.J. (1991) Segregation of MHC class II molecules from MHC class I molecules in the Golgi complex for transport to lysosomal compartments. Nature, 349, 669-676.

Pierre, P. and Mellman, I. (1998) Developmental regulation of invariant chain proteolysis controls MHC class II trafficking in mouse dendritic cells. Cell, 93, 1135-1145.

Raposo, G., Marks, M.S. and Cutler, D.F. (2007) Lysosome-related organelles: driving post-Golgi compartments into specialisation. Curr Opin Cell Biol, 19, 394-401.

Raposo, G., Nijman, H.W., Stoorvogel, W., Liejendekker, R., Harding, C.V., Melief, C.J. and Geuze, H.J. (1996) B lymphocytes secrete antigen-presenting vesicles. J Exp Med, 183, 1161-1172.

Riese, R.J. and Chapman, H.A. (2000) Cathepsins and compartmentalization in antigen presentation. Curr Opin Immunol, 12, 107-113.

Roche, P.A., Teletski, C.L., Stang, E., Bakke, O. and Long, E.O. (1993) Cell surface HLA-DR-invariant chain complexes are targeted to endosomes by rapid internalization. Proc Natl Acad Sci U S A, 90, 8581-8585.

Roche, P.A. and Cresswell, P. (1990) Invariant chain association with HLA-DR molecules inhibits immunogenic peptide binding. Nature, 345, 615-618.

Shi, G.P., Villadangos, J.A., Dranoff, G., Small, C., Gu, L., Haley, K.J., Riese, R., Ploegh, H.L. and Chapman, H.A. (1999) Cathepsin S required for normal MHC class II peptide loading and germinal center development. Immunity, 10, 197-206.

Shin, J.S., Ebersold, M., Pypaert, M., Delamarre, L., Hartley, A. and Mellman, I. (2006) Surface expression of MHC class II in dendritic cells is controlled by regulated ubiquitination. Nature, 444, 115-118.

Sloan, V.S., Cameron, P., Porter, G., Gammon, M., Amaya, M., Mellins, E. and Zaller, D.M. (1995) Mediation by HLA-DM of dissociation of peptides from HLA-DR. Nature, 375, 802-806.

van Ham, S.M., Tjin, E.P., Lillemeier, B.F., Gruneberg, U., van Meijgaarden, K.E., Pastoors, L., Verwoerd, D., Tulp, A., Canas, B., Rahman, D., Ottenhoff, T.H., Pappin, D.J., Trowsdale, J. and Neefjes, J. (1997) HLA-DO is a negative modulator of HLA-DM-mediated MHC class II peptide loading. Curr Biol, 7, 950-957.

van Niel, G., Wubbolts, R., Ten Broeke, T., Buschow, S.I., Ossendorp, F.A., Melief, C.J., Raposo, G., van Balkom, B.W. and Stoorvogel, W. (2006) Dendritic cells regulate exposure of MHC class II at their plasma membrane by oligoubiquitination. Immunity, 25, 885-894.

Vascotto, F., Lankar, D., Faure-Andre, G., Vargas, P., Diaz, J., Le Roux, D., Yuseff, M.I., Sibarita, J.B., Boes, M., Raposo, G., Mougneau, E., Glaichenhaus, N., Bonnerot, C., Manoury, B. and Lennon-Dumenil, A.M. (2007) The actin-based motor protein myosin II regulates MHC class II trafficking and BCR-driven antigen presentation. J Cell Biol, 176, 1007-1019.

Vasiljeva, O., Reinheckel, T., Peters, C., Turk, D., Turk, V. and Turk, B. (2007) Emerging roles of cysteine cathepsins in disease and their potential as drug targets. Curr Pharm Des, 13, 385-401.

Viville, S., Neefjes, J., Lotteau, V., Dierich, A., Lemeur, M., Ploegh, H., Benoist, C. and Mathis, D. (1993) Mice lacking the MHC class II-associated invariant chain. Cell, 72, 635-648.

Vyas, J.M., Kim, Y.M., Artavanis-Tsakonas, K., Love, J.C., Van der Veen, A.G. and Ploegh,

H.L. (2007) Tubulation of Class II MHC Compartments Is Microtubule Dependent and Involves Multiple Endolysosomal Membrane Proteins in Primary Dendritic Cells. J Immunol, 178, 7199-7210.

Wubbolts, R., Fernandez-Borja, M., Jordens, I., Reits, E., Dusseljee, S., Echeverri, C., Vallee, R.B. and Neefjes, J. (1999) Opposing motor activities of dynein and kinesin determine retention and transport of MHC class II-containing compartments. J Cell Sci, 112, 785-795.

Wubbolts, R., Fernandez-Borja, M., Oomen, L., Verwoerd, D., Janssen, H., Calafat, J., Tulp, A., Dusseljee, S. and Neefjes, J. (1996) Direct vesicular transport of MHC class II molecules from lysosomal structures to the cell surface. J Cell Biol, 135, 611-622.

Ziegler, H.K. and Unanue, E.R. (1982) Decrease in macrophage antigen catabolism caused by ammonia and chloroquine is associated with inhibition of antigen presentation to T cells. Proc Natl Acad Sci U S A, 79, 175-178.

Zwart, W., Griekspoor, A., Kuijl, C., Marsman, M., van Rheenen, J., Janssen, H., Calafat, J., van Ham, M., Janssen, L., van Lith, M., Jalink, K. and Neefjes, J. (2005) Spatial separation of HLA-DM/HLA-DR interactions within MIIC and phagosome-induced immune escape. Immunity, 22, 221-233.

Chapter 2

Activation of endosomal dynein motors by stepwise assembly of Rab7-RILP-ORP1L-p150^{Glued}, ORP1L, and the receptor βIII spectrin
Reproduced from J. Cell Biol. 2007. 176:459-71

Activation of endosomal dynein motors by stepwise assembly of Rab7–RILP–p150^{Glued}, ORP1L, and the receptor βIII spectrin

Marie Johansson,[1] Nuno Rocha,[2] Wilbert Zwart,[2] Ingrid Jordens,[2] Lennert Janssen,[2] Coenraad Kuijl,[2] Vesa M. Olkkonen,[1] and Jacques Neefjes[2]

[1]Department of Molecular Medicine, National Public Health Institute, Biomedicum, FI-00251 Helsinki, Finland
[2]Division of Tumor Biology, The Netherlands Cancer Institute, 1066CX Amsterdam, Netherlands

The small GTPase Rab7 controls late endocytic transport by the minus end–directed motor protein complex dynein–dynactin, but how it does this is unclear. Rab7-interacting lysosomal protein (RILP) and oxysterol-binding protein–related protein 1L (ORP1L) are two effectors of Rab7. We show that GTP-bound Rab7 simultaneously binds RILP and ORP1L to form a RILP–Rab7–ORP1L complex. RILP interacts directly with the C-terminal 25-kD region of the dynactin projecting arm p150^{Glued}, which is required for dynein motor recruitment to late endocytic compartments (LEs). Still, p150^{Glued} recruitment by Rab7–RILP does not suffice to induce dynein-driven minus-end transport of LEs. ORP1L, as well as βIII spectrin, which is the general receptor for dynactin on vesicles, are essential for dynein motor activity. Our results illustrate that the assembly of microtubule motors on endosomes involves a cascade of linked events. First, Rab7 recruits two effectors, RILP and ORP1L, to form a tripartite complex. Next, RILP directly binds to the p150^{Glued} dynactin subunit to recruit the dynein motor. Finally, the specific dynein motor receptor Rab7–RILP is transferred by ORP1L to βIII spectrin. Dynein will initiate translocation of late endosomes to microtubule minus ends only after interacting with βIII spectrin, which requires the activities of Rab7–RILP and ORP1L.

Introduction

The location and movement of intracellular vesiculotubular structures is controlled by microtubule-dependent kinesin and dynein motor proteins, as well as actin-dependent myosin motor proteins. Microtubule-based vesicle motility usually occurs in a bidirectional, stop-and-go manner because of the alternating activities of kinesin motors for plus-end movement and dynein motors for minus-end movement toward the microtubule organizing center (MTOC; Hirokawa, 1998; Wubbolts et al., 1999; Vale, 2003). How motor proteins are targeted to individual vesicles, how they dock on specific receptors, and how motor activity is controlled in a spatial and temporal manner are all processes that are poorly understood.

Cytoplasmic dynein is an ∼1.2-MD multisubunit protein complex, and it is the major motor for centripetal transport of membranous cargoes along microtubules (Schroer et al., 1989). Dynactin, which is also an ∼1.2-MD multisubunit complex, is a critical component of most, if not all, of the cytoplasmic dynein–driven activities. Dynactin participates in motor binding to microtubules (Waterman-Storer et al., 1995), increases motor processivity (King and Schroer, 2000; Culver-Hanlon et al., 2006), and acts as a multifunctional adaptor connecting cargo and dynein motor (Karki and Holzbaur, 1999; Schroer, 2004). At least 15 subunits of the dynein–dynactin motor are identified. The 1-MD dynein heavy chain dimer and the 300-kD p150^{Glued} dimer of the projecting arm of dynactin contact microtubules (Culver-Hanlon et al., 2006). p150^{Glued} is connected to the dynein heavy chain via the dynein intermediate chains (Waterman-Storer et al., 1995) and increases dynein motor processivity (King and Schroer, 2000; Culver-Hanlon et al., 2006). The actin-related protein 1 (Arp1) subunit forms a short filament at the base of dynactin and can bind membrane-associated βIII spectrin, which probably acts as the membrane receptor for the dynein–dynactin motor complex (Holleran et al., 2001; Muresan et al., 2001). αIβIII spectrin is located on the cytosolic side of late endocytic compartments (LEs), Golgi, and other subcellular compartments (De Matteis and Morrow, 2000),

M. Johansson and N. Rocha contributed equally to this paper.

Correspondence to Jacques Neefjes: j.neefjes@nki.nl

Abbreviations used in this paper: Arp, actin-related protein; FLIM, fluorescence lifetime imaging microscopy; FRET, fluorescence resonance energy transfer; LE, late endocytic compartment; MIIC, major histocompatibility complex class II–containing compartment; MBP, maltose-binding protein; mRFP, monomeric red fluorescent protein; MTOC, microtubule organizing center; ORD, oxysterol-binding protein–related domain; ORP, oxysterol-binding protein–related protein; RILP, Rab7-interacting lysosomal protein; shRNA, short hairpin RNA.

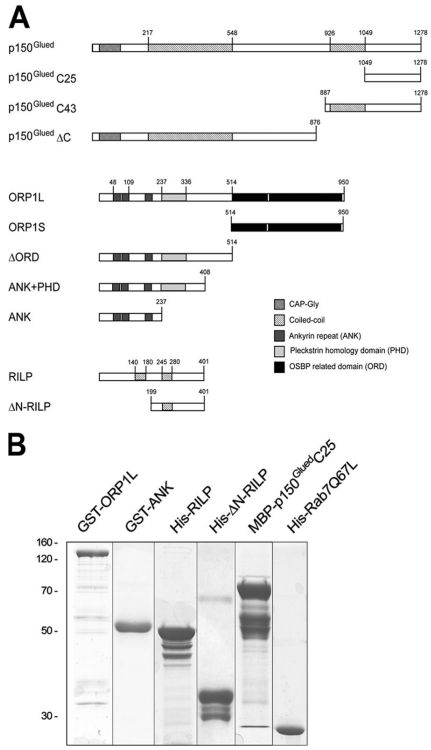

Figure 1. **The ORP1L, RILP, and p150^{Glued} constructs and purified recombinant proteins.** (A) Schematic representation of the constructs used in this study. The domains in ORP1L and p150^{Glued} are indicated. RILP contains predicted coiled-coil regions only. Numbers indicate amino acid residue positions. (B) Purified fusion proteins were resolved by 10% SDS-PAGE and Coomassie stained. Positions of the molecular weight markers and the fusion proteins are indicated.

implying that compartment-selective dynein motor recruitment cannot be controlled by βIII spectrin itself.

Small GTPases of the Rab family are present on specific subcellular compartments to regulate vesicle transport and fusion. They are ideal candidates for orchestrating the spatiotemporal regulation of motor-driven vesicle trafficking. Several Rab GTPases have been shown to interact directly or indirectly with motor proteins. These include members of the kinesin motor family (Rab4, Rab5, and Rab6), the dynein motor (Rab6 and Rab7), and the myosin motors (Rab8, Rab11, and Rab27a; Jordens et al., 2005). Rab6, which regulates Golgi transport, requires the effector bicaudal-D1 and -D2 (BicD1/2) to interact with the p50^{dynamitin} subunit of dynactin (Hoogenraad et al., 2003; Matanis et al., 2002) or a third protein, egalitarian (Egl), which directly interacts with the dynein light chain in *Drosophila melanogaster* (Navarro et al., 2004). An activation state–dependent interaction of Rab6 with p150^{Glued} has also been observed in a directed two-hybrid analysis (Short et al., 2002). We have studied another Rab protein, Rab7, which, through its effector Rab7-interacting lysosomal protein (RILP), recruits the dynein–dynactin motor to LEs, resulting in minus end–driven vesicular transport to the MTOC (Jordens et al., 2001). The Rab7–RILP–dynein motor cascade has been shown to act on many Rab7-containing compartments, including *Salmonella*-containing phagosomes (Harrison et al., 2004; Marsman et al., 2004), early melanosomes (Jordens et al., 2006), major histocompatibility complex class II–containing compartments (MIICs; Jordens et al., 2001), and cytolytic granules (Stinchcombe et al., 2006). The crystal structure of Rab7 in complex with a C-terminal domain of RILP revealed the details of this interaction. RILP forms a coiled-coil homodimer with two symmetric surfaces that bind two separate Rab7–GTP molecules to form a tetrameric complex (Wu et al., 2005), which has been confirmed in biochemical experiments (Colucci et al., 2005; Marsman et al., 2006). The recent finding that a member of the oxysterol-binding protein–related protein (ORP) family, ORP1L, also interacts with Rab7 and induces clustering of LEs (Johansson et al., 2005) complicated a simple interpretation of Rab7–RILP–controlled dynein motor recruitment. ORPs have been implicated in diverse aspects of cellular processes, including sterol and phospholipid metabolism, vesicle transport, and cell signaling (Lehto and Olkkonen, 2003). The mechanisms by which ORP proteins contribute to these processes have, however, remained largely unknown. We recently showed that ORP1L localizes to LEs and interacts via its ankyrin repeat region with the small GTPase Rab7 (Johansson et al., 2005). ORP1L was shown to stabilize the GTP-bound active form of Rab7 on LEs and to affect the subcellular distribution of these organelles, analogously, to RILP (Jordens et al., 2001). A third Rab7 effector, Rabring7 (Mizuno et al., 2003), clusters LEs, much like the other effectors, and induces lysosomal acidification, but dynein motor recruitment has not been shown. Surprisingly, no obvious sequence similarity is found between the three Rab7 effectors.

Apparently, multiple effectors interact with Rab7. They could be mutually exclusive, but they may also interact simultaneously with this Rab GTPase. How the Rab7 effector complexes recruit the dynein motor complex is also unclear. We have studied the interaction of RILP and ORP1L with the Rab7 GTPase, as well as their interactions with dynein–dynactin motor subunits. We show that Rab7 is part of a tripartite complex binding RILP and ORP1L simultaneously. RILP is essential for dynein motor recruitment through a direct interaction with the C-terminal portion of the p150^{Glued} subunit of the dynein–dynactin motor. ORP1L recruits this complex to βIII spectrin domains, which appears to be critical for dynein motor activation and minus-end transport of LEs. Rab7, thus, recruits two proteins with diverse functions in the control of dynein motor–driven transport: RILP for motor binding and ORP1L for transport to the membrane-associated late endocytic βIII spectrin receptor for motor activation. The dynein–dynactin motor, thus, requires two receptors before actively transporting LEs to the microtubule minus end. Its projecting arm, p150^{Glued}, is recruited by RILP bound by active Rab7 in LE membranes. The other Rab7 effector, ORP1L, then transfers the Rab7–RILP–p150^{Glued}–dynein motor complex to βIII spectrin interacting with the base of the dynactin complex Arp1. Only after completion of this "mass protein action" does the dynein motor transport LEs to the microtubule minus end.

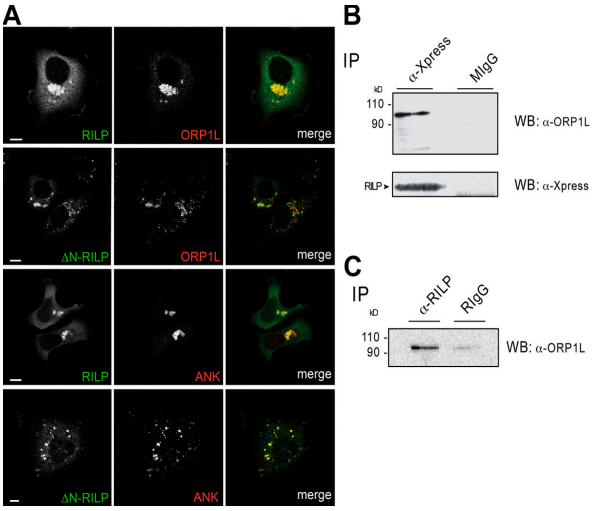

Figure 2. **ORP1L and RILP colocalize and are part of a physical complex.** (A) ORP1L and RILP colocalize on juxtanuclear late endocytic clusters. HeLa cells were transfected with GFP–RILP or GFP–ΔN-RILP, together with Xpress-tagged ORP1L or Xpress-tagged ORP1L–ANK domain (red), as indicated in the images. ANK and ORP1L colocalize with RILP or ΔN-RILP (right, merge). Bars, 10 μm. (B) ORP1L co-isolates with expressed RILP. HeLa cells were transfected with Xpress-tagged RILP and immunoprecipitated with anti-Xpress antibody (α-Xpress) or irrelevant mouse IgG (MIgG). The isolates were Western blotted with anti-ORP1L antibodies (WB: α-ORP1L). (bottom) Corresponding lanes probed with anti-Xpress antibody (WB: α-Xpress). (C) Coimmunoprecipitation of endogenous RILP and ORP1L. HeLa cell lysates were immunoprecipitated with rabbit anti-RILP serum (α-RILP) or irrelevant rabbit IgG (RIgG). The isolates were Western blotted with anti-ORP1L antibodies (WB: α-ORP1L).

Results

ORP1L and RILP colocalize on juxtanuclear late endocytic clusters as part of a physical complex

Both RILP and ORP1L have been reported to localize on LEs, and their overexpression induces juxtanuclear clustering of these compartments, suggesting involvement in microtubule-dependent LE motility (Jordens et al., 2001; Johansson et al., 2005). We studied the distribution of GFP-tagged RILP and Xpress-tagged ORP1L expressed in HeLa cells, and we visualized the proteins by confocal laser-scanning fluorescence microscopy. The proteins showed extensive colocalization on compact juxtanuclear organelle clusters (Fig. 2 A). We studied the contribution of their various domains to this phenotype (Fig. 1 A). The N-terminal portion of ORP1L, consisting of the ankyrin repeat region (ANK; aa 1–237; Fig. 2 A) or the ANK and the PH domain regions (ANK + PH; aa 1–408; not depicted), displayed colocalization with RILP similar to that of full-length ORP1L (Fig. 2 A), demonstrating that the N-terminal Rab7-interacting ANK region of ORP1L suffices to specify this localization. We have previously shown that the ANK and ANK + PH domain regions of ORP1L induce clustering of LEs in the absence of ectopically expressed RILP (Johansson et al., 2003, 2005). We tested whether a truncated RILP that fails to recruit the dynein–dynactin motor, but still binds to the switch and interswitch regions of small GTPase Rab7 (ΔN-RILP; Jordens et al., 2001; Wu et al., 2005), affects the LE-clustering phenotype induced by the ORP1L ANK domain (Fig. 2 A). Overexpression of ΔN-RILP inhibited clustering by ANK, although the two proteins still colocalized on the scattered LEs.

To determine whether ORP1L and RILP might interact physically, HeLa cells were transected with Xpress-tagged RILP and subjected to immunoprecipitation with the Xpress mAb or irrelevant mouse IgG. Western blotting of the isolates with anti-ORP1L antibody revealed coprecipitation of endogenous ORP1L with Xpress-RILP (Fig. 2 B). To study the interaction in an endogenous setting, HeLa cell lysates were incubated with anti-RILP antibody or irrelevant rabbit IgG. Endogenous ORP1L was detected in the immunoprecipitates by Western blotting (Fig. 2 C), suggesting that ORP1L and RILP not only colocalize on LEs but are also part of a physical complex in cells.

ORP1L and RILP interactions with Rab7 in living cells

We then applied fluorescence resonance energy transfer (FRET) techniques to test whether a RILP–Rab7–ORP1L interaction could be visualized in living cells using fluorescently labeled proteins. When two fluorophores are in close proximity (<8 nm) and the fluorophores show spectral overlap, FRET can occur (Förster, 1948). FRET can be detected by sensitized emission (when the acceptor emits light at the cost of donor fluorescence) or fluorescence lifetime imaging microscopy (FLIM). FLIM detects the time between photon absorbance by the donor fluorophore and its emission (in nanoseconds), which decreases when energy is transferred to acceptor fluorophores. FLIM, which, in principle, is more quantitative than sensitized emission for detecting FRET and FRET efficiencies (Wallrabe and Periasamy, 2005), was applied to study interactions between Rab7, RILP, and ORP1L in living HeLa cells.

HeLa cells transfected with GFP–RILP and monomeric red fluorescent protein (mRFP)–Rab7, GFP–ORP1L and mRFP–Rab7, or GFP–ORP1L and mRFP–RILP, were analyzed by FLIM, and the lifetime of the GFP fluorophore was measured. The cells were cocultured with Mel JuSo cells stably expressing histone 2B (H2B)–GFP, which were used as an internal null FRET control. Because RILP and Rab7 have been previously shown to interact (Cantalupo et al., 2001; Jordens et al., 2001) and cocrystallize (Wu et al., 2005), these proteins constituted a positive control for the experimental setup.

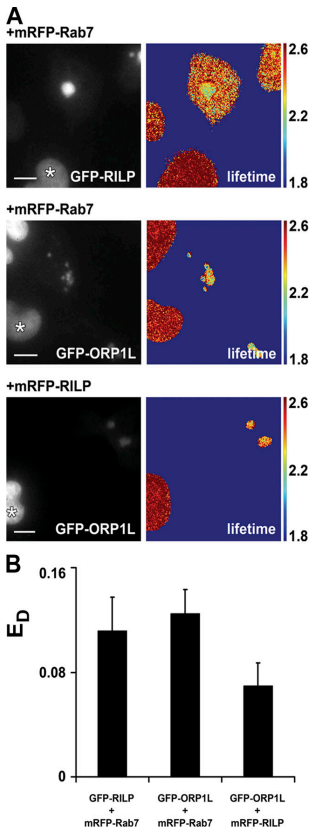

Figure 3. **FRET between ORP1L, Rab7, and RILP.** (A) HeLa cells were transfected with GFP–RILP or GFP–ORP1L and cotransfected with mRFP–Rab7 or mRFP–RILP, as indicated. The transfected HeLa cells were cocultured with Mel JuSo cells stably expressing H2B–GFP (indicated by *) as an internal marker with a lifetime of 2.6 ns. (left) Wide-field image of the transfected and internal control cells. (right) FLIM image of the same cells, in which the fluorescence lifetime is depicted in false colors. The color scale with the respective lifetimes (in nanoseconds) is indicated. The fluorescence lifetime of GFP–RILP or GFP–ORP1L was determined on vesicles immobile during data acquisition (~12 s). Bar, 10 μm. (B) The donor FRET efficiencies (E_D) between the GFP- and mRFP-tagged proteins were determined and plotted in the bar diagram. Mean ± the SD. $n > 20$.

When GFP–RILP and mRFP–Rab7 were coexpressed, discrete perinuclear clusters were formed. A substantial decrease in GFP fluorescence lifetime on the GFP–RILP–positive structures was observed in the presence of mRFP–Rab7. The measured lifetime was 2.29 ± 0.06 ns (Fig. 3 A), when the lifetime for H2B–GFP in control cells (indicated by an asterisk) was at 2.56 ± 0.03 ns (Bastiaens and Squire, 1999). The calculated donor FRET efficiency, or E_D (see Materials and methods), between GFP–RILP and mRFP–Rab7 was 11.2 ± 2.5% (Fig. 3 B), indicating efficient FRET and close spacing of RILP and Rab7 in living cells. Measuring FLIM between GFP–ORP1L and mRFP–Rab7 resulted in a comparable reduced lifetime of the GFP fluorophore, 2.23 ± 0.03 ns (Fig. 3 A), corresponding to an E_D of 12.5 ± 1.85% (Fig. 3 B).

To determine whether ORP1L and RILP are in close proximity not only to Rab7 but also to each other, FLIM was performed between GFP–ORP1L and mRFP–RILP. The decrease of fluorescence lifetime was somewhat less pronounced, but still significant (2.35 ± 0.04 ns; E_D = 7.0 ± 1.8%; Fig. 3, A and B). Similar results were obtained when measuring FRET by sensitized emission (unpublished data). These data suggest that ORP1L is part of the same complex as RILP and Rab7. The absolute distances between the proteins cannot, however, be determined from these data because FRET efficiency is not only determined by the Förster distance (distance between the fluorescent groups) but also by the orientation factor and flexibility of the fluorophores (Förster, 1948).

The Rab7-RILP-ORP1L tripartite complex

Having established that ORP1L and RILP are part of a physical complex (Fig. 2, A and B), we set out to study the interaction between the two proteins by a series of pull-down experiments. Endogenous RILP was pulled down from HeLa cell lysate using purified, matrix-immobilized GST–ORP1L (Fig. 4 A). To study whether this interaction between ORP1L and RILP is direct, we used purified His_6-tagged RILP or the constitutively active GTP-loaded Rab7 mutant Q67L, which is produced in *E. coli*, to pull down purified GST–ORP1L. These experiments revealed that, although His_6–Rab7Q67L efficiently pulled down GST–ORP1L in accordance with our previous results (Johansson et al., 2005), no interaction was detected between His_6–RILP and GST–ORP1L (Fig. 4 B). Because both RILP and ORP1L bind to Rab7, we next tested, using purified proteins, whether Rab7 is able to bridge the two effectors and thereby form a tripartite complex. Because soluble full-length recombinant GST–ORP1L is produced in limiting amounts, GST–ANK, which suffices to bind Rab7 and can be efficiently produced, was used to perform the binding assay. GST fusion proteins of the Rab7-interacting ORP1L ANK fragment (GST–ANK) were incubated with His_6–RILP, GTP-loaded His_6–Rab7Q67L, or a mixture of both His_6-tagged proteins. As expected, GST–ANK pulled down His_6–Rab7Q67L, but not His_6–RILP. However, His_6–RILP was pulled down by GST–ANK when the incubation was performed in the presence of GTP-loaded His_6–Rab7Q67L (Fig. 4 C). This indicated that Rab7 is required to bridge RILP and ORP1L, and that the two effectors do not compete for the same binding site on Rab7.

To test whether ORP1L and RILP interacted cooperatively with Rab7, we immobilized GTP-loaded GST–Rab7 and pulled down in vitro–translated and radiolabeled ORP1L or RILP. This experiment was performed in the presence of a step gradient of increasing amounts of purified RILP, ΔN-RILP, or ORP1L fusion proteins, respectively. GTP-loaded GST–Rab7 pulled down ^{35}S-labeled ORP1L to a significant extent in the absence of RILP, but further addition of His_6–RILP to the reaction mixture increased ORP1L binding to Rab7 in a dose-dependent manner. ^{35}S-labeled ORP1L binding to immobilized Rab7 increased up to approximately fourfold in the presence of His_6–RILP (Fig. 4, D [I] and E). Addition of His_6–RILP had no effect

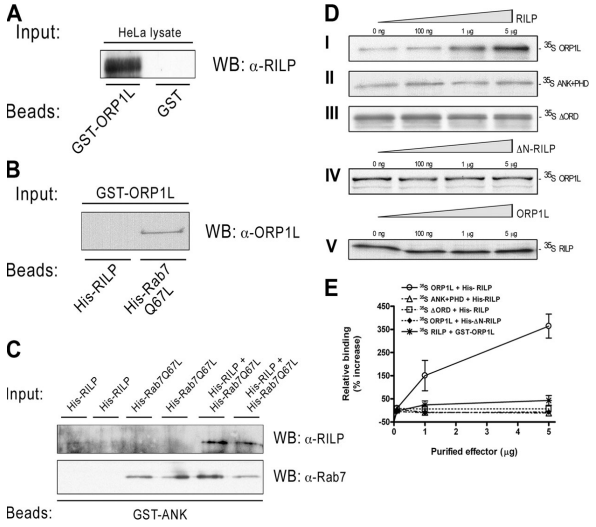

Figure 4. **The ORP1L–Rab7–RILP heterotrimeric complex.** (A) Proteins were pulled down from HeLa cell lysates with GST–ORP1L or GST and Western blotted with anti-RILP antiserum (WB: α-RILP). Pull-down assays were performed with purified proteins. (B) His_6–RILP or His_6–Rab7Q67L were immobilized on a matrix and used to pull down GST–ORP1L. Isolates were Western blotted with anti-ORP1L antibodies (WB: α-ORP1L). (C) GST–ORP1L ANK fragment (GST–ANK) was immobilized and incubated with His_6–RILP, GTP-loaded His_6–Rab7Q67L, or a mixture containing both His_6–RILP and GTP-loaded His_6–Rab7Q67L. The material pulled down by the ANK fragment was Western blotted with antibodies against Rab7 or RILP (indicated on the right). Duplicate samples are shown for each condition. (D) RILP enhances ORP1L binding to Rab7. GST–Rab7 was immobilized on a matrix, loaded with GTP, and incubated with in vitro–translated ^{35}S-labeled ORP1L in the presence of increasing amounts of His_6–RILP. ^{35}S-labeled ORP1L protein pulled down by GST–Rab7 was visualized by SDS-PAGE and autoradiography (I). Similar pull-down experiments were performed with in vitro–translated ^{35}S-labeled ORP1L ANK + PHD (II) or ^{35}S-labeled ORP1L ΔORD fragments (III). Pull-down of full-length ^{35}S-labeled ORP1L by active GST–Rab7 in the presence of increasing amounts of His_6–ΔN-RILP (indicated above the lanes) (IV). A reciprocal pull-down experiment in which in vitro–translated ^{35}S-labeled RILP was incubated with immobilized His_6–Rab7–GTP in the presence of increasing amounts of GST–ORP1L (indicated above the lanes; V). (E) Quantification of the radioactive bands in D by phosphorimaging. The plotted data shows the relative increase in binding of in vitro–translated proteins to immobilized Rab7–GTP in the presence of a step-gradient of effector proteins. Binding of ORP1L to Rab7 was enhanced up to fourfold in the presence of RILP. The plotted data represents the mean of three independent experiments ± the SD (error bars).

on the binding of ORP1L ANK (not depicted) or ANK + PHD fragments to Rab7–GTP (Fig. 4, D [II] and E). To further map the region of ORP1L involved in the observed stabilization, we extended the ANK + PHD domain to contain a region upstream of the oxysterol-binding protein–related domain (ORD) displaying a high probability of forming a coiled coil (ΔORD; Fig. 1 A; Lupas et al., 1991; Berger et al., 1995). Also this construct failed to produce the effect observed with full-length ORP1L (Fig. 4, D [III] and E), suggesting that the ORD of ORP1L is involved in the stabilization effect observed in the presence of His_6–RILP.

To determine if the N-terminal region of RILP, which is required for dynein–dynactin motor recruitment to LEs (Jordens et al., 2001), is necessary for facilitating the ORP1L–Rab7 interaction, the pull-down experiment with GTP-loaded Rab7 was repeated with in vitro–translated ^{35}S-labeled ORP1L in the presence of His_6–ΔN-RILP. This truncated form of RILP failed to increase ORP1L binding to Rab7–GTP (Fig. 4, D [IV] and E), demonstrating that the same domain of RILP essential in dynein–dynactin motor recruitment to LEs (Jordens et al., 2001) is also involved in the stabilization of the Rab7–ORP1L interaction.

To test if the observed cooperativity of ORP1L binding to Rab7 in the presence of RILP is reciprocal, we pulled down in vitro–translated ^{35}S-labeled RILP with immobilized His_6–Rab7–GTP, followed by incubation with increasing amounts of GST–ORP1L. RILP was observed to bind to immobilized Rab7, but the addition of GST–ORP1L had no effect on RILP binding (Fig. 4, D [V] and E). These experiments suggest that RILP might stabilize the Rab7–ORP1L interaction in a unidirectional manner, and again indicate that binding of the two effectors to Rab7 is not mutually exclusive.

RILP–Rab7 recruits $p150^{Glued}$ to LEs, whereas ORP1L is required for actual minus-end transport

GTP-loaded Rab7 collects RILP and ORP1L into a complex, and then recruits the dynein–dynactin motor protein complex to LE membranes. The dynein–dynactin motor complex interacts via the Arp1 filament with the β chain of membrane-associated αIβIII spectrin (Holleran et al., 2001), which thereby acts as a membrane receptor for the motor. Fluorescence microscopy analyses performed in HeLa cells demonstrated that the dynein–dynactin motor subunits Arp1, $p50^{dynamitin}$ (not depicted), and $p150^{Glued}$ were selectively recruited to LEs by myc-tagged RILP (Fig. 5 A). ΔN-RILP, in contrast, failed to recruit these dynein–dynactin motor subunits (Fig. 5 B).

To identify the dynein–dynactin motor subunit required for the RILP-mediated targeting to LEs, we tested whether ectopically expressed RILP or ORP1L could selectively stabilize particular dynein–dynactin motor subunits on LE membranes when the dynein–dynactin motor complex is dissociated. Overexpression of (GFP–)$p50^{dynamitin}$ displaces the projecting arm of dynactin from the rest of the dynactin complex, leaving Arp1 membrane associated, whereas $p150^{Glued}$ and other more distal dynein–dynactin motor subunits are dispersed in the cytosol (Echeverri et al., 1996; Burkhardt et al., 1997; Eckley et al., 1999). GFP–$p50^{dynamitin}$ was overexpressed in HeLa cells in the absence or presence of HA-RILP or Xpress–ORP1L. Cells were fixed and stained for endogenous $p150^{Glued}$ (Fig. 5 C). Expression of RILP alone, but not ORP1L (or ANK; unpublished data), sufficed to rescue $p150^{Glued}$ localization on LEs when the dynein motor complex was dissociated by $p50^{dynamitin}$ overexpression. It is noteworthy that the dynein–dynactin motor

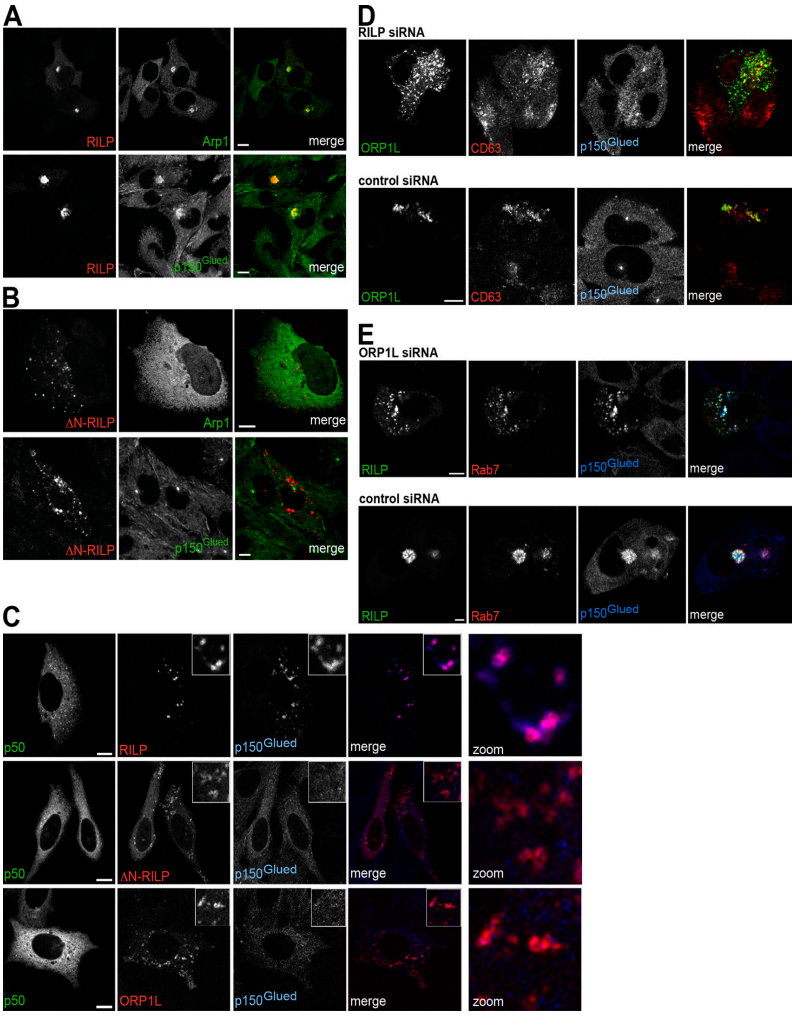

Figure 5. **Role of RILP and ORP1L in the recruitment of the p150^{Glued} subunit of the dynein–dynactin motor.** (A) HeLa cells were transfected with myc-tagged RILP (red), and the location of GFP–Arp1 and endogenous p150^{Glued} (green) was determined. (B) HeLa cells were transfected with VSV-tagged ΔN-RILP (red), and the location of GFP–Arp1 or endogenous p150^{Glued} (green) was determined. (C) HeLa cells were transfected with p50^{dynamitin} (green) and HA-tagged RILP, ΔN-RILP, or ORP1L (red), and subsequently stained for endogenous p150^{Glued} (blue), as indicated. The merge and the magnified merge (zoom) images only show the stainings in the red and blue images. (D) HeLa cells were transfected with GFP–ORP1L (green) and RILP siRNA or scrambled siRNA, as indicated. At 72 h after transfection, cells were fixed and stained for endogenous CD63 (red) and p150^{Glued} (blue). The merge shows only the ORP1L and CD63 labeling. (E) HeLa cells were transfected with GFP–RILP (green), mRFP–Rab7 (red), and ORP1L siRNA or a scrambled siRNA, as indicated, and fixed at 48 h after transfection. Cells were stained for endogenous p150^{Glued} (blue). Bars, 10 μm.

complex is no longer assembled into a functional motor when p50^{dynamitin} is overexpressed, resulting in scattered vesicles still containing RILP and p150^{Glued}. To further test the involvement of endogenous RILP or ORP1L in motor recruitment and minus end–directed transport, the proteins were down-regulated by specific siRNAs, and the localizations of RILP (ectopically expressed), ORP1L (ectopically expressed), late endocytic markers, and p150^{Glued} were determined (Fig. 5, D and E). Down-regulation of endogenous RILP or ORP1L induced scattering of LEs. p150^{Glued} was recruited to the scattered vesicles only when RILP was overexpressed (Fig. 5 E). Importantly, p150^{Glued} recruitment by RILP in the absence of ORP1L did not suffice to drive minus-end transport of LEs into a characteristic perinuclear cluster around the MTOC (Fig. 5 E). This suggests that RILP, but not ORP1L, interacts with the p150^{Glued} subunit of the dynein–dynactin motor complex. However, interactions

of RILP or ORP1L with other stabilizing motor subunits, or the involvement of additional proteins linking p150^{Glued} and RILP, cannot be excluded by these experiments.

RILP interacts with the C-terminal domain of p150^{Glued}

To identify the potential interaction between RILP and p150^{Glued}, we first determined the p150^{Glued} region recruited by RILP. ΔC, the GFP-tagged N-terminal 95-kD fragment of p150^{Glued} (aa 1–876) was coexpressed with mRFP–RILP (Fig. 6 A). Although decorating microtubules and the MTOC, this fragment failed to be recruited to the RILP cluster. This suggested that RILP interacts (directly or indirectly) with the C-terminal 55-kD portion of p150^{Glued}. The coiled coil–containing region in p150^{Glued} CC2 (aa 887–1,063) also failed to be recruited by RILP (not depicted), whereas GFP–p150^{Glued} C25 (aa 1,049–1,278), representing the most C-terminal 25-kD region after the coiled coil, was recruited to the mRFP–RILP cluster (Fig. 6 A). This construct did not colocalize with mRFP–ΔN-RILP (Fig. 6 A), in agreement with the observation that this dominant-negative RILP variant inhibits p150^{Glued} recruitment to LEs (Fig. 5, B–D; Jordens et al., 2001). These data suggest that the N-terminal half of RILP interacts with the most C-terminal region of p150^{Glued} to recruit the dynein–dynactin motor complex to LEs. To test whether this p150^{Glued} fragment also inhibited minus-end transport by acting as a dominant-negative dynein motor fragment, analogously to overexpression of p50^{dynamitin} (Burkhardt et al., 1997), the GFP-tagged versions of both proteins were overexpressed in HeLa cells, and late endocytic structures were visualized by labeling with anti-CD63 antibodies (Fig. 6 B). Overexpression of the C-terminal fragment of p150^{Glued} induced a mild, but reproducible, scattering of LEs, whereas the effect of p50^{dynamitin} overexpression was considerably more pronounced. This suggests that overexpression of the (presumably) monomeric version of the p150^{Glued} C-terminal fragment competes weakly with the endogenous p150^{Glued} homodimer for binding to the RILP homodimer.

A direct interaction between RILP and the most C-terminal region of p150^{Glued} can only be studied using purified proteins. GST–Rab7, GST–ORP1L, maltose-binding protein (MBP)–p150^{Glued} C25, His$_6$–RILP, and His$_6$–ΔN-RILP were expressed in *E. coli* and purified. GST–Rab7 was immobilized on beads and loaded with GTPγS. To reconstitute the tripartite complex in vitro, the beads were subsequently loaded with His$_6$–RILP or His$_6$–ΔN-RILP in the presence or absence of ORP1L. The beads were washed, and equal amounts of purified MBP–p150^{Glued} C25 were added to all reactions before another washing step. To determine specific binding, which is binding-dependent on the active GTP-bound conformation of Rab7, GTPγS was eluted by EDTA and replaced by excess GDP. The eluates were then incubated with amylose resin to capture the MBP–p150^{Glued} C25 fusions before extensive washing. The bound fractions were analyzed by SDS-PAGE and Western blotting (Fig. 6 C). Only RILP, but not ΔN-RILP or ORP1L, was recovered from the amylose-bound MBP–p150^{Glued} C25 fractions, in line with the observations above. This interaction was also reproduced in the absence of immobilized Rab7, suggesting that the GTPase is not required for binding in vitro of p150^{Glued} to RILP (unpublished data). These results support a model in which the C-terminal domain of RILP interacts with active GTP-loaded Rab7 and the N-terminal domain of RILP (which is absent in

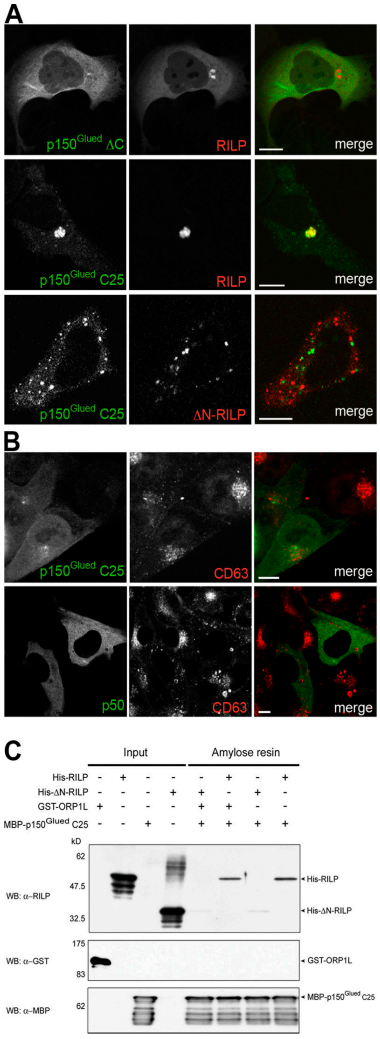

Figure 6. **RILP interacts with the C-terminal 25-kD fragment of p150^{Glued}.** (A) HeLa cells were transfected with mRFP–RILP or mRFP-tagged ΔN-RILP, along with GFP-tagged ΔC and C25 fragments of p150^{Glued}. (B) HeLa cells were transfected with GFP–p150^{Glued} C25 or GFP–p50^{dynamitin}, fixed, and stained with anti-CD63 antibodies. (C) Purified GTP-γS-loaded Rab7Q67L coupled to GST-beads was incubated with combinations of purified RILP, ΔN-RILP, ORP1L, or p150^{Glued} C25 (aa 1,049–1,278), as indicated above the gels. Proteins bound in a GTP-dependent manner were eluted with EDTA and the C-terminal MBP–p150^{Glued} fragments (C25) were captured on amylose resin. The input and resin-bound proteins were Western blotted with anti-RILP, -GST, or -MBP antibodies. Bars, 10 μm.

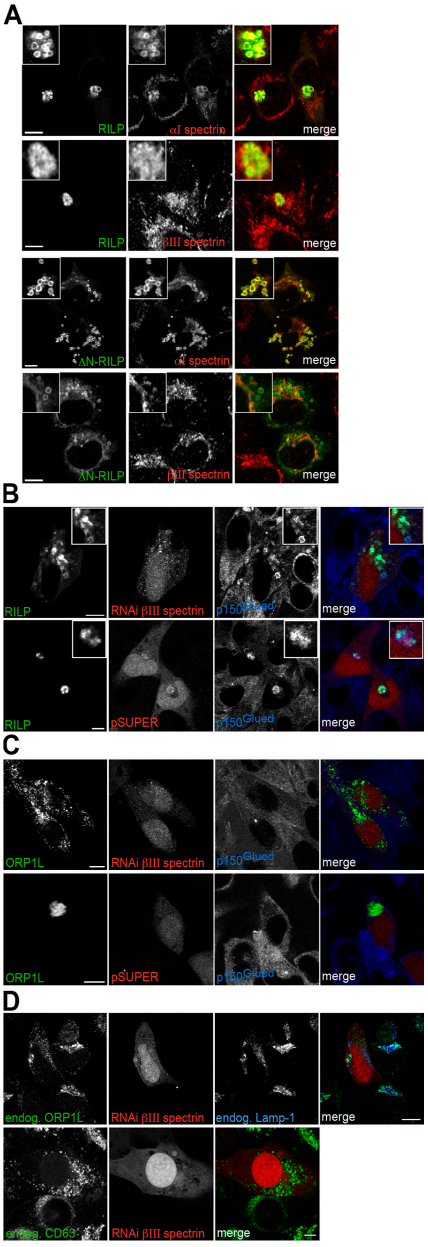

Figure 7. **αIβIII spectrin localizes to LEs for ORP1L-mediated RILP–p150^{Glued}–driven minus-end transport.** (A) Mel JuSo cells were transfected with GFP–RILP or GFP–ΔN-RILP for 48 h before fixation and staining for αI spectrin or βIII spectrin. αI and βIII spectrin (red) are located on RILP- and ΔN-RILP–labeled vesicles, as well as other subcellular structures. Note that βIII spectrin labeling localizes differently within the GFP–RILP– or GFP–ΔN-RILP–labeled vesicles. (insets) Magnification of vesicles showing the localization of RILP or ΔN-RILP and αI spectrin or βIII spectrin. (B) HeLa cells were transfected with GFP–RILP and pSUPER vector coexpressing mRFP and a control or βIII spectrin shRNA. Cells were fixed at 72 h after transfection and stained for endogenous p150^{Glued} (blue). (C) HeLa cells were transfected with GFP–ORP1L and pSUPER vector coexpressing mRFP and a control or βIII spectrin shRNA. At 72 h after transfection, cells were fixed and stained for endogenous p150^{Glued} (blue). (D) Endogenous ORP1L and spectrin. HeLa cells were transfected with a βIII spectrin shRNA pSUPER construct coexpressing mRFP. At 72 h after transfection, cells were fixed and stained for endogenous ORP1L (green) or endogenous CD63 (green) and the late endocytic marker Lamp-1 (blue). Bars, 10 μm.

ΔN-RILP) interacts with the C-terminal 25-kD fragment of the dynein–dynactin motor subunit p150^{Glued}.

ORP1L recruits the Rab7-RILP-p150^{Glued} complex to the membrane-associated receptor βIII spectrin

If the Rab7–RILP complex recruits the dynein motor through the p150^{Glued} stalk, it could act as a second dynein motor receptor in parallel with βIII spectrin on the membrane of LEs. βIII spectrin has an N-terminal actin-binding domain that interacts with the base of the dynein–dynactin motor Arp1 (Holleran et al., 2001) and is required for anchoring this motor to the membrane and for motor activity (Muresan et al., 2001). αIβIII spectrin is likely to be the only spectrin family member present on LEs (Stankewich et al., 1998; De Matteis and Morrow, 2000). To test whether αIβIII spectrin is located on LEs, and whether RILP or the dominant-negative form ΔN-RILP affects spectrin localization, we introduced GFP-tagged RILP or ΔN-RILP in Mel JuSo cells and stained these with antibodies for αI or βIII spectrin (Fig. 7 A). αI and βIII spectrin localized to various subcellular structures, including RILP- and ΔN-RILP–containing vesicles. Although full-length RILP was required for p150^{Glued} recruitment, αIβIII spectrin remained membrane associated, even when ΔN-RILP was expressed. The membrane association of αIβIII spectrin is, thus, independent of RILP, and probably occurs through association with various (unidentified) late endocytic transmembrane proteins and phospholipids (De Matteis and Morrow, 2000).

If RILP and βIII spectrin are receptors for the same motor protein, do they act in concert or independently? HeLa cells were transfected with GFP–RILP and a pSUPER construct that coexpresses mRFP and a control or βIII spectrin short hairpin RNA (shRNA). The cells were fixed and stained for endogenous p150^{Glued}. Although (GFP–)RILP recruited p150^{Glued}, down-regulation of βIII spectrin prevented transport of the RILP–p150^{Glued}–positive vesicles to the microtubule minus ends, which is similar to the situation observed after down-regulation of ORP1L (Fig. 7 B and Fig. 5 E). We subsequently tested whether the clustering of LEs imposed by ORP1L was also dependent on βIII spectrin. HeLa cells were transfected with GFP–ORP1L– and pSUPER vector–coexpressing mRFP and control or βIII spectrin shRNA. Cells were fixed and stained for p150^{Glued} (Fig. 7 C). GFP–ORP1L clustered vesicles without recruiting detectable p150^{Glued}, which is in accordance with the finding that RILP is responsible for recruiting p150^{Glued}. Silencing of βIII spectrin expression resulted in scattering of ORP1L-positive vesicles, implying that minus-end transport of ORP1L

and RILP-positive vesicles requires βIII spectrin (Fig. 7, B and C). Unlike RILP, endogenous ORP1L was detectable with the available antibodies. We tested whether down-regulation of βIII spectrin also induced scattering of organelles positive for endogenous ORP1L and other late endocytic markers. HeLa cells were transfected with the pSUPER vector coexpressing mRFP and a shRNA for βIII spectrin before labeling (Fig. 7 D). Scattering of the ORP1L-, Lamp-1–, and CD63-positive LEs was only detected in the mRFP-expressing transfected cells. These results suggest that βIII spectrin is required for minus-end transport of LEs labeled with endogenous or ectopically expressed ORP1L (Fig. 7, C and D). Notably, silencing of βIII spectrin (Fig. 7 B), as well as ORP1L (Fig. 5 E), prevents LEs labeled with Rab7–RILP–$p150^{Glued}$ complexes to be actively transported to the minus end of microtubules.

Discussion

Most intracellular organelles are transported along microtubules in a bidirectional manner, driven by at least two oppositely directed motor proteins. Late endosomes, like MIICs, move bidirectionally by the alternating activities of the dynein–dynactin motor (for minus-end transport) and the kinesin motor (for plus-end transport; Wubbolts et al., 1999). The function of motor proteins must be spatially and temporally coordinated to explain this complex pattern of organelle motility. We show how minus-end transport of LEs by the dynein–dynactin motor is regulated by the tripartite complex ORP1L–Rab7–RILP. We show that RILP directly interacts with the 25-kD C-terminal region of $p150^{Glued}$. This explains how activation of Rab7, via RILP, recruits the dynein–dynactin motor to LEs. However, we also show that this motor recruitment does not suffice for minus-end microtubular transport of LEs. ORP1L is presumably essential for translocation of Rab7–RILP–$p150^{Glued}$ to βIII spectrin, which acts as the general dynein receptor on LEs and other organelles (De Matteis and Morrow, 2000). Only then does dynein motor–driven minus-end transport ensue. Rab7–RILP is the late endocytic–specific dynein motor receptor that cooperates with the general dynein receptor βIII spectrin for active dynein motor activity on LEs. This $p150^{Glued}$–RILP–Rab7–ORP1L–βIII spectrin cascade explains one critical step in the spatiotemporal control of late endocytic motility.

βIII spectrin pairs with αI spectrin and the αIβIII spectrin heterodimer localizes to the cytosolic side of LEs, Golgi, and other organelles (Stankewich et al., 1998; De Matteis and Morrow, 2000). However, its presence does not suffice to recruit the dynein motor. Instead, activation of Rab7 specifies the target membrane for RILP- and ORP1L-mediated dynein–dynactin motor activities rather than the more ubiquitous spectrin receptor. Several Rab proteins have recently been found to control motor proteins either via a direct interaction or via effector proteins (Jordens et al., 2005). In all cases, it is unclear whether additional membrane motor receptors on specific compartments are also involved in RabGTPase-controlled, motor-driven transport.

We define a novel interaction where Rab7 recruits RILP to interact with the C terminus of $p150^{Glued}$. This may stabilize the projecting motor arm on the dynein–dynactin base comprised of Arp1, $p50^{dynamitin}$, and other subunits (Schroer, 2004). The C-terminal fragment of $p150^{Glued}$ also interacts with dynein intermediate chain and Arp1 (Kumar et al., 2001) in a manner that still leaves space for RILP interactions. That RILP interacts with a fragment near the dynein–dynactin motor base is not unexpected because the Rab7–RILP complex is membrane embedded and not likely to protrude far from the membrane. We have previously failed to detect this by cryoelectronmicroscopy (Jordens et al., 2001), probably because of the inefficiency of immunolabeling.

In this study, we have used a series of techniques to study the interaction between Rab7 and two of its effectors, RILP and ORP1L. The FRET results indicate that Rab7, RILP, and ORP1L are in close proximity in living cells, and our in vitro experiments indicate that RILP and ORP1L can bind simultaneously to the same active GTP-loaded Rab7 molecule. In fact, the binding of ORP1L to Rab7 is stabilized by RILP. The N-terminal ANK region of ORP1L specifies the Rab7 interaction (Johansson et al., 2005). We now show that the ANK region binds directly to active GTP-loaded Rab7, but additional determinants in the C-terminal half of ORP1L stabilize the RILP–Rab7–ORP1L tripartite complex. Because the crystal structure of the Rab7–RILP complex revealed that two GTP-loaded Rab7 molecules bind on opposite sides of a RILP homodimer (Wu et al., 2005), the RILP–Rab7–ORP1L complex is probably a heterotrimeric dimer with ORP1L positioned at the boundaries of the complex (Fig. 8).

How does the RILP–Rab7–ORP1L complex recruit the dynein motor to LEs? Rab7 associates with LEs after GTP binding and recruits the effectors RILP and/or ORP1L, thus forming a tripartite complex. In theory, both effectors could mediate the recruitment of the motor. When we overexpressed $p50^{dynamitin}$ to dissociate the dynein–dynactin motor complex such that the $p150^{Glued}$ subunit becomes solubilized, RILP, but not ORP1L, was able to recruit soluble $p150^{Glued}$ to LEs. $p150^{Glued}$ is in fact the most membrane-distal subunit that becomes detached from the Arp1 filament at the base of dynactin after $p50^{dynamitin}$ overexpression (Echeverri et al., 1996; Burkhardt et al., 1997; Ahmad et al., 1998; Eckley et al., 1999). Using $p150^{Glued}$ deletion constructs, we identified the RILP-interacting determinant as the most C-terminal 25-kD part of $p150^{Glued}$. In vitro reconstitution experiments confirmed that RILP, unlike ΔN-RILP or ORP1L, directly interacts with this C-terminal region of $p150^{Glued}$. Thus, the C-terminal half of RILP interacts with GTP–Rab7 and the N-terminal half interacts with the C-terminus of $p150^{Glued}$, and probably with the C-terminus of ORP1L (Fig. 8). The N-terminal half of RILP could not be successfully produced in *E. coli* because of aggregation of the expressed protein and was not recruited to LEs. Thus, a direct interaction of this domain with $p150^{Glued}$ could not be tested. Because both RILP and $p150^{Glued}$ are homodimers, these two proteins may bind as dimer–dimer, but this has not been experimentally verified.

If the Rab7–RILP complex recruits the dynein–dynactin motor complex by directly interacting with $p150^{Glued}$, the function of ORP1L remains elusive. RILP mainly contains coiled-coil

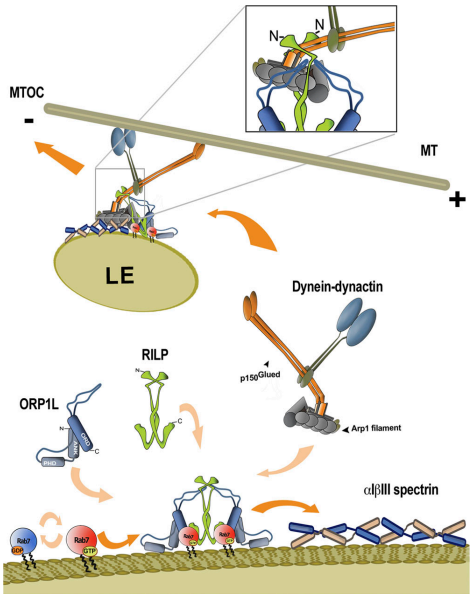

Figure 8. **Model for function of ORP1L in the translocation of the Rab7–RILP–p150^{Glued}–dynein motor complex to βIII spectrin for minus-end transport.** Active GTP-loaded Rab7 localizes to membranes of LEs and recruits the effectors RILP and ORP1L to form a dimer of a heterotrimeric complex. The C-terminal domain of RILP interacts with the switch and interswitch (RabSF1 and RabSF4) regions of Rab7, and the N-terminal half of RILP binds to the C-terminal domain of p150^{Glued} (shown in detail in the box). Subsequently, the 2.4-MD dynein–dynactin motor is recruited by the 0.35-MD ORP1L–Rab7–RILP complex on LEs. ORP1L is required to direct the entire complex to the 0.6-MD αIβIII spectrin. The interaction is mediated by Arp1 binding to βIII spectrin. αIβIII spectrin localizes to several different compartments, but it is not sufficient on its own to recruit dynein motors. Microtubule-based, dynein motor–driven minus-end transport of LEs can only occur after the specific late endocytic dynein receptor Rab7–RILP has interacted with the general dynein membrane receptor βIII spectrin, a process that is facilitated by ORP1L.

regions, whereas ORP1L is composed of multiple defined domains, including three ankyrin repeats, a PH domain, and an oxysterol-binding domain. Both βIII spectrin and ORP1L contain a PH domain with similar specificity (Rameh et al., 1997; Johansson et al., 2005). It is possible that ORP1L is required for Rab7–RILP–dynein motor targeting to specific microdomains on LEs to deliver the dynein motor to its spectrin receptor. This is likely to be the 622-kD αIβIII spectrin heterodimer (Stankewich et al., 1998; De Matteis and Morrow, 2000), which remains bound to late endosomes when RILP is inactivated (Fig. 7 A). The 272-kD βIII spectrin protein contains two Arp1-binding sites (Holleran et al., 2001), repeat regions involved in several protein–protein interactions and a C-terminal PH domain (De Matteis and Morrow, 2000). Via its various molecular interactions, spectrin is strongly associated with multiple membrane compartments, including LEs. Using RNAi, we show that βIII spectrin is critical for minus-end dynein-mediated transport of LEs. Surprisingly, inactivation of ORP1L or βIII spectrin prevented minus-end dynein-mediated transport of LEs, even when Rab7–RILP recruited the p150^{Glued} subunit of dynactin onto the membranes of LEs. The similarity of phenotypes suggests that ORP1L and spectrin are functionally connected. ORP1L could interact directly with αIβIII spectrin, perhaps via its ankyrin repeats. Because the PH domains of ORP1L and βIII spectrin have overlapping specificities (Rameh et al., 1997; Johansson et al., 2005), ORP1L may also transfer the Rab7–RILP–p150^{Glued} complex to the correct microdomains for docking the dynein motor on βIII spectrin. This transfer could be required for dynein motor activation by an unknown mechanism.

In addition, such microdomains may contain a GTPase-activating protein to inactivate GTP–Rab7 and dissociate the RILP–dynein motor complex from LEs. This may be essential because a kinesin and/or dynein motor should be cyclically recruited or activated to drive the bidirectional transport of LEs in a stop-and-go fashion (Wubbolts et al., 1999). How the kinesin motor is recruited and whether this requires dissociation of the Rab7–RILP–dynein motor complex is unclear. Kinesin II can associate with p150^{Glued} (Deacon et al., 2003; Gross, 2003), and the bidirectional movement may be driven by alternating activities of the kinesin and dynein motors on the ORP1L–Rab7–RILP-recruited–p150^{Glued} complex docked on βIII spectrin, which acts as a receptor for both motor activities.

Based on the data presented here, we propose the following model for Rab7-controlled recruitment of the dynein motor complex to its receptor αIβIII spectrin on LEs (Fig. 8). After GTP binding, Rab7 is recruited to late endocytic membranes. Active Rab7 binds two proteins with different functions. The RILP homodimer binds to the switch and interswitch regions of Rab7, arresting Rab7 in the active membrane-bound state (Jordens et al., 2001; Wu et al., 2005; Marsman et al., 2006). ORP1L binding to Rab7 is stabilized by RILP to form a 360-kD complex. Within this complex, the RILP dimer associates with the base of p150^{Glued} to facilitate the recruitment of the dynein–dynactin motor. ORP1L then targets the Rab7–RILP–dynein motor complex to the spectrin receptor on LEs. ORP1L and βIII spectrin are both required for a functional dynein motor, suggesting that RILP-mediated recruitment of the dynein motor to LEs does not suffice for correct docking on the LE–dynein receptor βIII spectrin. The dynein motor is apparently only activated with full cooperation of Rab7, RILP, and ORP1L. The complicated bidirectional motility of LEs is regulated by networks of macromolecular complexes controlled by the small GTPase Rab7.

Materials and methods

cDNA constructs and vectors

ORP1L, RILP, ΔN-RILP, and Rab7 cDNA constructs have been previously described (Fig. 1 A; Jordens et al., 2001; Johansson et al., 2003, 2005; Marsman et al., 2004). The mammalian expression vectors used were pcDNA4HisMax (Invitrogen), pcDNA3.1 (Invitrogen), and pEGFP-C (BD Biosciences). The mRFP–RILP and mRFP–Rab7 fusion constructs were generated by amplification of full-length mRFP by PCR (template plasmid provided by R.Y. Tsien, University of California, San Diego, La Jolla, CA) using forward primer 5′-CCCAGCTAGCACCACCATGGCCTCCTCCGAGGACGTCAT-3′ and reverse primer 5′-GAAGATCTGGCGCCGGTGGAGTG-3′. The mRFP fragment was ligated into the NheI and BglII sites in vector pEGFP-C1, from which the GFP moiety had been removed. The GFP–Arp1 construct was a gift from C. Hoogenraad (Erasmus Medical Centre,

Rotterdam, Netherlands). The C-terminal fragments of p150^{Glued} encoding aa 887–1,278 and 1,049–1,278 were generated by PCR and ligated into the EcoRI and BamHI sites of vector pEGFP-C2 (CLONTECH Laboratories, Inc.). For production of MBP–p150^{Glued} fusion proteins, the same fragments were cloned into the EcoRI and BamHI sites of vector pMAL-c2X (New England Biolabs). A pSUPER vector coexpressing mRFP (Bergink et al., 2006) was used to express short hairpins to down-regulate human βIII spectrin (the sequence targeted by the expressed RNAi is 5′-CGTGGCACGGCTCTGGGAC-3′). siRNA for human RILP was obtained from Dharmacon (ON-TARGETplus SMARTpool for accession no. NP_113618) and cotransfected with a vector expressing GFP–ORP1L (Johansson et al., 2005), using DharmaFECT 1 transfection reagent (Dharmacon). Human ORP1L siRNA oligos with sequence 5′-UrGrCrCrArGUrGrCrCrGrGrAUUrCUrGrATT -3′ were obtained from Proligo and were cotransfected with a vector expressing GFP–RILP (Marsman et al., 2006) using Lipofectamine 2000 (Invitrogen).

For production of hexahistidine (His_6)-tagged proteins, full-length Rab7, or Rab7Q67L, cDNAs were subcloned into the BamHI and XhoI sites of pET-28a (Novagen). A cDNA fragment encoding full-length RILP was subcloned into the NcoI–HindIII sites of vector pETM-11 (a gift from G. Stier, European Molecular Biology Laboratory, Heidelberg, Germany) for production of His_6-tagged RILP. ΔN-RILP was subcloned as a BglII fragment into a BamHI-digested vector pRSET-C (Invitrogen).

Vector pRP265, which is a derivative of pGEX-2T (GE Healthcare) with a modified multiple cloning site, was used to generate GST–Rab7 fusion protein. Full-length ORP1L, ORP1S, and ANK fragment inserts were subcloned into the BamHI site of vector pGEX-1λT (GE Healthcare) for production of GST fusion proteins. Constructs are depicted in Fig. 1 A.

Antibodies

GST–ORP1 and GST–RILP fusion proteins were used for generation of rabbit polyclonal antibodies (Jordens et al., 2001; Johansson et al., 2003, 2005). The other antibodies used were chicken anti-Rab7 (a gift from A. Wandinger-Ness, University of New Mexico, Albuquerque, NM), rabbit anti-Rab7 (Santa Cruz Biotechnology, Inc.), rabbit anti–human αI spectrin and rabbit anti–human βIII spectrin (Santa Cruz Biotechnology, Inc.), mouse anti-Xpress (Invitrogen), mouse anti-myc (Santa Cruz Biotechnology, Inc.), mouse anti-p150^{Glued} (BD Biosciences), HRP-conjugated monoclonal anti-MBP (New England Biolabs), and polyclonal goat anti-GST (GE Healthcare).

Protein purification

His_6-tagged RILP was produced in the *E. coli* strain Rosetta (DE3) pLysS (Novagen) in autoinduction high-density shaking cultures (Studier, 2005) at 24°C for 20 h. Cells were collected and resuspended in buffer A (25 mM Hepes, pH 7.5, 300 mM NaCl, Complete EDTA-free Protease Inhibitor Cocktail [Roche], 1 mM PMSF, 5 mM β-mercaptoethanol, 10 mM imidazole, and 0.05% [vol/vol] Triton X-100), and then lysed by sonication on ice. The cleared lysate was incubated with preequilibrated Talon Co^{2+} resin (CLONTECH Laboratories, Inc.) for 1 h. The resin was packed into a column and washed with buffer A containing 20 mM imidazole, and His_6-RILP was eluted by a step-gradient of imidazole in buffer A. The eluted protein was concentrated in 25 mM Hepes, pH 7.5, 300 mM NaCl, and 10% (vol/vol) glycerol in 10-kD cut-off concentrators (Vivaspin-2; Sartorius).

GST–ORP1L was produced in a similar manner at an induction temperature of 30°C for 18 h. Cells were harvested and lysed in buffer B (25 mM Hepes, pH 8.0, 150 mM NaCl, 1 mM PMSF, Complete Protease Inhibitor Cocktail, 0.1% Triton X-100, and 1 mM DTT). The soluble fraction was combined with glutathione–Sepharose 4B beads (GE Healthcare) and washed extensively with buffer (25 mM Hepes, pH 7.6, and 100 mM NaCl), and the protein was eluted with 15 mM reduced glutathione. The protein was concentrated in 25 mM Hepes, pH 7.6, 150 mM NaCl, 15% (vol/vol) glycerol, and 1 mM DTT.

GST–ANK expression was induced in BL21(DE3) (Stratagene) with 1.0 mM IPTG for 4 h at 37°C. Cells were harvested, resuspended in PBS, and lysed by freeze–thaw cycles followed by sonication. The cleared lysate was incubated with glutathione–Sepharose 4B and washed with PBS, and the protein was eluted with 20 mM reduced glutathione in PBS.

His_6-tagged Rab7 and His_6-tagged Rab7Q67L were expressed in BL21(DE3) (Stratagene) by induction with 0.5 mM IPTG for 5 h at 30°C. After harvesting, the cells were resuspended in 25 mM Hepes, pH 8.0, 300 mM NaCl, 5 mM $MgCl_2$, Complete EDTA-free Protease Inhibitor Cocktail, 1 mM PMSF, 5 mM β-mercaptoethanol, and 10 mM imidazole, and lysed by sonication on ice. The clarified lysates were passed through a HiTrap Chelating HP column (GE Healthcare) charged with Co^{2+} and further purified using a HiTrap SP HP column (GE Healthcare) in 20 mM Mes, pH 6.0, 100 mM NaCl, 5 mM $MgCl_2$, and 5 mM β-mercaptoethanol.

E. coli BL21(DE3) cells harboring the GST–Rab7 construct were induced with 0.5 mM IPTG for 5 h at 30°C. Cells were harvested, resuspended in a buffer containing 50 mM Tris-HCl, pH 7.5, 200 mM NaCl, 1 mM PMSF, Complete EDTA-Free Protease Inhibitor Cocktail, 5 mM $MgCl_2$, and 1 mM DTT, and lysed by sonication on ice. The cleared lysate was loaded on a preequilibrated GSTrap FF column (GE Healthcare) and washed extensively with the same buffer. GST–Rab7 was eluted with 50 mM Tris-HCl, pH 8.0, 100 mM NaCl, 5 mM $MgCl_2$, 1 mM DTT, and 20 mM reduced glutathione.

The MBP–p150^{Glued} fusion proteins were expressed in *E. coli* strain Rosetta (DE3) pLysS (Novagen) and affinity purified using an amylose resin column (New England Biolabs) according to the manufacturer's instructions. All fusion proteins made were analyzed by SDS-PAGE and Coomassie staining; they are depicted in Fig. 1 B.

Immunoprecipitations

Transfected HeLa cells (~2×10^6) were washed with ice-cold PBS and scraped into 400 μl of lysis buffer (20 mM Hepes, pH 7.6, 150 mM NaCl, 2 mM $MgCl_2$, 10% glycerol, 0.5% Triton X-100, and 1 mM DTT) with Complete EDTA-free Protease Inhibitor Cocktail. Cells were kept on ice for 15 min and centrifuged for 15 min at 16,000 *g* at 4°C, and the supernatant was preadsorbed at 4°C for 30 min with 30 μl of protein G–Sepharose 4 Fast Flow (GE Healthcare). The recovered supernatant was incubated with Xpress or irrelevant control antibodies at 4°C overnight. The lysate–antibody mixture was incubated at 4°C with protein G–Sepharose for 4 h, followed by washing with lysis buffer. For immunoprecipitation of endogenous ORP1L from HeLa lysates, cells (~10^7) were lysed and preadsorbed as described for supernatant. The recovered supernatant was incubated with RILP or irrelevant control antibodies at 4°C for 2 h. The lysate–antibody mixture was incubated at 4°C with protein G–Sepharose for 2 h, followed by washing with lysis buffer. The immunoprecipitates were analyzed by SDS-PAGE and Western blotting.

Pull-down of endogenous RILP

100 μg GST–ORP1L fusion protein and an approximately equimolar amount of 25 μg GST were coupled to 30 μl glutathione–Sepharose 4B beads in coupling buffer (PBS, 2 mM $MgCl_2$, and 1 mM DTT) for 2 h at 4°C. Beads were washed with coupling buffer and equilibrated in lysis buffer (20 mM Hepes, pH 7.6, 150 mM NaCl, 2 mM $MgCl_2$, 10% glycerol, 0.5% Triton X-100, and 1 mM DTT). HeLa cells were lysed as described in the immunoprecipitations section. After centrifugation of the lysates for 15 min at 16,000 *g* at 4°C, the supernatant was added to the beads and incubated for 2 h at 4°C. Beads were washed extensively with lysis buffer, and bound proteins were eluted with 20 mM glutathione. The eluted proteins were analyzed by SDS-PAGE and Western blotting.

Pull-down of in vitro–translated fragments

^{35}S-labeled full-length and truncated proteins were generated by in vitro transcription/translation using the TnT coupled reticulocyte system (Promega) according to the manufacturer's instructions. 50 μg wild-type GST–Rab7 fusion protein was coupled to 20 μl glutathione–Sepharose 4B beads in coupling buffer (PBS, 2 mM $MgCl_2$, and 1 mM DTT) for 2 h at 4°C. Beads were washed with coupling buffer and equilibrated in 20 mM Hepes, pH 7.5, 100 mM KAc, 0.5 mM $MgCl_2$, 1 mM DTT, 2 mM EDTA, and 10 mg/ml albumin. The beads were incubated with 10 μM GTP for 10 min at room temperature, after which $MgCl_2$ was added to a final concentration of 10 mM and the incubation was continued for an additional 30 min. Purified His_6–RILP, His_6–ΔN-RILP, or GST–ORP1L (0 ng, 100 ng, 1 μg, and 5 μg) and in vitro–translated proteins (22 μl) were added to the beads and incubated in a total volume of 0.5 ml for 2 h at 4°C. Beads were washed extensively with wash buffer (20 mM Hepes, pH 7.5, 100 mM KAc, 5 mM $MgCl_2$, and 1 mM DTT), and proteins were eluted with 20 mM glutathione in wash buffer and resolved by SDS-polyacrylamide gels, which were exposed on x-ray film (Kodak) or analyzed by phosphor imaging (FLA-3000; Fujifilm).

Pull-down of purified ORP1L

50 μg His_6–RILP and 50 μg His_6–Rab7Q67L were coupled to 20 μl Talon Co^{2+} resin (CLONTECH Laboratories, Inc.) in coupling buffer (20 mM Hepes, pH 7.5, 150 mM NaCl, 2 mM $MgCl_2$, 10% glycerol, and 5 mM β-mercaptoethanol) for 1 h at 4°C. Beads were washed and equilibrated in coupling buffer with 10 mM imidazole. 2.3 μg purified GST–ORP1L or 5 μg plain GST was added to the beads and incubated for 2 h at 4°C. Beads were

washed extensively with binding buffer (20 mM Hepes, pH 7.5, 150 mM NaCl, 2 mM $MgCl_2$, 10% glycerol, 5 mM β-mercaptoethanol, and 10 mM imidazole) and eluted with 750 mM imidazole in 20 mM Hepes, pH 7.5, 150 mM NaCl, 10% glycerol, and 5 mM β-mercaptoethanol. Samples were analyzed by SDS-PAGE and Western blotting.

Pull-down of purified His_6–RILP

100 μg GST–ANK was coupled to glutathione–Sepharose 4B beads in PBS for 2 h at 4°C, after which the beads were washed and equilibrated in binding buffer (20 mM Hepes, pH 7.5, 150 mM NaCl, 2 mM $MgCl_2$, 10% glycerol, 0.5% Triton X-100, and 1 mM DTT). 10 μg purified His_6–RILP and/or 20 μg His_6–Rab7Q67L were added to the beads and incubated for 4 h at 4°C. Beads were washed with binding buffer and eluted with 20 mM glutathione (30 μl) in binding buffer. Samples were analyzed by SDS-PAGE and Western blotting.

$p150^{Glued}$-binding assay

30 μg GST–Rab7 was coupled to 15 μl glutathione–Sepharose 4B beads and preloaded with GTPγS as described for the pull-down of in vitro–translated fragments. Beads were washed to remove unbound proteins, and recombinant purified His_6–RILP (3 μg), His_6–ΔN-RILP (2 μg), or GST–ORP1L (8 μg) was added to the beads and incubated in a total volume of 0.4 ml for 2 h at 4°C. Beads were washed extensively with detergent/salt buffer (20 mM Hepes, pH 7.5, 300 mM NaCl, 1 mM DTT, 2 mM $MgCl_2$, and 0.1% [vol/vol] Triton X-100), and 4 μg of either MBP–$p150^{Glued}$ (aa 887–1,278) or MBP–$p150^{Glued}$ (aa 1,049–1,278) was added to the beads. Proteins were incubated further in a total volume of 0.4 ml of detergent/salt buffer for 30 min at 22°C. Beads were washed and proteins bound to GTP–Rab7 were eluted by supplementing the 0.4 ml of detergent/salt reaction buffer with EDTA to a final concentration of 20 mM. To precipitate the MBP–$p150^{Glued}$ C25 fusion (aa 1,049–1,278), the elution fractions were combined with 20 μl of amylose resin and incubated for 1 h at 4°C. The resin was washed extensively with detergent/salt buffer before analysis by SDS-PAGE and Western blotting.

Immunofluorescence microscopy

Transfected cells were fixed either with 4% formaldehyde in PBS for 30 min and permeabilized for 5 min with 0.05% Triton X-100 in PBS or with methanol (−20°C) for 5 min. Nonspecific binding of antibodies was blocked by 10% FBS/PBS for 30 min, after which cells were incubated with primary antibody in 5% FBS/PBS for 30 min at 37°C. Bound primary antibodies were visualized with Alexa Fluor secondary antibody conjugates (Invitrogen). Cells were mounted in Mowiol (Calbiochem) containing 50 mg/ml 1,4-diazocyclo-[2,2,2]octane (Sigma-Aldrich) or in Vectashield mounting medium (Vector Laboratories). The specimens were analyzed with confocal laser scanning microscopes (TCS SP1 or TCS SP2) equipped with HCX PL APO and HCX PL APO lbd.bl 40×/NA 1.32 objective lenses (all Leica). The acquisition software used was Leica LCS.

FLIM

FLIM experiments were performed at 37°C in a 5% CO_2 culture hood on an inverted microscope (DM-IRE2; Leica) fitted with a TCS SP2 scanhead and HCX PL APO lbd.bl 40×/NA 1.32 objective lenses and equipped with Lambert Instruments frequency domain lifetime attachment, controlled by EZflim software (Lambert Instruments). Cells were cultured in Delta T dishes (Bioptechs) in CBS medium (140 mM NaCl, 5 mM KCl, 2 mM $MgCl_2$, 1 mM $CaCl_2$, 23 mM $NaHCO_3$, 10 mM [D-]glucose, and 10 mM Hepes, pH 7.3, under 5% CO_2 condition). GFP was excited with ~4 mW of 488-nm light from a LED modulated at 40 MHz, and emission was collected at 490−550 nm using an intensified charge-coupled device camera (CoolSNAP HQ; Roper Scientific). To calculate the GFP lifetime, the intensities from 40 phase-shifted images (modulation depth ~70%) were fitted with a sinus function, and lifetimes were derived from the phase shift between excitation and emission. For internal control, cells were cocultured with Mel JuSo cells expressing H2B–GFP only. Lifetimes were referenced to a 1-μM solution of rhodamine-G6 in saline that was set at a 4.11-ns lifetime. The donor FRET efficiency E_D was calculated as $E_D = 1 -$ (measured lifetime/GFP lifetime in control cells) (Zwart et al., 2005).

We are grateful to Seija Puomilahti and Pirjo Ranta for skilled technical assistance. Angela Wandinger-Ness, Roger Y. Tsien, Casper Hoogenraad, and Gunther Stier are acknowledged for providing antibodies and cDNA constructs; Ira Mellman, Marije Marsman, and Peter Peters for support and critical reading of the manuscript; and Kees Jalink for help with FLIM.

Marie Johansson was supported by the Helsinki Graduate School of Biotechnology and Molecular Biology, a European Molecular Biology Organization short-term fellowship, The Finnish Cultural Foundation, and the Alfred Kordelin Foundation. Nuno Rocha was supported by a Portuguese Foundation for Science and Technology FCT/ FSE PhD scholarship within the Third Framework Program and a grant from the Dutch Cancer Society KWF. This study was further supported by the Academy of Finland (grants 206298 and 113010), the Sigrid Juselius Foundation, and the Finnish Foundation for Cardiovascular Research (to V.M. Olkkonen).

Submitted: 15 June 2006
Accepted: 9 January 2007

References

Ahmad, F.J., C.J. Echeverri, R.B. Vallee, and P.W. Baas. 1998. Cytoplasmic dynein and dynactin are required for the transport of microtubules into the axon. *J. Cell Biol.* 140:391–401.

Bastiaens, P.I., and A. Squire. 1999. Fluorescence lifetime imaging microscopy: spatial resolution of biochemical processes in the cell. *Trends Cell Biol.* 9:48–52.

Berger, B., D.B. Wilson, E. Wolf, T. Tonchev, M. Milla, and P.S. Kim. 1995. Predicting coiled coils by use of pairwise residue correlations. *Proc. Natl. Acad. Sci. USA*. 92:8259–8263.

Bergink, S., F.A. Salomons, D. Hoogstraten, T.A. Groothuis, H. de Waard, J. Wu, L. Yuan, E. Citterio, A.B. Houtsmuller, J. Neefjes, et al. 2006. DNA damage triggers nucleotide excision repair-dependent monoubiquitylation of histone H2A. *Genes Dev.* 20:1343–1352.

Burkhardt, J.K., C.J. Echeverri, T. Nilsson, and R.B. Vallee. 1997. Overexpression of the dynamitin (p50) subunit of the dynactin complex disrupts dynein-dependent maintenance of membrane organelle distribution. *J. Cell Biol.* 139:469–484.

Cantalupo, G., P. Alifano, V. Roberti, C.B. Bruni, and C. Bucci. 2001. Rab-interacting lysosomal protein (RILP): the Rab7 effector required for transport to lysosomes. *EMBO J.* 20:683–693.

Colucci, A.M., M.C. Campana, M. Bellopede, and C. Bucci. 2005. The Rab-interacting lysosomal protein, a Rab7 and Rab34 effector, is capable of self-interaction. *Biochem. Biophys. Res. Commun.* 334:128–133.

Culver-Hanlon, T.L., S.A. Lex, A.D. Stephens, N.J. Quintyne, and S.J. King. 2006. A microtubule-binding domain in dynactin increases dynein processivity by skating along microtubules. *Nat. Cell Biol.* 8:264–270.

Deacon, S.W., A.S. Serpinskaya, P.S. Vaughan, M. Lopez Fanarraga, I. Vernos, K.T. Vaughan, and V.I. Gelfand. 2003. Dynactin is required for bidirectional organelle transport. *J. Cell Biol.* 160:297–301.

De Matteis, M.A., and J.S. Morrow. 2000. Spectrin tethers and mesh in the biosynthetic pathway. *J. Cell Sci.* 113:2331–2343.

Echeverri, C.J., B.M. Paschal, K.T. Vaughan, and R.B. Vallee. 1996. Molecular characterization of the 50-kD subunit of dynactin reveals function for the complex in chromosome alignment and spindle organization during mitosis. *J. Cell Biol.* 132:617–633.

Eckley, D.M., S.R. Gill, K.A. Melkonian, J.B. Bingham, H.V. Goodson, J.E. Heuser, and T.A. Schroer. 1999. Analysis of dynactin subcomplexes reveals a novel actin-related protein associated with the Arp1 minifilament pointed end. *J. Cell Biol.* 147:307–320.

Förster, T. 1948. Zwischenmolekulare energiewandering und fluoreszenz. *Annalen Physik*. 6:55–75.

Gross, S.P. 2003. Dynactin: coordinating motors with opposite inclinations. *Curr. Biol.* 13:R320–R322.

Harrison, R.E., J.H. Brumell, A. Khandani, C. Bucci, C.C. Scott, X. Jiang, B.B. Finlay, and S. Grinstein. 2004. *Salmonella* impairs RILP recruitment to Rab7 during maturation of invasion vacuoles. *Mol. Biol. Cell.* 15:3146–3154.

Hirokawa, N. 1998. Kinesin and dynein superfamily proteins and the mechanism of organelle transport. *Science*. 279:519–526.

Holleran, E.A., L.A. Ligon, M. Tokito, M.C. Stankewich, J.S. Morrow, and E.L. Holzbaur. 2001. beta III spectrin binds to the Arp1 subunit of dynactin. *J. Biol. Chem.* 276:36598–36605.

Hoogenraad, C.C., A. Akhmanova, S.A. Howell, B.R. Dortland, C.I. De Zeeuw, R. Willemsen, P. Visser, F. Grosveld, and N. Galjart. 2001. Mammalian Golgi-associated Bicaudal-D2 functions in the dynein-dynactin pathway by interacting with these complexes. *EMBO J.* 20:4041–4054.

Hoogenraad, C.C., P. Wulf, N. Schiefermeier, T. Stepanova, N. Galjart, J.V. Small, F. Grosveld, C.I. de Zeeuw, and A. Akhmanova. 2003. Bicaudal D induces selective dynein-mediated microtubule minus end-directed transport. *EMBO J.* 22:6004–6015.

Johansson, M., V. Bocher, M. Lehto, G. Chinetti, E. Kuismanen, C. Ehnholm, B. Staels, and V.M. Olkkonen. 2003. The two variants of oxysterol binding protein-related protein-1 display different tissue expression patterns, have different intracellular localization, and are functionally distinct. *Mol. Biol. Cell*. 14:903–915.

Johansson, M., M. Lehto, K. Tanhuanpaa, T.L. Cover, and V.M. Olkkonen. 2005. The oxysterol-binding protein homologue ORP1L interacts with Rab7 and alters functional properties of late endocytic compartments. *Mol. Biol. Cell*. 16:5480–5492.

Jordens, I., M. Fernandez-Borja, M. Marsman, S. Dusseljee, L. Janssen, J. Calafat, H. Janssen, R. Wubbolts, and J. Neefjes. 2001. The Rab7 effector protein RILP controls lysosomal transport by inducing the recruitment of dynein-dynactin motors. *Curr. Biol.* 11:1680–1685.

Jordens, I., M. Marsman, C. Kuijl, and J. Neefjes. 2005. Rab proteins, connecting transport and vesicle fusion. *Traffic*. 6:1070–1077.

Jordens, I., W. Westbroek, M. Marsman, N. Rocha, M. Mommaas, M. Huizing, J. Lambert, J. Naeyaert, and J. Neefjes. 2006. Rab7 and Rab27a control two motor protein activities involved in melanosomal transport. *Pigment Cell Res.* 19:412–423.

Karki, S., and E.L. Holzbaur. 1999. Cytoplasmic dynein and dynactin in cell division and intracellular transport. *Curr. Opin. Cell Biol.* 11:45–53.

King, S.J., and T.A. Schroer. 2000. Dynactin increases the processivity of the cytoplasmic dynein motor. *Nat. Cell Biol.* 2:20–24.

Kumar, S., Y. Zhou, and M. Plamann. 2001. Dynactin-membrane interaction is regulated by the C-terminal domains of p150(Glued). *EMBO Rep.* 2:939–944.

Lehto, M., and V.M. Olkkonen. 2003. The OSBP-related proteins: a novel protein family involved in vesicle transport, cellular lipid metabolism, and cell signalling. *Biochim. Biophys. Acta*. 1631:1–11.

Lupas, A., M. Van Dyke, and J. Stock. 1991. Predicting coiled coils from protein sequences. *Science*. 252:1162–1164.

Marsman, M., I. Jordens, C. Kuijl, L. Janssen, and J. Neefjes. 2004. Dynein-mediated vesicle transport controls intracellular *Salmonella* replication. *Mol. Biol. Cell*. 15:2954–2964.

Marsman, M., I. Jordens, N. Rocha, C. Kuijl, L. Janssen, and J. Neefjes. 2006. A splice variant of RILP induces lysosomal clustering independent of dynein recruitment. *Biochem. Biophys. Res. Commun.* 344:747–756.

Matanis, T., A. Akhmanova, P. Wulf, E. Del Nery, T. Weide, T. Stepanova, N. Galjart, F. Grosveld, B. Goud, C.I. De Zeeuw, et al. 2002. Bicaudal-D regulates COPI-independent Golgi-ER transport by recruiting the dynein-dynactin motor complex. *Nat. Cell Biol.* 4:986–992.

Mizuno, K., A. Kitamura, and T. Sasaki. 2003. Rabring7, a novel Rab7 target protein with a RING finger motif. *Mol. Biol. Cell*. 14:3741–3752.

Muresan, V., M.C. Stankewich, W. Steffen, J.S. Morrow, E.L. Holzbaur, and B.J. Schnapp. 2001. Dynactin-dependent, dynein-driven vesicle transport in the absence of membrane proteins: a role for spectrin and acidic phospholipids. *Mol. Cell*. 7:173–183.

Navarro, C., H. Puthalakath, J.M. Adams, A. Strasser, and R. Lehmann. 2004. Egalitarian binds dynein light chain to establish oocyte polarity and maintain oocyte fate. *Nat. Cell Biol.* 6:427–435.

Rameh, L.E., A. Arvidsson, K.L. Carraway III, A.D. Couvillon, G. Rathbun, A. Crompton, B. VanRenterghem, M.P. Czech, K.S. Ravichandran, S.J. Burakoff, et al. 1997. A comparative analysis of the phosphoinositide binding specificity of pleckstrin homology domains. *J. Biol. Chem.* 272:22059–22066.

Schroer, T.A. 2004. Dynactin. *Annu. Rev. Cell Dev. Biol.* 20:759–779.

Schroer, T.A., E.R. Steuer, and M.P. Sheetz. 1989. Cytoplasmic dynein is a minus end-directed motor for membranous organelles. *Cell*. 56:937–946.

Short, B., C. Preisinger, J. Schaletzky, R. Kopajtich, and F.A. Barr. 2002. The Rab6 GTPase regulates recruitment of the dynactin complex to Golgi membranes. *Curr. Biol.* 12:1792–1795.

Stankewich, M.C., W.T. Tse, L.L. Peters, Y. Ch'ng, K.M. John, P.R. Stabach, P. Devarajan, J.S. Morrow, and S.E. Lux. 1998. A widely expressed betaIII spectrin associated with Golgi and cytoplasmic vesicles. *Proc. Natl. Acad. Sci. USA*. 95:14158–14163.

Stinchcombe, J.C., E. Majorovits, G. Bossi, S. Fuller, and G.M. Griffiths. 2006. Centrosome polarization delivers secretory granules to the immunological synapse. *Nature*. 443:462–465.

Studier, F.W. 2005. Protein production by auto-induction in high density shaking cultures. *Protein Expr. Purif.* 41:207–234.

Vale, R.D. 2003. The molecular motor toolbox for intracellular transport. *Cell*. 112:467–480.

Wallrabe, H., and A. Periasamy. 2005. Imaging protein molecules using FRET and FLIM microscopy. *Curr. Opin. Biotechnol.* 16:19–27.

Waterman-Storer, C.M., S. Karki, and E.L. Holzbaur. 1995. The p150Glued component of the dynactin complex binds to both microtubules and the actin-related protein centractin (Arp-1). *Proc. Natl. Acad. Sci. USA*. 92:1634–1638.

Wu, M., T. Wang, E. Loh, W. Hong, and H. Song. 2005. Structural basis for recruitment of RILP by small GTPase Rab7. *EMBO J.* 24:1491–1501.

Wubbolts, R., M. Fernandez-Borja, I. Jordens, E. Reits, S. Dusseljee, C. Echeverri, R.B. Vallee, and J. Neefjes. 1999. Opposing motor activities of dynein and kinesin determine retention and transport of MHC class II-containing compartments. *J. Cell Sci.* 112:785–795.

Zwart, W., A. Griekspoor, C. Kuijl, M. Marsman, J. van Rheenen, H. Janssen, J. Calafat, M. van Ham, L. Janssen, M. van Lith, et al. 2005. Spatial separation of HLA-DM/HLA-DR interactions within MIIC and phagosome-induced immune escape. *Immunity*. 22:221–233.

Chapter 3

The molecular mechanism of cholesterol control of late endosomal transport by dynein motors
Submitted

The Molecular Mechanism of Cholesterol Control of Late Endosomal Transport by Dynein Motors

Nuno Rocha, Coenraad Kuijl[+], Rik van der Kant[+], Lennert Janssen, Wilbert Zwart[*] and Jacques Neefjes[*].

Division of Tumor Biology, The Netherlands Cancer Institute, Amsterdam, The Netherlands

[+]Equal contribution

Late endosomes and lysosomes exhibit bidirectional motility along microtubules by the alternating actions of kinesin and dynein motor proteins. The Rab7 effector RILP recruits the dynein motor to late endosomes for microtubular minus-end transport but how this complex is disassembled and what regulates the process to allow for the observed changes in direction is unclear. The Rab7-RILP complex interacts with the oxysterol-binding protein ORP1L. Here we show that the late endosomal cholesterol content determines the conformational state of ORP1L, acting as a switch to control dynein-dynactin motor complex binding to its Rab7-RILP receptor, thereby regulating the direction of transport. The cytosolic state of the cholesterol-sensing OSBP-related domain (ORD) of ORP1L exposes a FFAT motif to recruit the integral membrane protein VAP. VAP then binds to and removes the dynein-dynactin motor subunit p150^{Glued} from Rab7-RILP. The FFAT motif is not exposed when the ORD is membrane-associated allowing dynein motor binding and transport. This regulatory mechanism is disrupted in Niemann-Pick type C disease causing the characteristic clustering of cholesterol-laden late endosomes. Thus, cholesterol acts as a molecular switch, controlling the transport of late endosomes and lysosome-related organelles.

INTRODUCTION

Late endosomes, lysosomes and lysosome-related organelles, such as the MHC class II-containing compartment (MIIC), cytolytic granules and early melanosomes move along microtubules in a so-called bidirectional manner and in a stop-and-go fashion (Jordens et al., 2006; Wubbolts et al., 1996). This bidirectional nature of movement results from the alternate action of at least two microtubule-based motor proteins with opposite polarities. The dynein-dynactin motor is essential for minus-end (inward-directed) transport and at least two motor proteins have been implicated in plus-end transport; kinesin-1 (conventional kinesin or KIF5) and kinesin-2 (heterotrimeric kinesin or KIF3) (Brown et al., 2005; Hollenbeck and Swanson, 1990; Wubbolts et al., 1999). Although this explains bidirectional motility of late endosomes and lysosomes, it does not

[*] Corresponding authors. Division of Tumor Biology, The Netherlands Cancer Institute, Plesmanlaan 121, Amsterdam 1066 CX, The Netherlands. Tel.: + 31 20 5122012; Fax: + 31 20 5122029; E-mail: J.NEEFJES@NKI.NL; W.ZWART@NKI.NL

explain control of motor activities.

Rab GTPases specify organelle identity (Pfeffer, 2001; Zerial and McBride, 2001), making them ideal central regulators of selective motor activity. Increasing evidence implicates Rab GTPases and their effectors in the selective recruitment of motor proteins to particular vesicles (Echard et al., 1998; Hoepfner et al., 2005; Jordens et al., 2001; Jordens et al., 2005). The small GTPase Rab7 associates with late endosomal and lysosomal structures as well as to most lysosomal-related organelles (Zerial and McBride, 2001). Rab7 has multiple reported functions. The yeast Rab7 ortholog, Ypt7p, can recruit the class C VPS/HOPS complex that mediates homotypic fusion (Peterson and Emr, 2001; Seals et al., 2000; Wurmser et al., 2000). This complex probably contains a Rab7 guanine nucleotide exchange factor, which is also an effector of the early endosomal GTPase Rab5 acting in the process of Rab5-to-Rab7 conversion and thus endosomal maturation (Rink et al., 2005). Rab7 also supports dynein motor recruitment to late endosomes by sequentially recruiting its effector RILP and then the $p150^{Glued}$ subunit of the dynein-dynactin motor protein complex (Johansson et al., 2007; Jordens et al., 2001). Active transport of late endosomes by the dynein-dynactin motor towards the minus-end of microtubules involves an additional Rab7 effector—oxysterol-binding protein (OSBP)-related protein 1L (ORP1L) (Johansson et al., 2007). ORP1L is a member of a family of OSBP-related proteins (ORPs) and interacts with GTP-bound Rab7 via its N-terminal ankyrin repeats region (Johansson et al., 2005). ORP1L also contains a pleckstrin homology (PH) domain which binds phosphoinositides (Johansson et al., 2005), a protein-interacting FFAT (Two Phenylalanines (FF) in an Acidic Tract) motif (Loewen and Levine, 2005; Loewen et al., 2003) and a C-terminal OSBP-related domain (ORD) able to bind 25-hydroxycholesterol and possibly other cholesterol derivatives within membranes (Im et al., 2005; Suchanek et al., 2007). The FFAT motif can interact with cytosolic proteins that are embedded in the ER by a C-terminal transmembrane region, called vesicle-associated membrane protein (VAMP)-associated protein (VAP)-A and VAP-B (Loewen and Levine, 2005). VAP-A and -B can form homo- and hetero-dimers (Hamamoto et al., 2005; Nishimura et al., 1999) and interact with OSBP, an ER protein related to ORP1L, which drives ER export of proteins and lipids (Wyles et al., 2002).

The RILP-controlled recruitment of dynein motors is not only operational in late endosomes and lysosomes but in all Rab7-containing compartments tested, including specialized lysosomes like early melanosomes (Jordens et al., 2006), MHC class II-containing compartments (MIIC) (Jordens et al., 2001), cytolytic granules (Stinchcombe et al., 2006) and phagosomes (Harrison et al., 2003; Marsman et al., 2004). This mechanism is responsible for the characteristic steady-state perinuclear distribution pattern of late endosomal compartments (Burkhardt et al., 1997; Harada et al., 1998; King et al., 2003; Vaughan et al., 2001).

How direction of transport is controlled remains unclear, although three models have been proposed. Motors of opposite polarity are reciprocally coordinated thereby preventing their simultaneous activity on a given vesicle. In this model, dynein and kinesin motors may use the dynactin stalk $p150^{Glued}$ as a common adaptor to the Rab7-RILP receptor. The nature of the $p150^{Glued}$-associated motor then dictates the directionality of transport (Brown et al., 2005; Deacon et al., 2003). Alternatively, motors of opposite polarities may coexist on a given vesicle and directionality is decided in a "tug-of-war" on the cargoes (Gross et al., 2002; Muller et al., 2008). Finally, bidirectional movement can occur as a result of dynein motors being able to move in both directions on microtubules, as suggested from *in vitro* studies (Gennerich

et al., 2007; Ma and Chisholm, 2002; Ross et al., 2006), In all cases, the p150^{Glued} interaction with the Rab7-RILP complex seems critical to determine motility and thus retention of late endosomal compartments in close proximity to the nucleus.

Cells overexpressing Rab7 and/or RILP show dense clustering of late endosomal vesicles around the minus-end of microtubules in the perinuclear area (Bucci et al., 2000; Jordens et al., 2001). This is the result of continuous dynein motor activity on late endosomal vesicles and possible exclusion of kinesin motor activities (Lebrand et al., 2002). Conversely, overexpression of the dominant-negative RILP variant ΔN-RILP prevents p150^{Glued} recruitment causing dispersal of late endosomal vesicles throughout the cytosol (Jordens et al., 2001).

The Rab7-RILP interaction with the p150^{Glued} subunit may be controlled by factors altering the activity of Rab7, such as a GTPase activating protein (GAP) specific for Rab7 that would release RILP from Rab7 by stimulating GTP hydrolysis. Other factors might also be involved in the positioning and motility of late endosomes/lysosomes. Some have been hinted at in human diseases like the Niemann-Pick type C disease, which is phenotypically defined by cholesterol-laden late endosomes/lysosomes clustered around the microtubule-organizing centre at the minus-end of microtubules (Mukherjee and Maxfield, 2004). This phenotype is shared with a series of other lysosomal storage diseases including Tangier, Fabry and Gaucher disease (Maxfield and Tabas, 2005). Increasing intracellular cholesterol levels with the chemical compound U18666A mimics this phenotype (Koh and Cheung, 2006; Roff et al., 1991; Sobo et al., 2007) in a process involving Rab7 and Rab9 GTPases as well as RabGDI (Chen et al., 2008; Holtta-Vuori et al., 2000; Lebrand et al., 2002; Narita et al., 2005). Rab GTPases, cholesterol and motor protein activities may somehow be connected resulting in late endosomal/lysosomal clustering as observed in these lysosomal storage diseases.

Here, we identify cholesterol as a messenger sensed by ORP1L, a late endosomal Rab7-RILP receptor complex subunit. Cholesterol determines the conformation of ORP1L to expose a FFAT domain that recruits VAP. VAP then controls p150^{Glued}-dynein motor binding to RILP and microtubule minus-end transport of late endosomes. The characteristic clustering of late endosomes observed in Niemann-Pick type C and other lysosomal storage diseases are the result of this process.

RESULTS

Late endosomes exhibit variable timing of bidirectional stop-and-go motions

Late endosomes, like MIIC, move along microtubulules in a so-called bidirectional manner and in a stop-and-go fashion by the action of dynein and kinesin motor proteins (Wubbolts et al., 1996). We have visualized these motions in the human melanoma cell line MelJuSo expressing Green Fluorescent Protein (GFP) tagged MHC class II using time-lapse confocal microscopy (Figure 1A). The MIIC regularly stops before continuing or switching direction of movement. The motility was subsequently plotted in a rose diagram where the speed and direction relative to the previous movement are plotted (Figure 1B). About 40% of peripheral MIIC structures were immotile during the time of analysis. The motile MIIC structures moved at 0.4 ± 0.3 μm/s in all directions. A vesicle tends to move along a single microtubule in time, since directions are primarily forward or reverse (Figure 1B). The time a vesicle stops before moving again is plotted in Figure 1C. There appears to be no correlation between the direction before standstill and the direction after standstill (data not shown). This suggests that motor-driven vesicle transport occurs with variations in standstill, direction of movement and

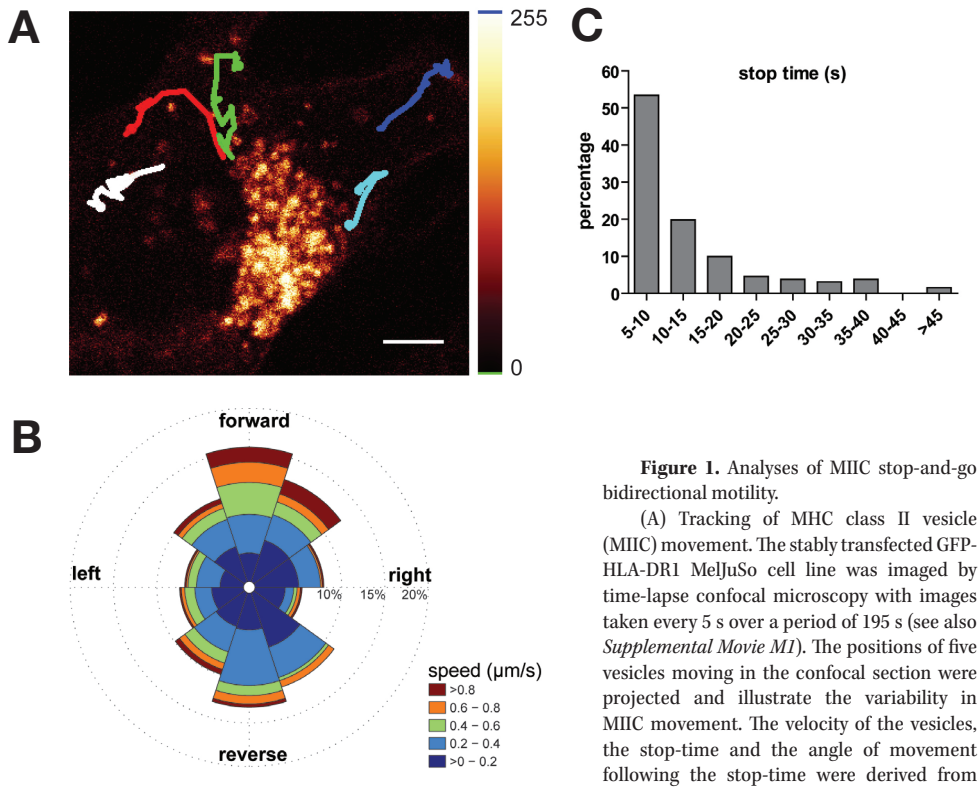

Figure 1. Analyses of MIIC stop-and-go bidirectional motility.

(A) Tracking of MHC class II vesicle (MIIC) movement. The stably transfected GFP-HLA-DR1 MelJuSo cell line was imaged by time-lapse confocal microscopy with images taken every 5 s over a period of 195 s (see also *Supplemental Movie M1*). The positions of five vesicles moving in the confocal section were projected and illustrate the variability in MIIC movement. The velocity of the vesicles, the stop-time and the angle of movement following the stop-time were derived from similar images.

(B) The velocity of vesicles was determined in the stable GFP-HLA-DR1 MelJuSo cell line. Vesicle velocity and direction relative to the previous direction from 36 tracks (820 data points) were quantified and plotted in a rose diagram. Each segment of 36 degrees (total 360 degrees) shows the direction of movement. Each segment is subdivided into 5 discrete compartments indicating the speed of vesicle movement in that direction.

(C) Vesicles stop before continuing or switching direction. The stop time (standstill) was determined from 36 tracks analyzed and binned over 5 s intervals. Total stop times were set at 100%.

progression after the standstill.

Rab7 is not a substrate for the TBC1D15 when in complex with RILP

Activated GTP-loaded Rab7 recruits its effector RILP that acts as a selective dynein motor receptor on late endosomal membranes by binding the p150^{Glued} subunit of the dynactin complex (Johansson et al., 2007). Inactivation of Rab7 by a Rab7-specific GTPase-activating protein could control dynein motor recruitment to late endosomes. We selected nine GAPs to generate shRNA constructs (Figure S1) which were introduced in MelJuSo cells expressing GFP-Rab7. Since GFP-Rab7 cycles between a membrane-associated GTP-bound active and a cytosolic inactive GDP-bound state, the Rab7 cycle can be monitored by photobleaching experiments (Jordens et al., 2001) (Figure 2A). Only downregulation of the RabGAP TBC1D15 by shRNA quenched the Rab7 cycle in living cells (Figures 2B and 2C). The TBC (Tre-2/Bub2/Cdc16) domain, a conserved catalytic domain that specifies most RabGAPs (Albert et al., 1999; Bernards, 2003), of TBC1D15 was subsequently expressed, isolated and tested in an *in vitro* GTPase assay with [γ–^{32}P]GTP-

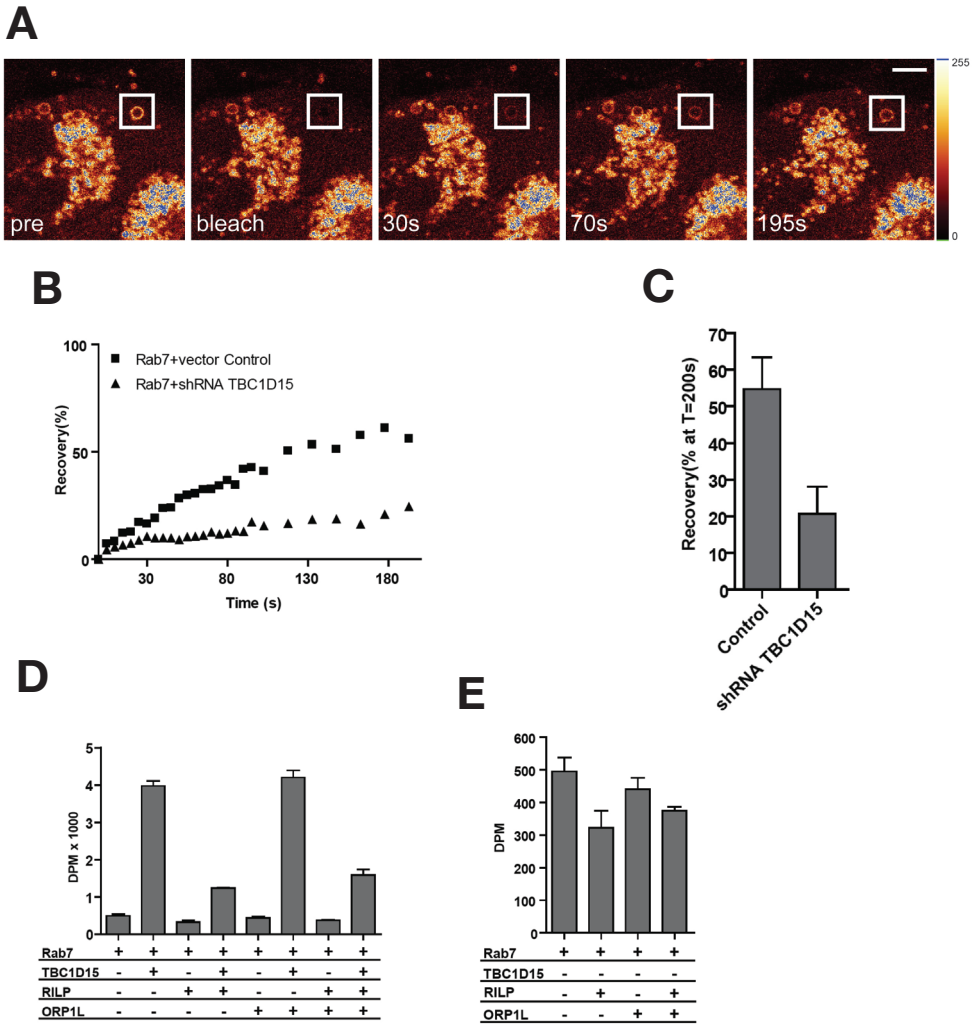

Figure 2. RILP prevents Rab7 GTPase activation by Rab7GAP. (A) The GFP-Rab7 cycle in living MelJuSo cells as determined by FRAP. GFP-Rab7-positive vesicles in living MelJuSo cells were photobleached and the recovery of fluorescence was followed in time. Single frames corresponding to a typical sequence with a GFP-Rab7-positive vesicle (inside white-box) prior to bleaching (pre), immediately after bleaching (bleach), and post-bleaching after different time intervals (30s, 70s, and 195s) are shown. (B) Quantification of fluorescence recovery of GFP-Rab7 on vesicles in living MelJuSo cells expressing a control shRNA or a shRNA for TBC1D15, as indicated. Nine potential RabGAPs (Figure S1) were tested with only one affecting the GFP-Rab7 cycle. shRNA-mediated silencing of TBC1D15 quenched the GFP-Rab7 cycle and the bleached membrane-bound Rab7 was less efficiently exchanged for fluorescent GFP-Rab7. (C) The recovery of fluorescence of GFP-Rab7 on vesicles in living MelJuSo cells expressing control or shRNA for the TBC1D15 was determined after 200 s. The cycle time of GFP-Rab7 was not significantly affected by intracellular localization but was strongly decreased by silencing Rab7GAP. The means and SD from five independent experiments are plotted. (D) RILP inhibits stimulation of the Rab7 GTPase activity by TBC1D15. [γ–^{32}P]GTP hydrolysis by purified GST-Rab7 was monitored in an *in vitro* reaction in the presence or absence of purified RILP, ORP1L and Rab7GAP, as indicated. The means and SD of duplicates in two independent experiments are shown. (E) Zoom-in on the effects of RILP and ORP1L on the intrinsic GTPase activity of Rab7 illustrating that RILP slows the intrinsic Rab7 GTPase activity. The means and SD of duplicates in two independent experiments are shown.

loaded Rab7 (Figure 2D). Consistent with recent data, we found that the TBC domain of TBC1D15 stimulated the low intrinsic GTPase activity of Rab7 (Zhang et al., 2005). To test whether this was also the case when Rab7 was complexed to RILP and ORP1L (Johansson et al., 2005; Johansson et al., 2007) we isolated RILP and ORP1L. Complexes of [γ–^{32}P]GTP-loaded Rab7 with RILP and/or ORP1L were assembled prior to adding the TBC domain of TBC1D15 to the reactions (Figure 2D). RILP but not ORP1L decreased the GTPase activity of Rab7 and TBC1D15. Simultaneous binding of RILP and ORP1L to [γ–^{32}P]GTP-loaded Rab7 did not further decrease GTPase activation of Rab7. This suggests that RILP limits access of TBC1D15 to Rab7 further slowing down the already slow Rab7 GTPase cycle (Figures 2B and 2S). The rapid mechanism of directional switching observed in late endosomal transport (Figures 1A and 1C) is therefore unlikely controlled by TBC1D15 since RILP delays the already slow intrinsic GTPase activity of Rab7 *in vitro* and in living cells (Jordens et al., 2001).

ORP1L controls p150^{Glued} binding to Rab7-RILP and late endosomal positioning.

ORP1L binds to Rab7-RILP via its N-terminal ankyrin repeats and is required for regulation of late endosomal transport by the dynein motor (Johansson et al., 2005; Johansson et al., 2007). To test which ORP1L domains are involved in late endosomal transport control, we constructed a series of C-terminal truncations of ORP1L fused to the monomeric Red Fluorescent Protein mRFP (Shaner et al., 2004) (Figure 3A) and co-expressed these with GFP-RILP in MelJuSo cells. Cells were fixed and stained for p150^{Glued}. Removal of the C-terminal ORD (ΔORD) prevented p150^{Glued} recruitment by RILP resulting in relocation of RILP-containing compartments to the cell periphery, further C-terminal truncations allowed p150^{Glued} binding to RILP and clustering at the minus-end of microtubules (Figure 3B). To test whether the ORD is directly involved in excluding p150^{Glued} binding to RILP, this domain was exchanged for two ORP1L PH domains in tandem (ΔORDPHDPHD). Tandem PH domains increase the avidity of binding to phosphoinositides considerably (Lemmon and Ferguson, 2000) and were used to mimic the ORD in a membrane-associated state. The ΔORDPHDPHD chimera allowed p150^{Glued} recruitment by RILP resulting in the clustering of RILP-positive compartments at the minus-end of microtubules (Figure 3B).

Thus, ORP1L allowed p150^{Glued} binding to RILP, unlike the mutant only lacking the cholesterol-interacting domain ORD. Further C-terminal truncations restored p150^{Glued} recruitment by RILP. This would fit a model where the ORD exists in two conformational states: a membrane-associated 'down' state when the ORD binds cholesterol, and a cytosolic-exposed 'up' state when not interacting with such sterols on late endosomal membranes. In the 'up' state, exposure of a region between the PH domain and the ORD would then affect binding of p150^{Glued} to Rab7-RILP. This region is exposed in ΔORD and prevents p150^{Glued}-RILP interactions whereas further C-terminal truncations eliminates this and restore the p150^{Glued}-RILP interaction (Figure 3B). Substitution of the ORD by tandem PH domains would impose a 'down' state conformation thereby preventing the exposure of the region between the PH domain and the ORD. Binding of p150^{Glued} to Rab7-RILP is then restored and RILP-containing compartments clustered as the result of prolonged p150^{Glued}-dynein motor binding to Rab7-RILP complexes (Figure 3B).

The ORP1L region between the PH domain and ORD (aa 408-514) then controls access of p150^{Glued} to RILP. This region contains a predicted coiled-coil region (aa 430-463) (Johansson et al., 2007) followed by a FFAT motif (aa 472-482; SEDEFYDALSD) (Loewen et al., 2003) (Figure 3A). This FFAT motif is

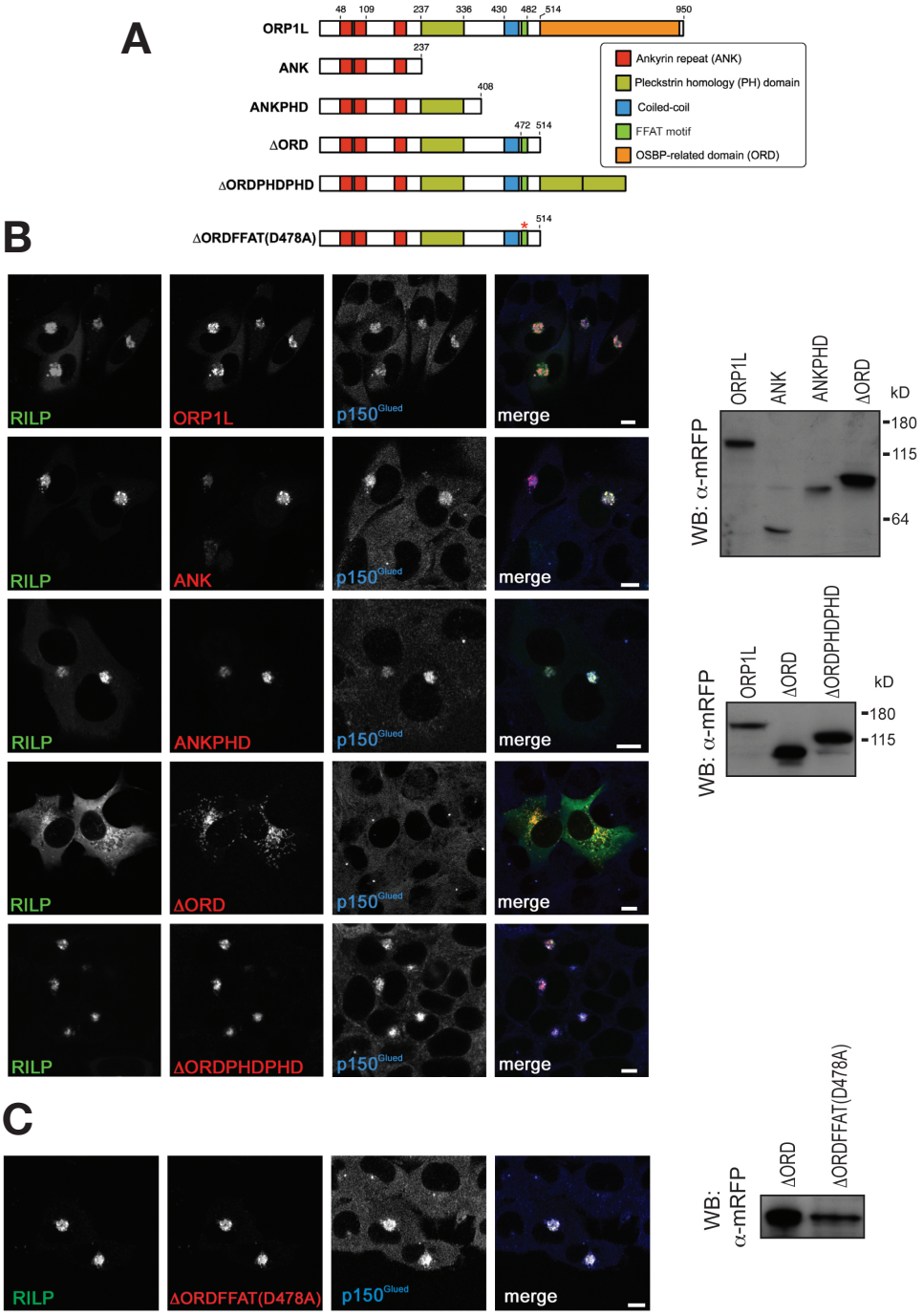

Figure 3. ORP1L controls recruitment of p150^{Glued} to the Rab7-RILP receptor. (A) ORP1L domain structure and constructs. Five domains can be distinguished in ORP1L. A series of C-terminal truncation mutants were generated. Numbers indicate amino acid residue positions. All constructs were N-terminally tagged with mRFP. The ΔORDPHDPHD

chimera had the ORD exchanged for a tandem PH domain derived from ORP1L. The ΔORDFFAT(D478A) mutant was obtained by inserting a point mutation (D478A) in the FFAT motif of ΔORD (marked by an asterisk). (B) Effect of ORP1L deletion or chimeric constructs on RILP-mediated p150^{Glued} recruitment. Left panel: MelJuSo cells were transfected with GFP-RILP and mRFP-ORP1L constructs prior to immunofluorescence confocal microscopy with anti-p150^{Glued} antibodies. n>200 for each condition. Scale bars, 10μm. Right panels: MelJuSo cells were transfected with the indicated mRFP-ORP1L, -ANK, -ANKPHD, -ΔORD, and -ΔORDPHDPHD constructs and whole-cell lysates were analyzed by SDS-PAGE and Western blotting with anti-mRFP antibodies (WB: α-mRFP). (C) Effect of mutating the FFAT motif in ΔORD on RILP-mediated p150^{Glued} recruitment. Left panel: MelJuSo cells transfected with GFP-RILP and mRFP-ΔORD carrying an inactivating point mutation in its FFAT motif, ΔORDFFAT(D478A), show clustering of RILP-positive compartments by immunofluorescence confocal microscopy with anti-p150^{Glued} antibodies. n>200. Scale bar, 10μm. Right panel: MelJuSo cells were transfected with the indicated mRFP-ΔORD or mRFP-ΔORDFFAT(D478A) constructs and whole-cell lysates were subjected to immunoblot analysis using anti-mRFP antibodies (WB: α-mRFP).

present in other ORP1L family members where it mediates interactions with Vesicle associated membrane (VAMP)-Associated Proteins (VAP) (Lehto et al., 2005; Wyles et al., 2002). To assess whether the FFAT motif is involved in excluding p150^{Glued} from RILP, an inactivating point mutation (D478A) in the FFAT motif (Loewen et al., 2003) was introduced in mRFP-ΔORD. This mutant was co-expressed with GFP-RILP in cells before fixation and staining for p150^{Glued} (Figure 3C). Whereas ΔORD excluded RILP-mediated recruitment of p150^{Glued} resulting in vesicle scattering, the single point mutation in the FFAT motif, ΔORDFFAT(D478A), rescued p150^{Glued} binding to RILP and clustering of RILP-positive compartments.

Cholesterol affects ORP1L conformation and positioning of late endosomes

The FFAT motif preceding the cholesterol-sensing domain ORD is apparently involved in excluding p150^{Glued}-dynein motor binding to the Rab7-RILP receptor. This motif could be exposed when the ORD adopts a cytosolic position as reflected by ΔORD and shielded when the ORD is membrane-bound as reflected by ΔORDPHDPHD. Recent studies suggest that OSBP/ORPs are involved in non-vesicular transport of sterols between specific donor and acceptor membranes through a functional cycle that involves ORD-dependent extraction of sterols from membranes and reciprocal conformational changes (Im et al., 2005; Lehto et al., 2008; Yang, 2006). The ORD is a cholesterol-interacting and extracting domain and it may adopt a membrane-bound conformation when extracting cholesterol from donor membranes, and a cytosol-exposed conformation following cholesterol extraction. If so, cholesterol would determine the orientation of the ORD relative to membranes and the exposure of the preceding FFAT motif. Late endosomal cholesterol content would then determine ORP1L conformation and vesicle positioning by regulating binding of p150^{Glued}-dynein motors to Rab7-RILP receptors

The intracellular cholesterol content of MelJuSo cells was manipulated to assess the role of cholesterol in ORP1L-mediated regulation of Rab7-RILP-p150^{Glued}-dynein motor transport of late endosomes. Cells were cultured in normal serum (FCS)-containing medium (F-medium), in delipidated serum-containing medium supplemented with a statin (Lovastatin) which inhibits 3-hydroxy-3-methylglutaryl coenzyme A (HMG-CoA) reductase and thus blocks endogenous cholesterol synthesis (S-medium), or in FCS-containing medium supplemented with U18666A (U-medium), a drug causing cholesterol accumulation in late endosomal compartments (Sobo et al., 2007; Sugii et al., 2006). Cells were fixed and cholesterol detected by filipin staining (Bornig and Geyer, 1974) (Figure 4A).

Filipin labelled the plasma membrane and intracellular vesicles. Labelling was

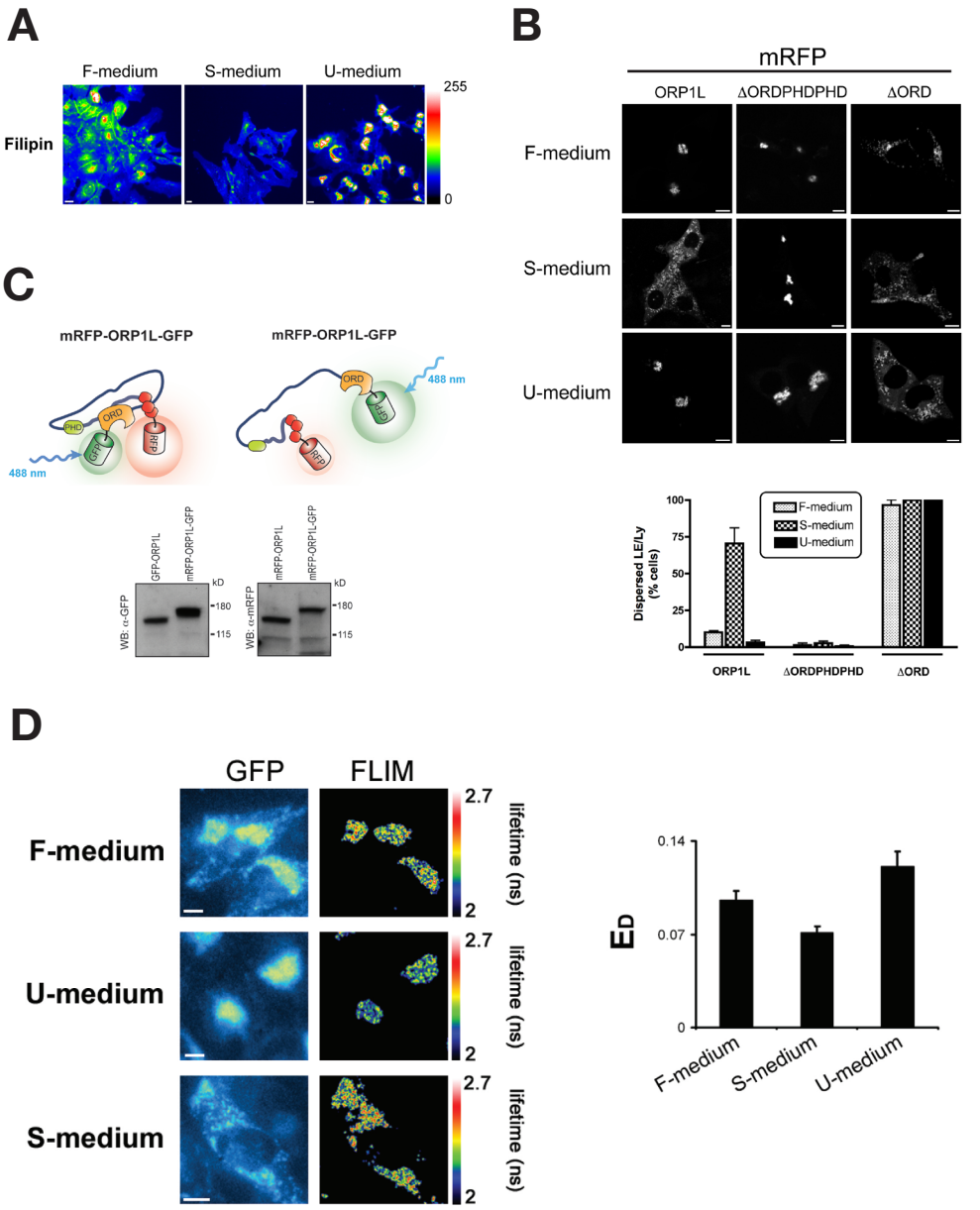

Figure 4. Different ORP1L conformations control cholesterol-dependent late endosomal minus-end transport and positioning. (A) Modulation of intracellular cholesterol. MelJuSo cells were cultured in normal (F-medium), cholesterol-depleted medium supplemented with Lovastatin to block synthesis of endogenous cholesterol (S-medium) or in normal medium supplemented with U18666A (U-medium) which elicits cholesterol accumulation in late endosomal compartments. Cells were fixed and stained with filipin to detect cholesterol. Images were obtained using identical settings on the microscope. A colour LUT is applied to illustrate the differences in filipin staining and cholesterol in cells. n>100 for each condition. Scale bars, 10µm. (B) ORP1L controls cholesterol-dependent vesicle positioning. MelJuSo cells expressing mRFP-ORP1L, -ΔORDPHDPHD or -ΔORD were cultured in normal (F-medium), medium decreasing (S-medium) or enhancing (U-medium) intracellular content of cholesterol. ORP1L-bearing vesicles disperse in S-medium treated cells unless the cholesterol-insensitive ORP1L variant ΔORDPHDPHD is expressed. Scale bars, 10µm. Bar chart

shows the percentage of cells showing dispersed late endosomes/lysosomes (LE/Ly) under the different cholesterol-manipulating treatments, as indicated. The means and SD from 150 cells analyzed in three independent experiments for each condition are shown. (C) Concept of intramolecular FRET for mRFP-ORP1L-GFP. Top: The intramolecular ORP1L FRET probe was created by tagging of ORP1L with mRFP and GFP at the N- and C-terminus, respectively. The lifetime of GFP is determined by excitation with 488 nm light. The GFP lifetime decreases when energy is transferred from GFP to mRFP which is dependent on the distance and orientation between the two fluorophores. From this lifetime the donor FRET efficiency E_D is calculated. Bottom: Immunoblotting analyses of whole-cell lysates of MelJuSo cells stably expressing mRFP-ORP1L-GFP or transiently expressing GFP-ORP1L or mRFP-ORP1L, as indicated, using anti-GFP (WB: α-GFP) and anti-mRFP (WB: α-mRFP) antisera. (D) Cholesterol affects the conformation of ORP1L. MelJuSo cells expressing the intramolecular mRFP-ORP1L-GFP FRET probe were treated with control (F-medium), cholesterol-enhancing (U-medium) or -depleting (S-medium) conditions prior to imaging with a wide-field FLIM microscope. Left panel: GFP fluorescence as detected by wide-field microscopy and lifetime as detected by FLIM. The colour LUT depicts the different lifetimes detected. Scale bars, 10 μm. Right panel: Donor FRET efficiency (E_D) as calculated from images as shown in the Left panel. The mean and SD from three independent experiments (70 cells analyzed for each condition) are shown.

respectively decreased or markedly increased under cholesterol-depleting (S-medium) or -enhancing (U-medium) treatments. Cells transiently expressing mRFP-ORP1L, -ΔORD or - ΔORDPHDPHD were cultured in F-, S-, or U-medium (Figure 4B). Late endosomal structures labelled by ORP1L, unlike those labelled by ΔORDPHDPHD, scattered in the cytosol under cholesterol-depleting conditions (S-medium). Under cholesterol-enhancing conditions (imposed by U18666A in the U-medium), ORP1L-labelled vesicles, unlike ΔORD labelled vesicles, clustered in a perinuclear region (Figure 4B; quantification data in bar chart).

To determine whether late endosomal cholesterol content indeed affected the conformation of ORP1L, a mRFP-ORP1L-GFP fusion protein was expressed in MelJuSo cells to monitor intramolecular Fluorescence Resonance Energy Transfer (FRET). FRET is the radiationless energy transfer from a donor fluorophore to a suitable acceptor (Förster, 1948). This is affected by alterations in distance or orientation between GFP and mRFP (Calleja et al., 2003; Förster, 1948) and thus reveals conformational changes within ORP1L. FRET was determined by fluorescence lifetime imaging microscopy (FLIM) on living cells cultured at 37°C, where the fluorescence lifetime of the donor fluorophore, GFP, is measured. The lifetime of GFP is typically 2,7 ns (Pepperkok et al., 1999), but decreases in the case of FRET, when energy is transferred to the acceptor fluorophore, mRFP (Figure 4C). As internal control, the cells were co-cultured with MelJuSo cells expressing Histone2B-GFP only. FLIM was determined in cells stably expressing mRFP-ORP1L-GFP under control (F-medium), cholesterol-depleting (S-medium), or -enhancing (U-medium) conditions. The donor FRET efficiencies (E_D) (calculated from the GFP lifetimes) were affected by the different cholesterol-manipulating treatments (Figure 4D), suggesting that cholesterol content variations in late endosomal compartments elicit different ORP1L conformations.

These results demonstrate that the Rab7-RILP interacting protein ORP1L uses its ORD to sense variations in cholesterol content. Cholesterol concentrations affect ORD conformation and exposure of the FFAT motif that is critical for preventing the interaction of the dynein motor subunit $p150^{Glued}$ with its receptor Rab7-RILP, and thereby determine late endosomal vesicle positioning.

ORP1L and Niemann-Pick type C disease

Various lysosomal storage diseases characteristically accumulate cholesterol in late endosomal compartments clustered at the microtubular minus-end in a perinuclear area. Best characterized is Niemann-Pick type C (NPC) where usually the multispanning membrane late endosomal protein NPC protein 1 (NPC1) is mutated or deleted (Carstea et al.,

1997). NPC1 binds 25-hydroxycholesterol and other sterols (Infante et al., 2008a) but it is unclear whether it actually transports these over the late endosomal limiting membrane like another multispanning membrane protein ATP-binding cassette transporter A1 (ABCA1) (Chen et al., 2001). ABCA1 may expose the high cholesterol content in the lumen of late endosomes in Niemann-Pick C cells to the cytosolic leaflet of these compartments. ORP1L would then sense this cholesterol resulting in effects on Rab7-RILP-p150^{Glued}-dynein motor mediated transport and clustering of late endosomes.

siRNA-mediated downregulation of NPC1 in MelJuSo cells induced clustering of CD63-positive vesicles in the perinuclear area (Figure 5A) that accumulate cholesterol (Figure 5B), as characteristic for Niemann-Pick C disease. To test whether late endosomal cholesterol increase—as a result of NPC1 downregulation—was sensed by ORP1L, intramolecular FRET between the two extremities of mRFP-ORP1L-GFP was measured by FLIM in control or NPC1 siRNA-transfected MelJuSo cells (Figure 5C). The GFP-lifetime of mRFP-ORP1L-GFP decreased (donor FRET efficiency E_D increased) when NPC1 was downregulated by siRNA, suggesting that ORP1L adopts a different conformation in the absence of NPC1. The calculated donor FRET efficiencies (E_D) for mRFP-ORP1L-GFP in NPC1-downregulated cells are similar to those observed with U-medium treatment, which phenomimics NPC1 deficiency (Koh and Cheung, 2006; Sobo et al., 2007) (Figure 4D).

The increase in cholesterol caused by siRNA-mediated downregulation of NPC1 may be sensed by ORP1L and translated into Rab7-RILP-controlled dynein motor transport thus initiating late endosomal clustering. If so, the deletion mutant of ORP1L lacking the cholesterol-interacting domain (ΔORD) should prevent late endosomal clustering following downregulation of NPC1. To test this, MelJuSo cells were transfected with siRNA for NPC1 along with various mRFP-labelled ORP1L constructs, as indicated (Figure 5D). Cells were fixed and stained for NPC1 and the late endosomal marker CD63 (Infante et al., 2008b; Patel et al., 1999). NPC1 was efficiently downregulated since only nuclear background staining with the NPC1 antibody was observed. Whereas ORP1L and ΔORDPHDPHD efficiently clustered the CD63-positive late endosomes, these compartments left the microtubule minus-end when ΔORD was expressed. This was also observed in MelJuSo cells treated with U18666A, a compound that phenomimics Niemann-Pick type C (Figure 5E).

Despite their redistribution to the cell periphery, ΔORD-bearing vesicles still showed accumulation of cholesterol following siRNA-mediated silencing of NPC1 (Figure 5F). This suggests that the accumulation of cholesterol observed in NPC1-deficient cells is not a result but a cause of late endosomal clustering.

The characteristic clustering of cholesterol-laden late endosomal compartments at the microtubule minus-end, as typical in Niemann-Pick type C and other lysosomal storage diseases, is the result of cholesterol sensing by ORP1L. ORP1L transmits this signal to the Rab7-RILP-p150^{Glued}-dynein motor complex for microtubule minus-end driven vesicle transport and clustering.

To examine if ORP1L significantly contributes to the control of cholesterol levels in late endosomes or is it primarily using cholesterol to control Rab7-RILP-mediated p150^{Glued}-dynein motor transport without influencing its cholesterol levels, MelJuSo cells were transfected with mRFP-ORP1L or mRFP-ΔORDPHDPHD, fixed and labelled with filipin to detect cholesterol (Figure 5G). Overexpressing ΔORDPHDPHD did not significantly alter cholesterol levels in late endosomal structures. This suggests that ORP1L uses cholesterol as a messenger rather than contributing directly to the intracellular distribution of cholesterol.

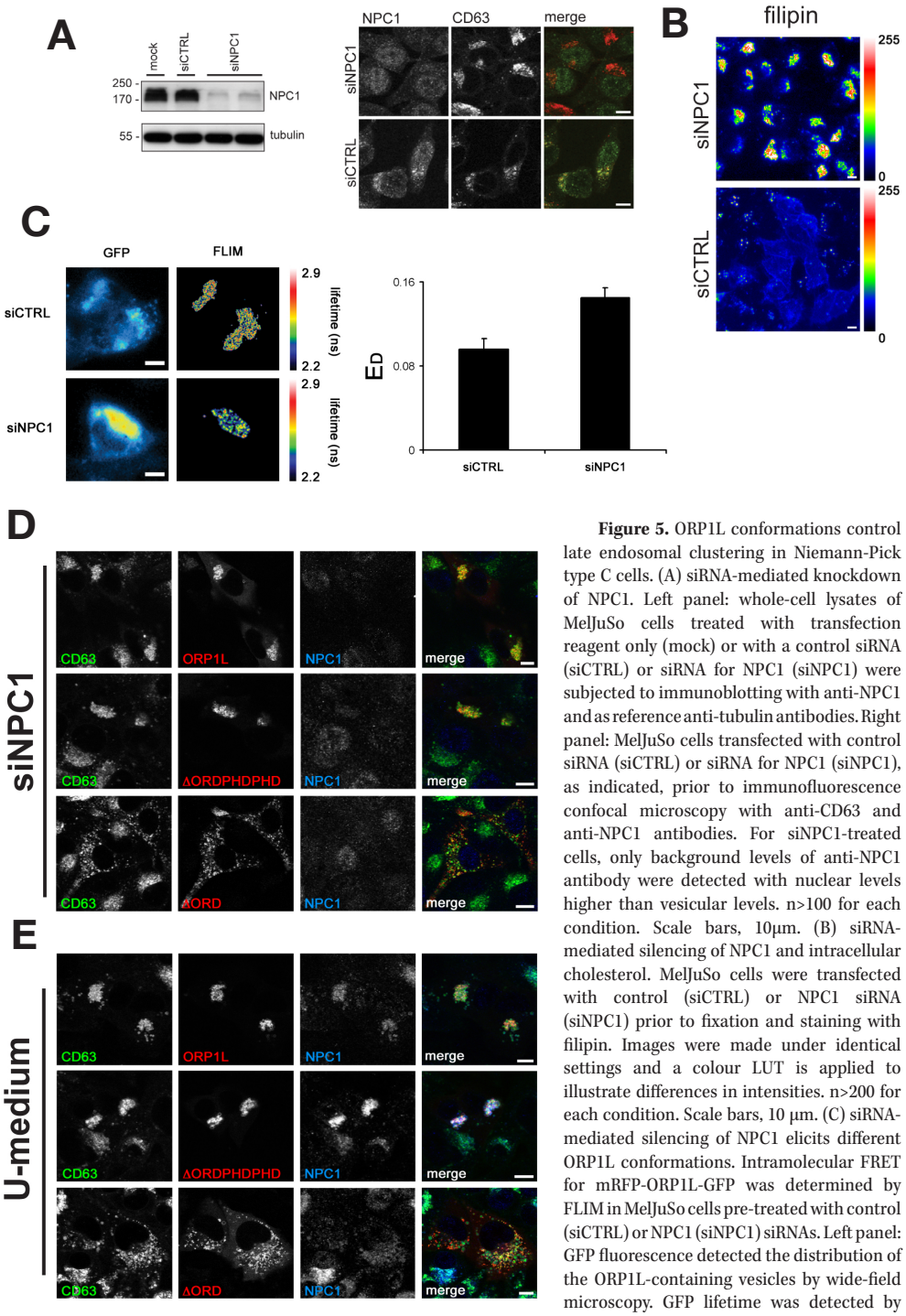

Figure 5. ORP1L conformations control late endosomal clustering in Niemann-Pick type C cells. (A) siRNA-mediated knockdown of NPC1. Left panel: whole-cell lysates of MelJuSo cells treated with transfection reagent only (mock) or with a control siRNA (siCTRL) or siRNA for NPC1 (siNPC1) were subjected to immunoblotting with anti-NPC1 and as reference anti-tubulin antibodies. Right panel: MelJuSo cells transfected with control siRNA (siCTRL) or siRNA for NPC1 (siNPC1), as indicated, prior to immunofluorescence confocal microscopy with anti-CD63 and anti-NPC1 antibodies. For siNPC1-treated cells, only background levels of anti-NPC1 antibody were detected with nuclear levels higher than vesicular levels. n>100 for each condition. Scale bars, 10μm. (B) siRNA-mediated silencing of NPC1 and intracellular cholesterol. MelJuSo cells were transfected with control (siCTRL) or NPC1 siRNA (siNPC1) prior to fixation and staining with filipin. Images were made under identical settings and a colour LUT is applied to illustrate differences in intensities. n>200 for each condition. Scale bars, 10 μm. (C) siRNA-mediated silencing of NPC1 elicits different ORP1L conformations. Intramolecular FRET for mRFP-ORP1L-GFP was determined by FLIM in MelJuSo cells pre-treated with control (siCTRL) or NPC1 (siNPC1) siRNAs. Left panel: GFP fluorescence detected the distribution of the ORP1L-containing vesicles by wide-field microscopy. GFP lifetime was detected by FLIM. The lifetime was determined (in ns) and plotted in false colours. Colour relates to the lifetime (in ns) as indicated in the colour LUT. Scale bars, 10 μm. Right panel: The donor FRET efficiencies (ED) as calculated from the FLIM data. The

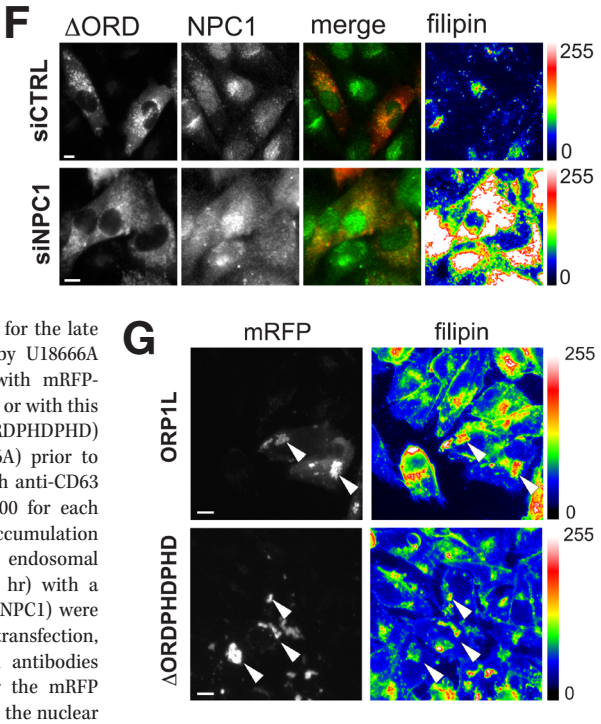

mean and SD from 75 cells analyzed in three independent experiments are shown. (D) The ORD of ORP1L is critical for late endosomal clustering following NPC1 silencing. MelJuSo cells pre-treated (for 48 hr) with siRNA for NPC1 (siNCP1) were transfected with mRFP-tagged ORP1L, ORP1L lacking the ORD (ΔORD) or with this domain replaced for a tandem PH domain (ΔORDPHDPHD), prior to immunofluorescence confocal microscopy with anti-CD63 and anti-NPC1 antibodies, as indicated. n>200 for each condition. Scale bars, 10 μm. (E) The ORD of ORP1L is critical for the late endosomal characteristic clustering caused by U18666A treatment. MelJuSo cells were transfected with mRFP-tagged ORP1L, ORP1L lacking the ORD (ΔORD) or with this domain replaced for a tandem PH domain (ΔORDPHDPHD) and cultured in U-medium (contains U18666A) prior to immunofluorescence confocal microscopy with anti-CD63 and anti-NPC1 antibodies, as indicated. n>200 for each condition. Scale bars, 10 μm. (F) Cholesterol accumulation in NPC1-deficient cells is not a result of late endosomal clustering. MelJuSo cells pre-treated (for 48 hr) with a control siRNA (siCTRL) or siRNA for NPC1 (siNPC1) were transfected with mRFP-ΔORD. At 24 hr post-transfection, cells were fixed and stained with anti-NPC1 antibodies and filipin to detect cholesterol. Except for the mRFP signal in the siNPC1 series (enhanced to detect the nuclear background anti-NPC1 staining), identical settings were used to produce the images. Merge shows only mRFP-ΔORD and anti-NPC1 antibody fluorescence signals. A colour LUT is applied to illustrate differences in filipin staining. n>50 for each condition. Scale bars, 10 μm. (G) Intracellular cholesterol levels are not affected by the ORD of ORP1L. MelJuSo cells were transfected with mRFP-ORP1L or mRFP-ΔORDPHDPHD and cultured under normal conditions (F-medium) prior to fixation and staining with filipin, as indicated. A colour LUT is applied to visualize intensities in filipin staining. Arrowheads indicate some of the transfected cells. n>100 for each condition. Scale bars, 10 μm.

ORP1L conformation, recruitment of VAP and removal of the p150^{Glued}-dynein motor

The FFAT motif in ORP1L is critical for p150^{Glued} binding to RILP (Figure 3C). This FFAT motif in the ORP1L homologue OSBP interacts with ER proteins VAP-A and VAP-B, which regulates protein and lipid export from the ER (Loewen and Levine, 2005; Wyles et al., 2002). VAP-A and –B can form heterodimers (Hamamoto et al., 2005). To test whether VAP is involved in controlling recruitment of p150^{Glued} to RILP, MelJuSo cells were transfected with ΔORD and RILP. In these cells, VAP-A was silenced by siRNA. Subsequently, cells were fixed and stained for p150^{Glued} (Figure 6A). Impaired recruitment of p150^{Glued} to RILP by ΔORD co-expression could be restored by silencing the expression of VAP-A. Identical results were obtained when VAP-B was silenced (data not shown), which was expected since VAP-A and -B can form heterodimers (Hamamoto et al., 2005). This suggests that VAP-A and –B are critical for translating the inhibitory effect of ΔORD to p150^{Glued} recruitment of RILP.

VAP-A and –B are cytosolic proteins with a hydrophobic C-terminus embedded in the ER membrane and thus not obvious candidates for regulating transport processes in late endosomes. We tested whether VAP-A and –B could appear on late endosomes dependent on OPR1L. MelJuSo cells were transfected with YFP-tagged VAP-A or –B in the presence of CFP-RILP and mRFP-ΔORD or mRFP-ΔORDPHDPHD. Cells were fixed and stained

for VAP and p150^{Glued} before analyses by CLSM (Figure 6B). VAP-A (and –B, data not shown) accumulated on late endosomes only when the FFAT motif was exposed as with mRFP-ΔORD. This suggests that the cholesterol content of vesicles determines the exposure of the FFAT motif of ORP1L and thereby the recruitment of VAP.

To follow how VAP is recruited to late endosomes, photoactivatable (PA)-GFP tagged VAP-A was expressed with various mRFP-tagged ORP1L constructs in MelJuSo cells. VAP-A/PA-GFP was photoactivated in the ER with 405 nm light, at the position of the nucleus with ER structures underneath and on top, preventing activation of any VAP-A/PA-GFP already present on the vesicles. This was verified by a Z-stack projection of the cell analyzed (Figure 6C). The transfer of VAP-A to the mRFP-ΔORD-, -ORP1L- or -ΔORDPHDPHD-labelled late endosomes was followed by time-lapse microscopy (Figure 6C, Supplemental movie M2-4). VAP-A photoactivated at the ER swiftly accessed late endosomes labelled by mRFP-ΔORD or –ORP1L but not -ΔORDPHDPHD. This suggests that the conformation of ORP1L determines VAP-A recruitment to late endosomes. The exact mechanism is unclear but transfer could be inhibited when cells were cultured at 4°C (data not shown).

VAP is recruited to late endosomes by ORP1L and is involved in p150^{Glued} exclusion. To test how VAP affects p150^{Glued} binding to RILP, the reaction was reconstituted with purified proteins. The (GTP-loaded)Rab7-RILP complex was generated to which either ORP1L or the C-terminus of p150^{Glued} (C25) were added before VAP-A was titrated into the reaction (Figure 6D, top panel). VAP-A removed C25 from the Rab7-RILP complex. ORP1L is not required for direct removal of C25 under *in vitro* conditions. However, ORP1L is essential *in vivo* to recruit VAP-A to the RILP-p150^{Glued} complex for subsequent motor removal (Figure 6CD). To test whether VAP-A directly interacted with the C25-fragment of p150^{Glued}, GST/VAP-A or GST (as a control) was bound to GST-beads and purified C25 added. A direct interaction between VAP-A and the C-terminal p150^{Glued} fragment was detected (Figure 6D, bottom panel). This *in vitro* reconstitution experiment reveals that we have defined a minimal unit controlling dynein motor binding to late endosomes with Rab7, RILP, ORP1L, p150^{Glued} and VAP. ORP1L is required to recruit VAP in a cholesterol-dependent manner to the Rab7-RILP complex and VAP then binds to and removes the dynein motor subunit p150^{Glued} from the Rab7-RILP receptor.

DISCUSSION

Cholesterol is a hydrophobic molecule essential for fluidity and microdomain formation in biomembranes. Although cells produce cholesterol in the ER, most cholesterol is acquired by uptake of HDL or LDL particles by the LDL receptor for transport to late endosomes and lysosomes (Ikonen, 2008). Most cholesterol is stored in the internal vesicles of multivesicular bodies for later transport to other cellular compartments (Mobius et al., 2003). Transfer of cholesterol over membranes requires transporters like ABCA1 and, possibly, NPC1 (Ikonen, 2008), and for further transfer, specific chaperones. A series of proteins with cholesterol-binding domains, like StAR-related lipid transfer (StART) domain and ORD, have been identified in various compartments to ensure correct cholesterol distribution in cells (Holthuis and Levine, 2005). Two such proteins, MLN64 and ORP1L, are located in late endosomes. MLN64 is a tetraspanin with a cytosolic StART domain and ORP1L a Rab7-interacting protein with an ORD (Ikonen, 2008).

High cholesterol content in late endosomes is typical for a series of lysosomal storage diseases with characteristic late endosomal clustering at the minus-end of microtubules.

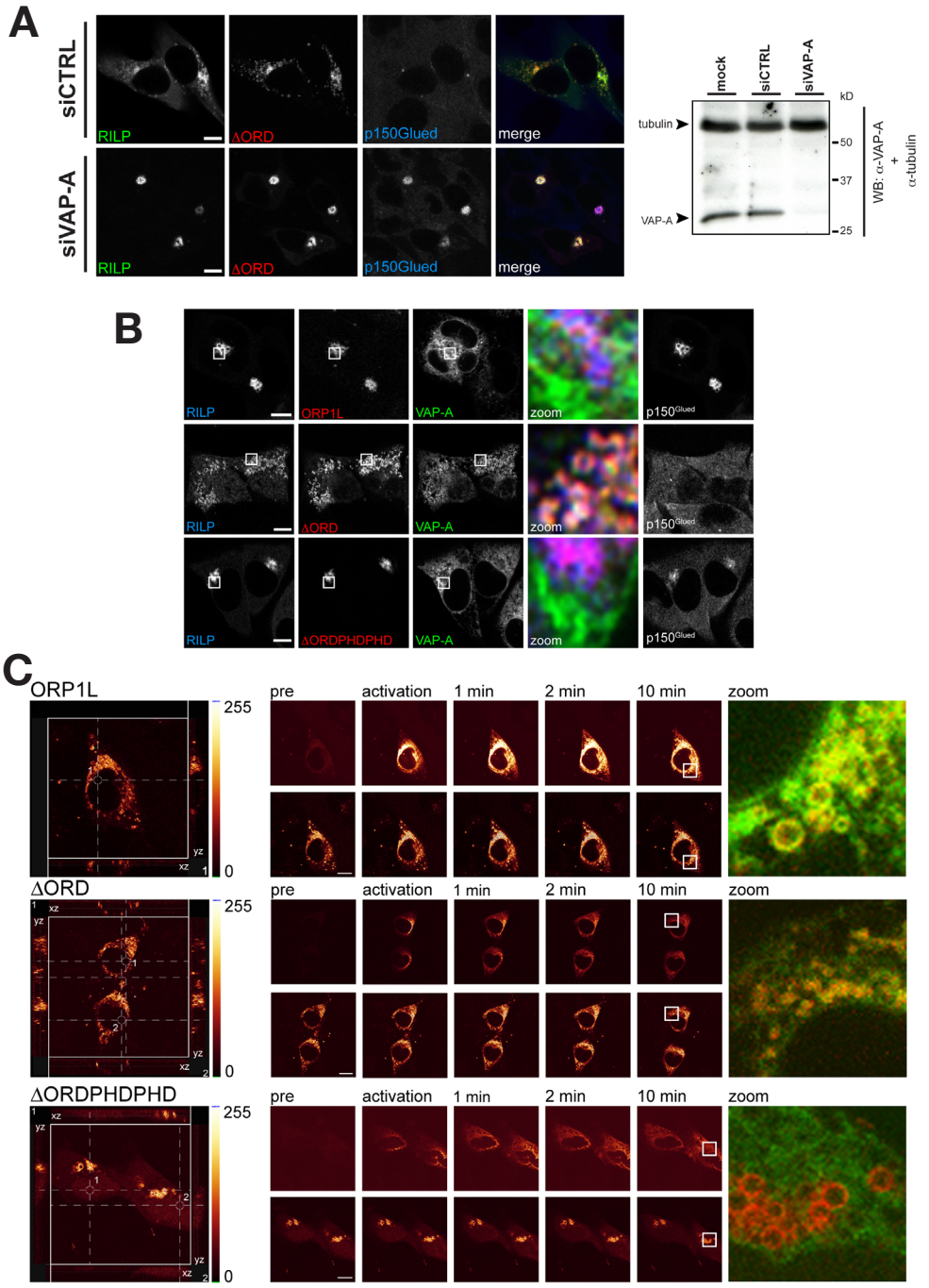

Figure 6. ORP1L recruits VAP to bind and remove p150^{Glued} for Rab7-RILP. (A) p150^{Glued} exclusion by ΔORD and VAP-A. VAP-A was silenced by siRNA in cells expressing GFP-RILP and mRFP-ΔORD. Left: Cells were fixed and stained for p150^{Glued} before analyses by confocal microscopy. n>100 for each condition. Scale bars, 10 µm. Right: Western blot analyses of cells transfected with transfection reagent only (mock), control (siCTRL) or VAP-A siRNA (siVAP-A) and subjected

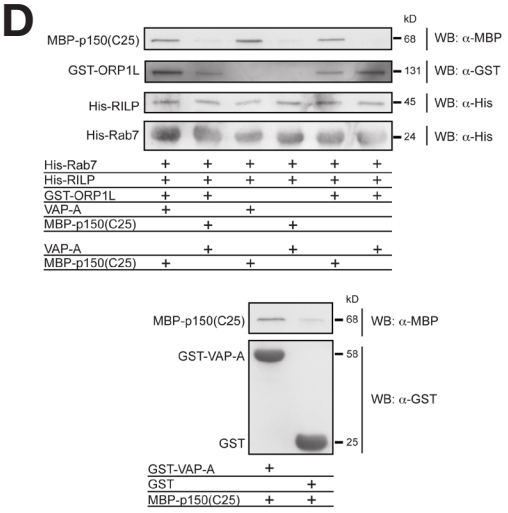

to immunobloting with α-VAP-A and α-tubulin (as reference) antibodies. (B) ΔORD recruits VAP-A and excludes p150^{Glued} from RILP-Rab7 complexes. MelJuSo cells expressing GFP-RILP and mRFP–ΔORD, -ORP1L or -ΔORDPHDPHD (as indicated) were fixed and stained for p150^{Glued} and VAP-A respectively. The different antigens are indicated. Zoom: overlay in three colours of CFP-RILP (blue), mRFP-ORP1L constructs (red) and YFP-VAP-A (in green). n>100 for each condition. Scale bars, 10 μm. (C) ORP1L recruits VAP-A from the ER. PA-GFP tagged VAP-A in living MelJuSo cells also expressing either mRFP-tagged ΔORDPHDPHD, ΔORD or ORP1L was photoactivated with a 405nm light to follow transport of ER located PA-GFP/VAP-A to late endosomes by time-lapse microscopy. Firstly, a z-stack of cells was made to identify a location for selective photoactivation of the ER pool of VAP-A. Left panel shows an x-y, x-z and y-z projection through the location of photoactivation (the 405nm laser spot position shown as a circle). Subsequently, the cells were followed by time-lapse confocal microscopy and various snapshots of the mRFP and GFP channels, prior and post-photoactivation of PA-GFP/VAP-A, are shown. Right panel is a zoom-in on late endosomes (indicated by the box) and merge of the mRFP and GFP channel. n>10 for each condition. Scale bars, 10μm. Movies are shown in Supplemental M2-4. (D) In vitro protein reconstitution experiment. Top: GTP-locked His-Rab7(Q67L) was coupled to TALON-beads and loaded with GTP before any of the isolated proteins indicated below were added to form another complex. After washing, these complexes were exposed to isolated VAP-A or the 150^{Glued}(C25) fragment, as indicated, and the effects on the pre-formed complex assessed by SDS-PAGE and Western blot analyses with specific antibodies, as indicated. A representative example of duplicate independent experiments is shown. Bottom: GST or GST-VAP-A were coupled to GST beads before exposure to the p150^{Glued}(C25) fragment. After washing, the complexes were analyzed by SDS-PAGE and Western blotting.

This suggests that cholesterol influences late endosomal transport in a process involving Rab GTPases, for which the precise mechanisms remain unknown (Holtta-Vuori et al., 2000). Vesicles are transported to the microtubule minus-end by the dynein-dynactin motor which is recruited to late endosomes by first binding the late endosomal specific Rab7-RILP receptor and then—supported by ORP1L—binding to a more general receptor spectrin βIII (Johansson et al., 2007). Both receptors are required for active dynein motor driven transport to the microtubule minus-end. Motor activities switch rapidly as visualized by the bidirectional motion of late endosomes. This switching is usually preceded by a 'stop' or immobile phase. Since the stop-time is rather variable, this is probably not a timely controlled process. The majority of the vesicles move in one line (supposedly the same microtubule) but another fraction continues under a different angle apparently switching microtubules. This suggests that vesicles do not switch direction by the same motor. We tested whether the mechanism of directional switching could be controlled by inactivating the Rab7 GTPase by TBC1D15. The Rab7 GAP TBC1D15 was identified using shRNA silencing of potential candidates in combination with photobleaching experiments to visualize the GFP-Rab7 GTPase cycle in living cells. However, RILP inhibited stimulation of the already low intrinsic Rab7 GTPase activity by TBC1D15, possibly by sharing overlapping binding sites with TBC1D15 in activated Rab7 (Figure S2). Consequently, Rab7GAP cannot be responsible for the swift mechanism of the directional switching in late endosomal transport. Rab7-RILP has been identified as the late endosomal/lysosomal receptor for the p150^{Glued}-dynein motor. Since ORP1L also binds Rab7-RILP (Johansson et al., 2007), we tested whether this protein could control dynein motor binding to RILP. Using intramolecular

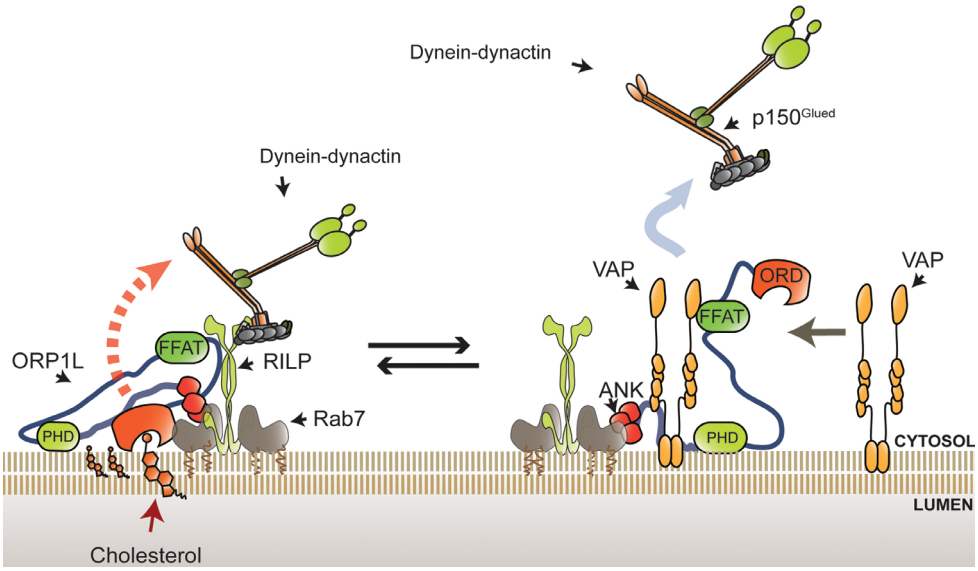

Figure 7. How cholesterol controls ORP1L conformations, VAP recruitment and p150^{Glued}-dynein motor binding to late endosomal Rab7-RILP receptors. Rab7 recruits the homodimeric effector RILP to late endosomes and lysosomes. The p150^{Glued} subunit of the dynein-dynactin motor directly interacts with RILP. ORP1L binds to the Rab7-RILP complex. Reciprocal ORP1L conformations reflect the C-terminal cholesterol-sensing domain of ORP1L (ORD) associated to cholesterol on the cytosolic leaflet of late endosomal membranes (left) or otherwise cytosolic (right). In the latter case, the FFAT motif preceding the ORD is exposed and recruits VAP. VAP binds to and removes p150^{Glued} from the Rab7-RILP receptor thus preventing minus-end transport and resulting in centrifugal translocation of late endosomal compartments. Cholesterol levels in late endosomes thus determine the conformation of ORP1L and VAP recruitment resulting in scattering under cholesterol-poor conditions and clustering of cholesterol-laden late endosomes/lysosomes, as in Niemann-Pick type C disease.

FRET, we showed that the C-terminal ORD of ORP1L senses cholesterol in late endosomes resulting in a conformational change. Removal of the ORD prevents p150^{Glued} binding to RILP whereas a further 11 kDa C-terminal truncation (aa 408-514 in ORP1L) restored binding. These data suggest that variations in late endosomal cholesterol levels elicit conformational changes in ORP1L which orchestrate motor protein binding. When the ORD is membrane-associated to bind cholesterol, the FFAT motif-containing ORP1L region preceding the ORD (aa 408-514 in ORP1L) allows binding of p150^{Glued} to RILP. Conversely, when the ORD is in its cytosolic orientated state or absent (as in the truncation mutant ΔORD), the 11 kDa region preceding the ORD (aa 408-514) prevents access of p150^{Glued}-dynein motor complexes to Rab7-RILP. Thereby, vesicles disperse by moving to the microtubule plus-end. This 11 kDa region is comprised of a predicted coiled-coil and a FFAT motif that is critical in preventing p150^{Glued} interactions in the ΔORD mutant. The FFAT motif in the ORP1L homologue OSBP interacts with VAPs in the ER (Loewen and Levine, 2005; Loewen et al., 2003) and modifies protein and lipid export from the ER (Wyles et al., 2002) and mutations in VAP-B cause familial amyotrophic lateral sclerosis (ALS) type 8 (Nishimura et al., 2004). Given the location in the ER, VAP would not be an obvious candidate for regulation of late endosomal transport, but we show VAP-A and –B accumulation on late endosomes driven by ΔORD (that exposes the FFAT motif) but not ΔORDPHDPHD (where FFAT is inaccessible). In addition, we showed using photoactivation, that ER-located VAP-A travels to late endosomes but the exact

transport pathway has not been resolved yet. Given the rapid transport and Brefeldin A-insensitivity (not shown), this unlikely is the result of classical transport through the Golgi. ORP1L may then interact in transit with VAP or actively recruit VAP from the ER membrane to control the dynein motor on late endosomes. Silencing VAP restores $p150^{Glued}$ binding to ΔORD-Rab7-RILP vesicles, suggesting that VAP is directly involved in removal of this dynein-dynactin motor subunit from the Rab7-RILP complex. This was confirmed using isolated proteins where purified VAP-A removed $p150^{Glued}$ from the RILP-Rab7-ORP1L complex (which also indicated that we have identified the minimal unit of proteins in this process). These experiments furthermore showed that ORP1L is not required for executing removal of $p150^{Glued}$ from the Rab7-RILP complex by VAP (in *in vitro* conditions), and that VAP directly interacts with the C-terminal segment of $p150^{Glued}$. However, cholesterol-dependent distinct ORP1L conformations determine VAP recruitment to the Rab7-RILP-$p150^{Glued}$ complex and subsequent removal of $p150^{Glued}$ from the Rab7-RILP receptor. This mechanism may be more general then described here, since the ORP1L homologue OSBP also uses VAP to modify ER export (Wyles et al., 2002), which is also driven by the dynein-dynactin motor complex. The motor receptor is unknown in this case. Whether other vesicles use sensors for cholesterol and VAP to control the dynein-dynactin motor, remains to be established.

When NPC1 is depleted, as in Niemann-Pick type C disease (Carstea et al., 1997), or when chemical drugs raise late endosomal cholesterol levels (Roff et al., 1991; Sobo et al., 2007), the ORD of ORP1L is membrane-associated excluding VAP. This allows enduring binding of $p150^{Glued}$-dynein motors complexes to Rab7-RILP and transport to the microtubule minus-end. Cholesterol depletion results in microtubule plus-end transport of late endosomes unless the cholesterol-insensitive ORP1L variant ΔORDPHDPHD is expressed. The positioning of vesicles bearing this chimera is independent of cholesterol levels as these remain densely clustered even when cholesterol-levels are lowered in late endosomes.

This mechanism explains how late endosomal cholesterol levels are associated with late endosomal positioning through cholesterol orchestrated recruitment of VAP by ORP1L that controls the Rab7-RILP-$p150^{Glued}$-dynein motor interaction (Figure 7). Since overexpression of ORP1L or ΔORDPHDPHD did not affect late endosomal cholesterol levels, ORP1L apparently uses local cholesterol levels (at the cytosolic leaflet of late endosomal membranes) as a messenger rather than actively contributing to cholesterol distribution in cells. Why cholesterol is selected for this purpose rather than lysobisphosphatidic acid (LBPA) or other lipids or molecules specific for late endosomes (Gruenberg and Stenmark, 2004), is unclear. It may be that cholesterol represents one of the few molecules present in the interior as well as the cytosolic leaflet of late endosomes allowing cytosolic exposure of intraluminal conditions. If cholesterol levels increase with maturation of late endosomes and lysosomes, the resulting ORP1L controlled Rab7-RILP-$p150^{Glued}$-dynein motor interactions would position the most mature compartments at the extreme minus-end of microtubules with 'shells' of less mature vesicles surrounding these at more plus-end locations. Newly arriving late endosomes would then first encounter the 'youngest' late endosomes automatically resulting in spatial maturation before encountering lysosomes. Cholesterol would thus control the positioning of these organelles.

We have visualized how the Rab7-RILP complex controls transport of late endosomes. This process is controlled by cholesterol levels that direct ORP1L. The cholesterol-interacting protein ORP1L has two conformational states dependent on late endosomal cholesterol

content and determines the dynein motor interaction with Rab7-RILP by selectively exposing its FFAT motif. The cytosolic exposed FFAT motif recruits VAP from the ER membrane. VAP then interacts with and removes the p150^{Glued} dynein motor subunit from the Rab7-RILP receptor of late endosomal and lysosomal membranes (Figure 7). This explains why cholesterol depletion causes late endosomal scattering and why high cholesterol levels induce lysosomal clustering, as observed in Niemann-Pick type C disease. Cholesterol in late endosomes is a messenger sensed by ORP1L to recruit VAP that binds to and removes dynein-dynactin motor complexes from late endosomal Rab7-RILP receptors and thus controls transport.

EXPERIMENTAL PROCEDURES

DNA constructs, Reagents, and Antibodies

Rab7, RILP, VAP-A, VAP-B, p150^{Glued}(C25) and ORP1L cDNA constructs have been described previously (Johansson et al., 2007; Jordens et al., 2001; Marsman et al., 2004; Wyles et al., 2002). GFP, mRFP, GST, MBP and His-tagged constructs were constructed by PCR modification and cloning and described in *Supplemental Experimental Procedures*. All constructs were sequenced verified and controlled by Western blot analyses. Reagents for manipulation of cellular cholesterol levels, cholesterol staining with filipin and antibodies for protein isolation, Western blotting and fluorescence microscopy are described in *Supplemental Experimental Procedures*.

Protein isolation and reconstitution studies

All proteins were expressed in *E. coli* with the exception of His-TBC1D15 that was isolated from 293T cells. Details on production and isolation are in *Supplemental Experimental Procedures*. Removal of GST from GST-VAP-A was by thrombin-cleavage followed by PMSF-precipitation of thrombin. The proteins were further purified by a GST-column and the flow-through contained GST-free VAP-A. Purity and correct molecular weight of the fusion proteins was controlled by SDS-PAGE and Coomassie staining. Proteins were stored in 8.7% glycerol at -80°C until use in protein reconstitution experiments. For Rab7GAP experiments, His-Rab7 was loaded with [γ-^{32}P]GTP before addition of His-RILP and GST-ORP1L in different combinations. His-TBC1D15 was added before the reaction was transferred from 4°C to 25°C. [γ-^{32}P]GTP-labelled His-Rab7 and [γ-^{32}P]GTP was precipitated by active charcoal unlike released ^{32}P-label which was quantified by scintillation counting. For *in vitro* effects of VAP-A on the ORP1L-Rab7-RILP-C25 protein complex, the GTPase-deficient His-Rab7(Q67L) was loaded onto TALON-beads and loaded with GTP (Sigma). Subsequently, the complex was formed by adding one or more of the following purified proteins: GST-OPR1L, His-RILP, MBP-p150^{Glued}(C25) and/or VAP-A. The complex was washed before addition of purified VAP-A or MBP-p150^{Glued}(C25) for 30 min at 20°C. Beads were washed before analysis by SDS-PAGE and Western Blotting. Alternatively, GST-VAP-A or purified GST were loaded onto GST-beads before addition of p150^{Glued}(C25) for 30 min at 20°C. After washing the beads were analyzed by SDS-PAGE and Western Blotting. Details are described in *Supplemental Experimental Procedures*.

Microscopy

Three and four-colour images on fluorescent fixed-samples were made using rabbit and mouse primary antibodies and mRFP- and GFP-labelled proteins. Images are made using Leica confocal laser scanning microscopes. Time-lapse imaging and Fluorescence Recovery After Photobleaching (FRAP) experiments were performed on a Leica TCS SP2 microscope equipped with a 37°C culture chamber. Vesicle motility analysis was performed using images analyzed by recovery curves of the time-

lapse images which were generated using the MATLAB plug-in curve fitting toolbox. Photoactivation experiments were performed using a 405 nm laser on a Leica AOBS system equipped with a 37°C culture chamber. Movies were made using IMAGE J programming. Lifetime imaging were taken on a Leica inverted DM-IRE2 microscope equipped with a Lambert Instruments (LI) frequency domain lifetime attachment (Leutingewolde, The Netherlands), controlled by the manufacturers' LI FLIM software. This microscope was also equipped with a 37°C culture chamber. Filipin signal was recorded using a 365 nm excitation filter with 397 nm long pass emission using a Zeiss Axiovert 200 microscope equipped with an AxioCam CCD camera and a 20x Achroplan Ph2 dry lens. For further details on microscopy and data analyses, see *Supplemental Experimental Procedures*.

ACKNOWLEDGEMENTS

We thank K. Jalink for support with FLIM measurements and V. Olkkonen and M. Johansson for ORP1L reagents and constructs; N. Ridgway, M. Hardy, K. Ettayebi, and C. Hoogenraad for VAP-A and –B reagents. We thank W. Moolenaar, H. Pickersgill and V. Menendez-Benito for critically reading the manuscript and S. Krom for helping with experiments. Nuno Rocha was supported by a Portuguese Foundation for Science and Technology FCT/ FSE PhD scholarship within the Third Framework Program. This work was supported by grants from the Dutch Cancer Society KWF and the Chemical Sciences Section of NWO.

REFERENCES

Albert, S., Will, E., and Gallwitz, D. (1999). Identification of the catalytic domains and their functionally critical arginine residues of two yeast GTPase-activating proteins specific for Ypt/Rab transport GTPases. Embo J *18*, 5216-5225.

Bernards, A. (2003). GAPs galore! A survey of putative Ras superfamily GTPase activating proteins in man and Drosophila. Biochim Biophys Acta *1603*, 47-82.

Bornig, H., and Geyer, G. (1974). Staining of cholesterol with the fluorescent antibiotic "filipin". Acta Histochem *50*, 110-115.

Brown, C.L., Maier, K.C., Stauber, T., Ginkel, L.M., Wordeman, L., Vernos, I., and Schroer, T.A. (2005). Kinesin-2 is a motor for late endosomes and lysosomes. Traffic *6*, 1114-1124.

Bucci, C., Thomsen, P., Nicoziani, P., McCarthy, J., and van Deurs, B. (2000). Rab7: a key to lysosome biogenesis. Mol Biol Cell *11*, 467-480.

Burkhardt, J.K., Echeverri, C.J., Nilsson, T., and Vallee, R.B. (1997). Overexpression of the dynamitin (p50) subunit of the dynactin complex disrupts dynein-dependent maintenance of membrane organelle distribution. J Cell Biol *139*, 469-484.

Calleja, V., Ameer-Beg, S.M., Vojnovic, B., Woscholski, R., Downward, J., and Larijani, B. (2003). Monitoring conformational changes of proteins in cells by fluorescence lifetime imaging microscopy. Biochem J *372*, 33-40.

Carstea, E.D., Morris, J.A., Coleman, K.G., Loftus, S.K., Zhang, D., Cummings, C., Gu, J., Rosenfeld, M.A., Pavan, W.J., Krizman, D.B., *et al.* (1997). Niemann-Pick C1 disease gene: homology to mediators of cholesterol homeostasis. Science *277*, 228-231.

Chen, H., Yang, J., Low, P.S., and Cheng, J.X. (2008). Cholesterol level regulates endosome motility via Rab proteins. Biophys J *94*, 1508-1520.

Chen, W., Sun, Y., Welch, C., Gorelik, A., Leventhal, A.R., Tabas, I., and Tall, A.R. (2001). Preferential ATP-binding cassette transporter A1-mediated cholesterol efflux from late endosomes/lysosomes. J Biol Chem *276*, 43564-43569.

Deacon, S.W., Serpinskaya, A.S., Vaughan,

P.S., Lopez Fanarraga, M., Vernos, I., Vaughan, K.T., and Gelfand, V.I. (2003). Dynactin is required for bidirectional organelle transport. J Cell Biol *160*, 297-301.

Echard, A., Jollivet, F., Martinez, O., Lacapere, J.J., Rousselet, A., Janoueix-Lerosey, I., and Goud, B. (1998). Interaction of a Golgi-associated kinesin-like protein with Rab6. Science *279*, 580-585.

Förster, T. (1948). Zwischenmolekulare energiewandering und fluoreszenz. . Annalen Physik *6*, 55–75.

Gennerich, A., Carter, A.P., Reck-Peterson, S.L., and Vale, R.D. (2007). Force-induced bidirectional stepping of cytoplasmic dynein. Cell *131*, 952-965.

Gross, S.P., Welte, M.A., Block, S.M., and Wieschaus, E.F. (2002). Coordination of opposite-polarity microtubule motors. J Cell Biol *156*, 715-724.

Gruenberg, J., and Stenmark, H. (2004). The biogenesis of multivesicular endosomes. Nat Rev Mol Cell Biol *5*, 317-323.

Hamamoto, I., Nishimura, Y., Okamoto, T., Aizaki, H., Liu, M., Mori, Y., Abe, T., Suzuki, T., Lai, M.M., Miyamura, T., *et al.* (2005). Human VAP-B is involved in hepatitis C virus replication through interaction with NS5A and NS5B. Journal of virology *79*, 13473-13482.

Harada, A., Takei, Y., Kanai, Y., Tanaka, Y., Nonaka, S., and Hirokawa, N. (1998). Golgi vesiculation and lysosome dispersion in cells lacking cytoplasmic dynein. J Cell Biol *141*, 51-59.

Harrison, R.E., Bucci, C., Vieira, O.V., Schroer, T.A., and Grinstein, S. (2003). Phagosomes fuse with late endosomes and/or lysosomes by extension of membrane protrusions along microtubules: role of Rab7 and RILP. Mol Cell Biol *23*, 6494-6506.

Hoepfner, S., Severin, F., Cabezas, A., Habermann, B., Runge, A., Gillooly, D., Stenmark, H., and Zerial, M. (2005). Modulation of receptor recycling and degradation by the endosomal kinesin KIF16B. Cell *121*, 437-450.

Hollenbeck, P.J., and Swanson, J.A. (1990). Radial extension of macrophage tubular lysosomes supported by kinesin. Nature *346*, 864-866.

Holthuis, J.C., and Levine, T.P. (2005). Lipid traffic: floppy drives and a superhighway. Nat Rev Mol Cell Biol *6*, 209-220.

Holtta-Vuori, M., Maatta, J., Ullrich, O., Kuismanen, E., and Ikonen, E. (2000). Mobilization of late-endosomal cholesterol is inhibited by Rab guanine nucleotide dissociation inhibitor. Curr Biol *10*, 95-98.

Ikonen, E. (2008). Cellular cholesterol trafficking and compartmentalization. Nat Rev Mol Cell Biol *9*, 125-138.

Im, Y.J., Raychaudhuri, S., Prinz, W.A., and Hurley, J.H. (2005). Structural mechanism for sterol sensing and transport by OSBP-related proteins. Nature *437*, 154-158.

Infante, R.E., Abi-Mosleh, L., Radhakrishnan, A., Dale, J.D., Brown, M.S., and Goldstein, J.L. (2008a). Purified NPC1 protein. I. Binding of cholesterol and oxysterols to a 1278-amino acid membrane protein. J Biol Chem *283*, 1052-1063.

Infante, R.E., Radhakrishnan, A., Abi-Mosleh, L., Kinch, L.N., Wang, M.L., Grishin, N.V., Goldstein, J.L., and Brown, M.S. (2008b). Purified NPC1 protein: II. Localization of sterol binding to a 240-amino acid soluble luminal loop. J Biol Chem *283*, 1064-1075.

Johansson, M., Lehto, M., Tanhuanpää, K., Cover, T.L., and Olkkonen, V.M. (2005). The oxysterol-binding protein homologue ORP1L interacts with Rab7 and alters functional properties of late endocytic compartments. Mol Biol Cell *16*, 5480-5492.

Johansson, M., Rocha, N., Zwart, W., Jordens, I., Janssen, L., Kuijl, C., Olkkonen, V.M., and Neefjes, J. (2007). Activation of endosomal dynein motors by stepwise assembly of Rab7-RILP-p150Glued, ORP1L, and the receptor betalll spectrin. J Cell Biol *176*, 459-471.

Jordens, I., Fernandez-Borja, M., Marsman, M., Dusseljee, S., Janssen, L., Calafat, J., Janssen,

H., Wubbolts, R., and Neefjes, J. (2001). The Rab7 effector protein RILP controls lysosomal transport by inducing the recruitment of dynein-dynactin motors. Curr Biol *11*, 1680-1685.

Jordens, I., Marsman, M., Kuijl, C., and Neefjes, J. (2005). Rab proteins, connecting transport and vesicle fusion. Traffic *6*, 1070-1077.

Jordens, I., Westbroek, W., Marsman, M., Rocha, N., Mommaas, M., Huizing, M., Lambert, J., Naeyaert, J.M., and Neefjes, J. (2006). Rab7 and Rab27a control two motor protein activities involved in melanosomal transport. Pigment Cell Res *19*, 412-423.

King, S.J., Brown, C.L., Maier, K.C., Quintyne, N.J., and Schroer, T.A. (2003). Analysis of the dynein-dynactin interaction in vitro and in vivo. Mol Biol Cell *14*, 5089-5097.

Koh, C.H., and Cheung, N.S. (2006). Cellular mechanism of U18666A-mediated apoptosis in cultured murine cortical neurons: bridging Niemann-Pick disease type C and Alzheimer's disease. Cell Signal *18*, 1844-1853.

Lebrand, C., Corti, M., Goodson, H., Cosson, P., Cavalli, V., Mayran, N., Faure, J., and Gruenberg, J. (2002). Late endosome motility depends on lipids via the small GTPase Rab7. Embo J *21*, 1289-1300.

Lehto, M., Hynynen, R., Karjalainen, K., Kuismanen, E., Hyvarinen, K., and Olkkonen, V.M. (2005). Targeting of OSBP-related protein 3 (ORP3) to endoplasmic reticulum and plasma membrane is controlled by multiple determinants. Exp Cell Res *310*, 445-462.

Lehto, M., Mayranpaa, M.I., Pellinen, T., Ihalmo, P., Lehtonen, S., Kovanen, P.T., Groop, P.H., Ivaska, J., and Olkkonen, V.M. (2008). The R-Ras interaction partner ORP3 regulates cell adhesion. J Cell Sci *121*, 695-705.

Lemmon, M.A., and Ferguson, K.M. (2000). Signal-dependent membrane targeting by pleckstrin homology (PH) domains. Biochem J *350 Pt 1*, 1-18.

Loewen, C.J., and Levine, T.P. (2005). A highly conserved binding site in vesicle-associated membrane protein-associated protein (VAP) for the FFAT motif of lipid-binding proteins. J Biol Chem *280*, 14097-14104.

Loewen, C.J., Roy, A., and Levine, T.P. (2003). A conserved ER targeting motif in three families of lipid binding proteins and in Opi1p binds VAP. Embo J *22*, 2025-2035.

Ma, S., and Chisholm, R.L. (2002). Cytoplasmic dynein-associated structures move bidirectionally in vivo. J Cell Sci *115*, 1453-1460.

Marsman, M., Jordens, I., Kuijl, C., Janssen, L., and Neefjes, J. (2004). Dynein-mediated vesicle transport controls intracellular Salmonella replication. Mol Biol Cell *15*, 2954-2964.

Maxfield, F.R., and Tabas, I. (2005). Role of cholesterol and lipid organization in disease. Nature *438*, 612-621.

Mobius, W., van Donselaar, E., Ohno-Iwashita, Y., Shimada, Y., Heijnen, H.F., Slot, J.W., and Geuze, H.J. (2003). Recycling compartments and the internal vesicles of multivesicular bodies harbor most of the cholesterol found in the endocytic pathway. Traffic *4*, 222-231.

Mukherjee, S., and Maxfield, F.R. (2004). Lipid and cholesterol trafficking in NPC. Biochim Biophys Acta *1685*, 28-37.

Muller, M.J., Klumpp, S., and Lipowsky, R. (2008). Tug-of-war as a cooperative mechanism for bidirectional cargo transport by molecular motors. Proc Natl Acad Sci U S A *105*, 4609-4614.

Narita, K., Choudhury, A., Dobrenis, K., Sharma, D.K., Holicky, E.L., Marks, D.L., Walkley, S.U., and Pagano, R.E. (2005). Protein transduction of Rab9 in Niemann-Pick C cells reduces cholesterol storage. Faseb J *19*, 1558-1560.

Nishimura, A.L., Mitne-Neto, M., Silva, H.C., Richieri-Costa, A., Middleton, S., Cascio, D., Kok, F., Oliveira, J.R., Gillingwater, T., Webb, J., *et al.* (2004). A mutation in the vesicle-trafficking protein VAPB causes late-onset

spinal muscular atrophy and amyotrophic lateral sclerosis. American journal of human genetics *75*, 822-831.

Nishimura, Y., Hayashi, M., Inada, H., and Tanaka, T. (1999). Molecular cloning and characterization of mammalian homologues of vesicle-associated membrane protein-associated (VAMP-associated) proteins. Biochemical and biophysical research communications *254*, 21-26.

Patel, S.C., Suresh, S., Kumar, U., Hu, C.Y., Cooney, A., Blanchette-Mackie, E.J., Neufeld, E.B., Patel, R.C., Brady, R.O., Patel, Y.C., *et al.* (1999). Localization of Niemann-Pick C1 protein in astrocytes: implications for neuronal degeneration in Niemann- Pick type C disease. Proc Natl Acad Sci U S A *96*, 1657-1662.

Pepperkok, R., Squire, A., Geley, S., and Bastiaens, P.I. (1999). Simultaneous detection of multiple green fluorescent proteins in live cells by fluorescence lifetime imaging microscopy. Curr Biol *9*, 269-272.

Peterson, M.R., and Emr, S.D. (2001). The class C Vps complex functions at multiple stages of the vacuolar transport pathway. Traffic *2*, 476-486.

Pfeffer, S.R. (2001). Rab GTPases: specifying and deciphering organelle identity and function. Trends Cell Biol *11*, 487-491.

Rink, J., Ghigo, E., Kalaidzidis, Y., and Zerial, M. (2005). Rab conversion as a mechanism of progression from early to late endosomes. Cell *122*, 735-749.

Roff, C.F., Goldin, E., Comly, M.E., Cooney, A., Brown, A., Vanier, M.T., Miller, S.P., Brady, R.O., and Pentchev, P.G. (1991). Type C Niemann-Pick disease: use of hydrophobic amines to study defective cholesterol transport. Dev Neurosci *13*, 315-319.

Ross, J.L., Wallace, K., Shuman, H., Goldman, Y.E., and Holzbaur, E.L. (2006). Processive bidirectional motion of dynein-dynactin complexes in vitro. Nat Cell Biol *8*, 562-570.

Seals, D.F., Eitzen, G., Margolis, N., Wickner, W.T., and Price, A. (2000). A Ypt/Rab effector complex containing the Sec1 homolog Vps33p is required for homotypic vacuole fusion. Proc Natl Acad Sci U S A *97*, 9402-9407.

Shaner, N.C., Campbell, R.E., Steinbach, P.A., Giepmans, B.N., Palmer, A.E., and Tsien, R.Y. (2004). Improved monomeric red, orange and yellow fluorescent proteins derived from Discosoma sp. red fluorescent protein. Nature biotechnology *22*, 1567-1572.

Sobo, K., Le Blanc, I., Luyet, P.P., Fivaz, M., Ferguson, C., Parton, R.G., Gruenberg, J., and van der Goot, F.G. (2007). Late endosomal cholesterol accumulation leads to impaired intra-endosomal trafficking. PLoS ONE *2*, e851.

Stinchcombe, J.C., Majorovits, E., Bossi, G., Fuller, S., and Griffiths, G.M. (2006). Centrosome polarization delivers secretory granules to the immunological synapse. Nature *443*, 462-465.

Suchanek, M., Hynynen, R., Wohlfahrt, G., Lehto, M., Johansson, M., Saarinen, H., Radzikowska, A., Thiele, C., and Olkkonen, V.M. (2007). The mammalian oxysterol-binding protein-related proteins (ORPs) bind 25-hydroxycholesterol in an evolutionarily conserved pocket. Biochem J *405*, 473-480.

Sugii, S., Lin, S., Ohgami, N., Ohashi, M., Chang, C.C., and Chang, T.Y. (2006). Roles of endogenously synthesized sterols in the endocytic pathway. J Biol Chem *281*, 23191-23206.

Vaughan, P.S., Leszyk, J.D., and Vaughan, K.T. (2001). Cytoplasmic dynein intermediate chain phosphorylation regulates binding to dynactin. J Biol Chem *276*, 26171-26179.

Wubbolts, R., Fernandez-Borja, M., Jordens, I., Reits, E., Dusseljee, S., Echeverri, C., Vallee, R.B., and Neefjes, J. (1999). Opposing motor activities of dynein and kinesin determine retention and transport of MHC class II-containing compartments. J Cell Sci *112 (Pt 6)*, 785-795.

Wubbolts, R., Fernandez-Borja, M., Oomen, L., Verwoerd, D., Janssen, H., Calafat, J., Tulp, A., Dusseljee, S., and Neefjes, J. (1996). Direct vesicular transport of MHC class II molecules

from lysosomal structures to the cell surface. J Cell Biol *135*, 611-622.

Wurmser, A.E., Sato, T.K., and Emr, S.D. (2000). New component of the vacuolar class C-Vps complex couples nucleotide exchange on the Ypt7 GTPase to SNARE-dependent docking and fusion. J Cell Biol *151*, 551-562.

Wyles, J.P., McMaster, C.R., and Ridgway, N.D. (2002). Vesicle-associated membrane protein-associated protein-A (VAP-A) interacts with the oxysterol-binding protein to modify export from the endoplasmic reticulum. J Biol Chem *277*, 29908-29918.

Yang, H. (2006). Nonvesicular sterol transport: two protein families and a sterol sensor? Trends Cell Biol *16*, 427-432.

Zerial, M., and McBride, H. (2001). Rab proteins as membrane organizers. Nat Rev Mol Cell Biol *2*, 107-117.

Zhang, X.M., Walsh, B., Mitchell, C.A., and Rowe, T. (2005). TBC domain family, member 15 is a novel mammalian Rab GTPase-activating protein with substrate preference for Rab7. Biochemical and biophysical research communications *335*, 154-161.

SUPPLEMENTAL EXPERIMENTAL PROCEDURES

Reagents

Rabbit anti-GFP and rabbit anti-mRFP antibodies were generated using purified His-mRFP or His-GFP recombinant proteins as immunogens, respectively. Cross-reactivity was excluded by Western blot analyses with various mRFP- or GFP-labelled fusion proteins. Rabbit polyclonal anti-NPC1 was from Novus Biologicals, Inc. (Littleton, CO, USA), rat monoclonal anti-tubulin antibody was from Abcam plc (Cambridge, UK), rabbit anti-human VAP antiserum was a kind gift of Dr. N. Ridgway (Dalhousie University, Canada). Rabbit- anti HA tag was from Santa Cruz. Fluorescent secondary antibodies were from Molecular Probes.

Lovastatin (or Mevinolin) was purchased from Calbiochem (Darmstadt, Germany) and converted from its inactive prodrug form to its open acid form prior to use, by first dissolving the prodrug in ethanol and heating to 50°C for 2 hr in NaOH. Sodium-phosphate buffer was then added and this solution was heated to 40°C for 30 min. Finally, the pH was adjusted to 7.3 with concentrated HCl. Mevalonate was prepared by dissolving Mevalonolactone (Sigma-Aldrich, Schnelldorf, Germany) in a 0.05 M NaOH solution. The pH was adjusted to 7.0 with 0.1 M HCl.

U18666A (Calbiochem) was dissolved in ethanol to a final concentration of 10 mg/ml.

The lipoprotein-deficient serum (LPDS) was prepared as described (Goldstein et al., 1983) and was a kind gift from Dr. M. Jauhiainen at the National Public Health Institute (Helsinki, Finland).

cDNA constructs and vectors

Rab7, RILP and ORP1L cDNA constructs have been described previously (Johansson et al., 2007; Jordens et al., 2001; Marsman et al., 2004). GST-VAP-A was a kind gift from Dr. M. Hardy and K. Ettayebi (Montana State University, USA) and HA-VAP-A and HA-VAP-B from Dr. C. Hoogenraad (Teuling et al., 2007). VAP-A was cut with BamHI and XhoI and cloned into both a pAGFP-C1 vector and an YFP-C1 vector (using the BglII and SalI sites). GFP-ANKPHD and mRFP-ANKPHD were generated by subcloning the ANKPHD fragment from pCDNA4-ANKPHD (Johansson et al., 2007) into a pEGFP-C1 (BD Biosciences Clonetech, USA) or into a custom made pmRFP-C1 vector (Johansson et al., 2007), respectively, using the BamHI and XbaI sites.

ΔORD was generated by PCR using primers 5'-ACTCGGATCCATGAACACAGAAGCGGAGCAACA-3' and 5'-AAAGGATCCCTATCTGTGTTTTCTACTGCCCAAATGC-3' and inserted into the BamHI site of pcDNA4HisMax-C (Invitrogen) and the BglII site of pmRFP-C1 (Johansson et al., 2007) vectors.

To generate mRFP-ΔORDPHDPHD, mRFP-ΔORD was digested with XbaI and EcoRI. The remainder of ΔORD was amplified by PCR using primers 5'-CTCAAAATGATTAAGGAGTGTGA-CATGGCTA-3' and 5'-CCGGAATTCCATTCTGTGTTTTCTACTGCCCAAATGCTC-3'. The amplified fragment was inserted into the XbaI and EcoRI sites of the previously digested mRFP-ΔORD vector. The first PH domain was generated by PCR using primers 5'-CCGGAATTCCGATAT-GAGGGCCCTCTCTGGAAGA-3' and 5'-CGGGGTACCGCTGTAAGCAGAATGTTCTTCTATTGC-3' and ligated into the EcoRI and KpnI sites. Subsequently, the second PH domain was also generated by PCR using primers 5'-CGGGGTACCCGATATGAGGGCCCTCTCTGGAAGA-3' and 5'-CGGGATCCATTCTAGCTGTAAGCAGAATGTTCTTCTATTGC-3' and inserted using the KpnI and BamHI sites.

mRFP-ΔORDFFAT(D478A) was generated by PCR using mRFP-ΔORD as

template and 5'-CCCAGAATTCTATGCGGCGCTGTCAGATTCCGAGTC-3' and 5'-AAGCAAGTAAAACCTCTACAAATG-3' as primers, followed by swapping of the wild-type FFAT motif in mRFP-ΔORD for the mutated FFAT using the EcoRI and BamHI restriction sites.

The ORP1L-FRET construct (mRFP-ORP1L-GFP) was generated in two steps. Firstly, mRFP-ORP1L was digested with NheI and SacI (internal site in ORP1L) which was subsequently cloned into pEGFP-N1 (Clontech) to obtain an N-terminal region of ORP1L which was N-terminally tagged to mRFP and C-terminally tagged to GFP. In the second step, the C-terminal part of ORP1L was produced by PCR using primers 5'-GGAGTGTGACATGGCTAA-3' and 5'-CGGGATTCCATAAATGTCAGGCAAATTGAAG-3', mutating the ORP1L stop codon. The PCR product was digested using SacI and BamHI, and cloned into the intermediate construct described.

TBC1D15 was a kind gift from Xiang-Ming Zhang (Zhang et al., 2005). shRNA targeting TBC1D15 were made using the pSUPER vector system (Brummelkamp et al., 2002) and the sequences 5'-AATGGGACATGGTTAATACAGTT-3' and 5'-AAGGCATGAAGACCCAGCTAATT-3'. siRNA for human NPC1 was obtained from Dharmacon (ON-TARGETplus SMARTpool for accession no. NM_000271) and transfected using DharmaFECT 1 transfection reagent (Dharmacon).

All constructs were sequence verified. Expressed proteins had the expected molecular weight as confirmed by SDS-PAGE and Western blotting analyses.

Cell culture and drug treatment

Monolayers of MelJuSo cells were maintained in Iscoves Modified Dulbecco's Medium (IMDM) medium (Gibco) supplemented with 5% FCS, in 5% CO_2 at 37°C.

For S-medium treatment, MelJuSo cells were washed with PBS and then cultured in IMDM supplemented with 5% LPDS, 50 μM lovastatin to inhibit HMG-CoA reductase, and 230 μM mevalonate to supply essential non-sterol isoprenoids for cell growth and survival (Liscum et al., 1989; Sugii et al., 2006), for 4 hr before analyses. For U-medium treatment, cells were washed with PBS and cultured in IMDM supplemented with 5% FCS and 3 μg/ml of U18666A for 15 hr before analyses.

Microscopy

Transfected cells were fixed at 48 hr (DNA), 48 hr (RNAi) or 72 hr (RNAi and DNA) post-transfection with 4% formaldehyde in PBS for 30 min and permeabilized for 5 min with 0.05% Triton X-100 in PBS, at room temperature. Nonspecific binding of antibodies was blocked by 0.5% BSA/PBS for 40 min, after which cells were incubated with a primary antibody in 0.5% BSA/PBS for 1 hr at room temperature. Bound primary antibodies were visualized with Alexa Fluor secondary antibody conjugates (Invitrogen). Cells were mounted in Vectashield mounting medium (Vector Laboratories, USA). The specimens were analyzed with confocal laser scanning microscopes (TCS-SP1, -SP2 or AOBS) equipped with HCX PL APO 63x/NA 1.32 and HCX PL APO lbd.bl 63×/NA 1.4 oil-corrected objective lenses (all from Leica, Mannheim, Germany). The acquisition software used was Leica LCS.

Live imaging of MelJuSo cells stably expressing GFP-MHC class II (Wubbolts et al., 1999) was performed on a Leica TCS SP2 System (Leica, Mannheim, Germany) at 37°C in a 5% CO_2 culture hood surrounding the objective stage of the microscope. Vesicle movement was analyzed with the ImageJ plugin "Manual Tracking". Obtained tracking data was further processed in Microsoft Excel.

FRAP experiments were performed as described previously (Jordens et al., 2001; Reits et al., 2000). Briefly, MelJuso cells expressing GFP-Rab7 were microinjected with constructs expressing an shRNAi targeting a GAP protein. Approximately 24 hr after microinjection GFP-Rab7 vesicles were bleached with a high-intensity laser beam. Subsequently, the recovery of fluorescence in the bleached spot was quantified. Lysosomes and late endosomes with little lateral movement were selected. Because the vesicles were not completely stationary, their position was tracked and intensity measured by a program written in Matlab (Mathworks, Natick, MA) and the percentage of fluorescence recovery after 200 s was determined. Independent experiments were analyzed.

Photo-activation experiments were performed in MelJuSo cells transfected with photo-activatable GFP tagged to VAP-A, cotransfected with mRFP-tagged-ORP1L, -ORP1LΔORD or -ORP1LΔORDPDHPDH. Cells were mounted in phenol-red-free DMEM (Invitrogen), limiting medium autofluorescence. All measurements were performed on a Leica AOBS system equipped with a 37°C culture chamber and HCX PL APO lbd.bl 63×/NA 1.4 oil-corrected objective lenses. Cells were imaged using a 488 nm and 561 nm laser, to visualize the activated PA-GFP and mRFP tagged proteins, respectively. Point-activation with full power from the 405 nm laser was performed for 3 seconds at the nuclear region, where ER could be activated outside of the confocal plain. To prevent PA-GFP/VAP-A activation already present on late endosomal/lysosomal structures, a Z-stack was performed before activation.

Fluorescence Lifetime Imaging Microscopy (FLIM)

FLIM experiments were performed with MelJuSo cells stably expressing GFP-ORP1L-mRFP cultured on Delta T dishes (Bioptechs). Prior to measurements, cells were mounted in bicarbonate-buffered saline medium (140 mM NaCl, 5 mM KCl, 2 mM $MgCl_2$, 1 mM $CaCl_2$, 23 mM $NaHCO_3$, 10 mM [D-]glucose, and 10 mM Hepes, pH 7.3) and analyzed at 37°C in a 5% CO_2 culture hood surrounding the objective stage of the microscope. Images were taken on a Leica inverted DM-IRE2 microscope with a HCX PL APO 63x/NA 1.35 glycerol corrected objective lens equipped with a Lambert Instruments (LI) frequency domain lifetime attachment (Leutingewolde, The Netherlands), controlled by the manufacturer's LI FLIM software. GFP was excited with ~4 mW of 488 nm light from a LED modulated at 40 MHz, and emission was collected at 490–550 nm using an intensified charge-coupled device camera (CoolSNAP HQ; Roper Scientific). To calculate the GFP lifetime, the intensities from 12 phase-shifted images (modulation depth ~70%) were fitted with a sinus function, and lifetimes were derived from the phase shift between excitation and emission. For internal controls, cells were co-cultured with MelJuSo cells expressing H2B–GFP only. Lifetimes were referenced to a 1 μM solution of rhodamine-G6 in saline that was set at a 4.11 ns lifetime. The donor FRET efficiency E_D was calculated as $E_D = 1 -$ (measured lifetime/GFP lifetime in control cells) (Zwart et al., 2005).

Filipin stainings

Filipin staining was performed on formaldehyde fixed cells for 2 hr at room temperature with 0.05 mg/ml freshly dissolved filipin (Sigma) in PBS supplemented with 0.5 % BSA, and imaged using a Zeiss Axiovert 200 microscope equipped with an AxioCam CCD camera and a 20 x Achroplan Ph2 dry lens. Filipin signal was recorded using a 365 nm excitation filter with 397 nm long pass emission. mRFP signal was recorded with a 546 nm excitation filter with 590 nm long pass emission (Zeiss). For data acquisition, the manufacturers' software was used.

Protein purification

His-Rab7, His-RILP, and GST-ORP1L were produced as previously described (Johansson et al., 2007). His-tagged mTBC1D15 was purified from human HEK293T cells. Cells were lysed in 0.5% Triton X-100, 20 mM Hepes (pH 7.5), 200 mM NaCl, 8 mM β-mercaptoethanol and Complete EDTA-free Protease Inhibitors Cocktail (Roche Diagnostics). The lysates was cleared by centrifugation and the supernatant was incubated with preequilibrated Talon Co^{2+} resin (Clontech Laboratories, Inc.) for 30 min. The resin was then washed extensively with 20 mM Hepes (pH 7.5), 200 mM NaCl and 8 mM β-mercaptoethanol. His-tagged mTBC1D15 was eluted with washing buffer supplemented with 500 mM imidazole. The purity and concentration of the eluted protein was determined by SDS-PAGE and Coomassie staining. GST-VAP-A construct in pGEX was a kind gift of Dr. N. Ridgway (Wyles et al., 2002). GST was removed by cleavage with thrombin by incubation at 30°C for 2 hr before inactivation and precipitation by 0.1 mM PMSF. GST was removed by glutathione beads and purity of the free VAP-A was checked by SDS-PAGE and Coomassie staining.

In vitro GTPase assay

The GTPase assay was performed as described previously (Askjaer et al., 1999). Briefly, His-Rab7 was loaded with [γ-^{32}P]GTP (10 mCi/ml, >5000 Ci/mmol, Amersham) in the presence of 10 mM EDTA. Loading was stopped by adding $MgCl_2$ to a concentration of 20 mM followed by gel filtration on a Bio-Spin 6 column (BioRad) equilibrated with buffer (0.1 M Tris-HCl pH 7.5, 10 mM $MgCl_2$, 2 mM dithiothreitol, 0.5 M NaCl). Reaction mixtures containing [γ-^{32}P]GTP Rab7 were pre-incubated with GST-ORP1L (3 μM) and/ or His-RILP (3 μM) in reaction buffer (40 mM Tris-HCl [pH 8.0], 50 mM NaCl, 8 mM $MgCl_2$, 1 mM DTT, 0.5 mM GTP, 0.1 mg/ml BSA, 1 mM phosphate, 1% glycerol) on ice for 10 min. To test the accessibility of TBC1D15 towards Rab7 in complex with ORP1L and/or RILP, His-tagged TBC1D15 (0.9 μM) was added to the reaction mixture. Reactions were incubated at 25°C and stopped after 15 min by addition of 1 ml of charcoal suspension (7% w/v charcoal, 10% v/v ethanol, 0.1 M HCl, 10 mM KH_2PO_4) (Bischoff and Ponstingl, 1995). The mixture was centrifuged for 2 min in a tabletop centrifuge. Release of free [^{32}P]orthophosphate was determined by scintillation counting in the supernatant.

The reconstitution assay was performed in a detergent/salt buffer (20 mM Hepes, pH 7.5, 200 mM NaCl, 4 mM β-mercaptoethanol, 5 mM $MgCl_2$, 0.05% [vol/vol] Triton X-100, and 50 μM GTP). 15 μg His-Rab7(Q67L) was coupled to 3 μl TALON beads and preloaded with GTP. Beads were washed to remove unbound His-Rab7(Q67L) and recombinant purified His-RILP (3 μg), GST-ORP1L (8.7 μg), VAP-A (2.2 μg) and MBP-p150^{Glued}(C25) (4.5 μg) were added to the beads as indicated and incubated in a total volume of 0.4 ml for 2 h at 4°C. Beads were washed extensively and MBP-p150^{Glued}(C25) (4.5 μg) or VAP-A (2.2 μg) was added to the beads as indicated. Proteins were subsequently incubated in a total volume of 0.4 ml of detergent/salt buffer for 30 min at 22°C. Beads were washed extensively and proteins bound to His-Rab7(Q67L) were analyzed by SDS-PAGE and Western blotting. Proteins were detected with the following antibodies: α-His (Amersham Biosciences), α-MBP (New England Biolabs), α-GST (kind gift of W. Moolenaar, NKI, Amsterdam). Direct binding of p150^{Glued} to VAP-A was assayed as follows. 30 μg GST-VAP-A or 15 μg GST was coupled to 15 μl glutathione-Sepharose 4B beads. Beads were washed to remove unbound proteins, and MBP-p150^{Glued}(C25) (4.5 μg) was added to the beads in a total volume of 0.4 ml for 30 min at 22°C. Beads were washed extensively and proteins bound to the glutathione-Sepharose

4B beads were analyzed by SDS-PAGE and Western blotting.

REFERENCES

Askjaer, P., Bachi, A., Wilm, M., Bischoff, F.R., Weeks, D.L., Ogniewski, V., Ohno, M., Niehrs, C., Kjems, J., Mattaj, I.W., et al. (1999). RanGTP-regulated interactions of CRM1 with nucleoporins and a shuttling DEAD-box helicase. Mol Cell Biol 19, 6276-6285.

Bischoff, F.R., and Ponstingl, H. (1995). Catalysis of guanine nucleotide exchange of Ran by RCC1 and stimulation of hydrolysis of Ran-bound GTP by Ran-GAP1. Methods Enzymol 257, 135-144.

Brummelkamp, T.R., Bernards, R., and Agami, R. (2002). A system for stable expression of short interfering RNAs in mammalian cells. Science 296, 550-553.

Goldstein, J.L., Basu, S.K., and Brown, M.S. (1983). Receptor-mediated endocytosis of low-density lipoprotein in cultured cells. Meth Enzymol 98, 241-260.

Johansson, M., Rocha, N., Zwart, W., Jordens, I., Janssen, L., Kuijl, C., Olkkonen, V.M., and Neefjes, J. (2007). Activation of endosomal dynein motors by stepwise assembly of Rab7-RILP-p150Glued, ORP1L, and the receptor betalll spectrin. J Cell Biol 176, 459-471.

Jordens, I., Fernandez-Borja, M., Marsman, M., Dusseljee, S., Janssen, L., Calafat, J., Janssen, H., Wubbolts, R., and Neefjes, J. (2001). The Rab7 effector protein RILP controls lysosomal transport by inducing the recruitment of dynein-dynactin motors. Curr Biol 11, 1680-1685.

Liscum, L., Ruggiero, R.M., and Faust, J.R. (1989). The intracellular transport of low density lipoprotein-derived cholesterol is defective in Niemann-Pick type C fibroblasts. J Cell Biol 108, 1625-1636.

Marsman, M., Jordens, I., Kuijl, C., Janssen, L., and Neefjes, J. (2004). Dynein-mediated vesicle transport controls intracellular Salmonella replication. Mol Biol Cell 15, 2954-2964.

Reits, E.A., Vos, J.C., Gromme, M., and Neefjes, J. (2000). The major substrates for TAP in vivo are derived from newly synthesized proteins. Nature 404, 774-778.

Sugii, S., Lin, S., Ohgami, N., Ohashi, M., Chang, C.C., and Chang, T.Y. (2006). Roles of endogenously synthesized sterols in the endocytic pathway. J Biol Chem 281, 23191-23206.

Teuling, E., Ahmed, S., Haasdijk, E., Demmers, J., Steinmetz, M.O., Akhmanova, A., Jaarsma, D., and Hoogenraad, C.C. (2007). Motor neuron disease-associated mutant vesicle-associated membrane protein-associated protein (VAP) B recruits wild-type VAPs into endoplasmic reticulum-derived tubular aggregates. J Neurosci 27, 9801-9815.

Wubbolts, R., Fernandez-Borja, M., Jordens, I., Reits, E., Dusseljee, S., Echeverri, C., Vallee, R.B., and Neefjes, J. (1999). Opposing motor activities of dynein and kinesin determine retention and transport of MHC class II-containing compartments. J Cell Sci 112 (Pt 6), 785-795.

Wyles, J.P., McMaster, C.R., and Ridgway, N.D. (2002). Vesicle-associated membrane protein-associated protein-A (VAP-A) interacts with the oxysterol-binding protein to modify export from the endoplasmic reticulum. J Biol Chem 277, 29908-29918.

Zhang, X.M., Walsh, B., Mitchell, C.A., and Rowe, T. (2005). TBC domain family, member 15 is a novel mammalian Rab GTPase-activating protein with substrate preference for Rab7. Biochem Biophys Res Commun 335, 154-161.

Supplemental Figure S1

Supplemental Table a

Symbol	Domain(s)
USP6NL (RNTRE)	
TBC1D17	
TBC1D15	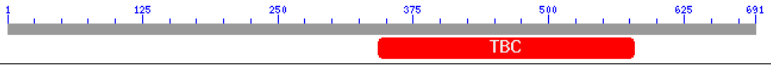
TBC1D5	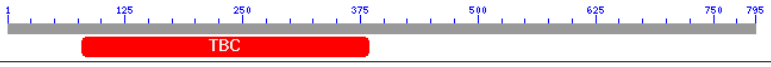
TBC1D2	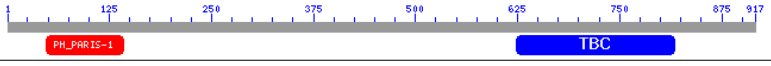
TBC1D2B	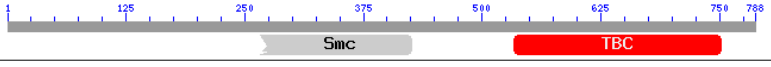
RABGAP1L	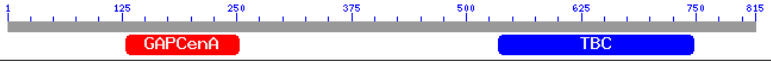
TBC1D4 (AS160)	
SGSM3	

Supplemental Table b

Symbol	shRNAi sequences
USP6NL (RNTRE)	AAGTCACAGATAGATTTGGCTTT AAAGCTTAAAGATGAGGCAGATT
TBC1D17	AATTCCCCTTCCCGGATGTCCTT
TBC1D15	AATGGGACATGGTTAATACAGTT AAGGCATGAAGACCCAGCTAATT
TBC1D5	AAGGTTGTTGGCCAACAAGATTT AACTGTTAGCACCTATAGTCTTT
TBC1D2	AAGCCTTCTCTGACCATCAGTTT AAGGTGGTGTTTCGCTATGCCTT
TBC1D2B	AAATTCCATTAATTTTTACTCTT AAGTACAAGGAAGAGGAGATTTT
RABGAP1L	AAAAACCTCAACTGAAGATAGTT AAAGGCCAAGCAGTCTTCTTGTT
TBC1D4 (AS160)	AACAGCCACGACCTCACCTACTT AATGTGAGAGCTTTGAAAATATT
SGSM3	AACCCCCTTGGTGGGCCTGTGTT AAGTGGTACCAGCCCTGGTCCTT

Supplemental Figure S1. Table a: Domain structure of the nine potential Rab GTPase GAPs tested by shRNA-mediated silencing. Name (Symbol), domain structure (Domain(s)) and size (numbers indicate amino acid residues) are indicated. The TBC domain is typical for GAPs for Rab GTPases. Table b: Sequences of primers cloned into pSUPER used for silencing of potential GAP proteins.

Supplemental Figure S2

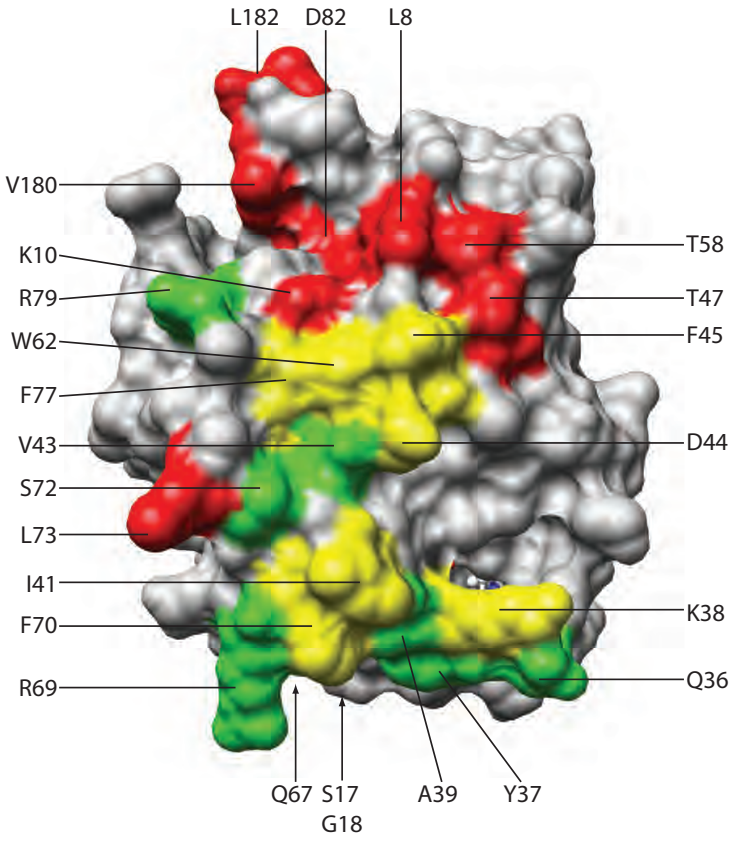

Rab7 interacting with RILP or TBC1D15.

Supplemental Figure S2. Overlapping interaction surfaces in GTP-Rab7 for TBC1D15 and RILP. Residues interacting with RILP are coloured red. The interaction with RILP is based on the crystal structure of the RILP-Rab7 complex (Wu et al., 2005). Residues predicted to interact with TBC1D15 are coloured green. The prediction is based on the structure of GYP1 and Rab33 (Pan et al., 2006). Given that both TBC1D15 and GYP1 contain a conserved TBC domain which interacts with the cognate GTPase, the interaction of TBC1D15 with Rab7 is likely similar to that of GYP1 with Rab33. Residues shared by RILP and TBC1D15 are coloured yellow.

The large surface area predicted to be shared between RILP and TBC1D15 suggests that binding of RILP to Rab7 will prevent binding of TBC1D15. In this way, RILP not only locks Rab7 in the GTP-bound active state (Marsman et al., 2006), but also prevents access of the GTPase-activating protein TBC1D15.

Chapter 4

A splice variant of RILP induces lysosomal clustering independent of dynein recruitment

Reproduced from Biochem Biophys Res Commun.2006.344:747-56

A splice variant of RILP induces lysosomal clustering independent of dynein recruitment

Marije Marsman [1], Ingrid Jordens [1], Nuno Rocha, Coenraad Kuijl, Lennert Janssen, Jacques Neefjes *

Division of Tumor Biology, The Netherlands Cancer Institute, Amsterdam 1066CX, The Netherlands

Received 14 March 2006
Available online 6 April 2006

Abstract

The small GTPase Rab7 controls fusion and transport of late endocytic compartments. A critical mediator is the Rab7 effector RILP that recruits the minus-end dynein–dynactin motor complex to these compartments. We identified a natural occurring splice variant of RILP (RILPsv) lacking only 27 amino acids encoded by exon VII. Both variants bind Rab7, prolong its GTP-bound state, and induce clustering of late endocytic compartments. However, RILPsv does not recruit the dynein–dynactin complex, implicating exon VII in motor recruitment. Clustering might still occur via dimerization, since both RILP and RILPsv are able to form hetero- and homodimers. Moreover, both effectors compete for Rab7 binding but with different outcome for dynein–dynactin recruitment and transport. Hence, RILPsv provides an extra dimension to the control of vesicle fusion and transport by the small GTPase Rab7.

Keywords: Rab7; RILP; Late endosomes; Lysosomes; Dynein; MTOC

Compartments of the biosynthetic and endocytic pathways continuously undergo fusion and fission events to maintain their integrity. The family of Rab GTPases regulates these processes. Beside regulating membrane fusion, Rab GTPases also regulate membrane transport [1–4]. In principle, one single Rab can regulate distinct steps in these processes by binding to one or more effector proteins. Moreover, each Rab member localizes to a specific compartment and cycles between an active GTP-bound state and an inactive GDP-bound state, thereby providing a temporal and spatial resolution in the regulation of membrane transport and fusion, for review see [4–8].

Rab7 is a key regulator in transport and fusion of late endosomes and lysosomes [9–14]. Three Rab7 effectors have been described, Rab7-interacting lysosomal protein (RILP), oxysterol-binding protein (OSBP)-related protein-1L (ORP1L), and Rabring7 [1,15–17]. Rabring7 has a zinc finger domain and specifically interacts with Rab7-GTP. Expression of Rabring7 results in clustering of late endosomes and lysosomes in the perinuclear area [16]. ORP1L expression can also induce lysosomal clustering. ORP1L has a conserved OSBP-related ligand-binding domain, an N-terminal extension with three ankyrin repeats, and a pleckstrin homology domain (PHD). RILP, which is unrelated to ORP1L and Rabring7, also interacts with Rab7-GTP and overexpression induces clustering of late endosomes and lysosomes [1,15]. In addition, both RILP and ORP1L can induce recruitment of the motor complex dynein–dynactin onto late endosomes and lysosomes, which facilitates their transport towards the minus-end of the microtubules [1,17].

Recently, the Golgi-restricted Rab34 has been implicated in lysosomal positioning [18]. Overexpression of wild type or constitutively active Rab34 resulted in clustering of late endosomal and lysosomal compartments in the perinuclear area. Although the precise mechanism has not

* Corresponding author. Fax: +31 02 5122029.
E-mail address: j.neefjes@nki.nl (J. Neefjes).
[1] These authors contributed equally to this work.

been revealed, it could be due to interaction with RILP [18].

Two RILP-like proteins have been identified, RLP1 and RLP2 [19], which share two highly conserved RILP homology domains, RH1 and RH2. Interestingly, both RLP1 and RLP2 are unable to bind to Rab7 and cannot induce lysosomal clustering. Yet, insertion of a domain of RILP (aa 274–333), containing the recently identified Rab7-binding domain, causes RLP1 to interact with Rab7 and to induce clustering of late endosomes and lysosomes [20].

Here, we describe a splice variant of RILP (RILPsv) lacking exon VII (aa 315–342). RILPsv still interacts with Rab7-GTP, but it lacks the ability to induce recruitment of the dynein–dynactin complex. However, like RILP, RILPsv can dimerize and is able to induce clustering of Rab7-positive compartments. Co-expression of full-length RILP can restore motor recruitment in RILPsv-expressing cells indicating that RILP can compete with RILPsv for Rab7 binding in vivo. Thus, splice variants can add an additional layer of complexity to regulation of intracellular vesicle transport.

Materials and methods

Plasmids. Wild type Rab7 [11,21] and Rab5 [22,23] were subcloned into the bacterial expression vectors pRP261 to generate glutathione-*S*-transferase (GST) fusion proteins. For myc-tagging Rab7 was cloned into pcDNA3. For yeast two-hybrid assay, the Rab7 binding half of RILP and RILPsv were both cloned into pACT. Rab7wt, Rab7Q67L, Rab7T22N, and Rab7I125N were after deletion of the CAAX box cloned into the pGBT9 (Stratagene). GFP-Rab7wt, GFP-RILPdeltaN (aa 199–401), and RILP-myc were described before [1].

RILPsv was subcloned into eukaryotic expression vector pcDNA3 (Invitrogen) with or without myc-tag introduced by PCR. All PCR products were sequence verified. For GFP-tagging both RILP and RILPsv were subcloned into the eukaryotic EGFP-C1 vector (Clontech).

RT-PCR. Human tissue RNAs were obtained from D. Atsma (Pathology, Netherlands Cancer Institute) isolated from lung, lymph node, and intestine. RNAs were isolated from the cell lines T47D (breast carcinoma), 603D (melanoma), and WiDR, and Colo205 (colon carcinoma) by TriZol following the manufacturer's protocol. mRNAs transcribed using SuperScript™ II reverse transcriptase (Invitrogen) by oligo(dT). The first-strand cDNA synthesis was performed using oligo's QS (654–673 bp) and QAS3 (1218–1238 bp). This product was used in a second nested PCR using WTS (751–768 bp) and QAS3.

Antibodies and markers. The following antibodies were used: rabbit polyclonal anti-CD63 [24] and mouse monoclonal anti-CD63 (Cymbus Biotechnology), mouse monoclonal anti-EEA-1 (BD Transduction laboratories), mouse monoclonal anti-Golgin-97 (Molecular Probes), mouse monoclonal anti-dynactin p50 and mouse monoclonal anti-p150^{Glued} (BD Transduction laboratories), mouse monoclonal anti-vsv (P5D4F7) and mouse monoclonal anti-myc (9E10), and rabbit polyclonal anti-RILP [1]. For immuno-staining, antibodies were diluted in PBS containing 0.5% BSA. Alexa 488- or Texas Red/Alexa 568-conjugated mouse or rabbit secondary antibodies were used (Molecular Probes, Leiden, The Netherlands).

For living cell analyses, lysosomal compartments were labeled by LysoTracker Red (Molecular Probes, Leiden).

Tissue culture. The human melanoma cell line Mel JuSo was maintained in Iscoves medium (GIBCO-BRL) supplemented with 7.5% FCS, 2 mM glutamine, 100 U/ml penicillin, and 100 μg/ml streptomycin. Mel JuSo stably transfected with GFP-Rab7 [1] were maintained in the same medium supplemented with 500 μg/ml G418 (GIBCO-BRL). The cells were grown at 37 °C under 5% CO_2. HeLa cells were maintained in Iscoves medium (GIBCO-BRL) supplemented with 7.5% FCS, 2 mM glutamine, 100 U/ml penicillin, and 100 μg/ml streptomycin. Cells were transiently transfected by polyethylenimine 25 kDa (PEI) transfection (Polysciences). The transfectants were cultured for 24–48 h prior to fixation or further processing.

Micro-injection and confocal analyses. For micro-injection, cells were seeded on coverslips in medium lacking G418 24 h before the experiment, to achieve 40–60% confluency at the time of injection. Cells were injected on a heated xy stage of an Olympus XL70 microscope equipped with an Eppendorf manipulator 5171/transjector 5246 system. Usually, 50–100 cells were injected intranuclearly with a mix of cDNAs (100–200 ng/μl). Texas Red Dextran-70 (Molecular Probes, Leiden) was used as injection marker. Cells were subsequently cultured at 37 °C and, 3–7 h after micro-injection, living cells were analyzed or cells were fixed and immuno-stained before analysis. Fixation was either in 3.7% formaldehyde for 15 min followed by permeabilization in 0.1% Triton X-100 or in methanol (−20 °C) for 2 min. All experiments presented were repeated several times on different days and results were consistent and reproducible.

Confocal analyses were performed using a Leica TCS SP confocal laser-scanning microscope (CLSM) equipped with an Argon/Krypton laser (Leica Microsystems, Heidelberg, Germany). Green fluorescence was detected at $\lambda > 515$ nm after excitation at $\lambda = 488$ nm. For dual analyses, green fluorescence was detected at $\lambda = 520$–560 nm. Red fluorochromes were excited at $\lambda = 568$ nm and detected at $\lambda > 585$ nm.

Fluorescence recovery after photobleaching. Fluorescence recovery after photobleaching (FRAP) experiments were performed as described [1,25]. In brief, Mel JuSo cells expressing GFP-Rab7 were grown on coverslips in Iscoves medium lacking G418 at least 48 h before the experiment. cDNA encoding RILP or RILPsv mixed with 70 kDa TxR-dextran were introduced by micro-injected and cells were analyzed in culture chamber at 37 °C by CLSM. A small set of fluorescent vesicles was bleached for 1 s by a high intensity laser beam and the fluorescence recovery in the bleached spot was quantified. LysoTracker Red was used to identify the bleached vesicles. When RILP or RILPsv was introduced, FRAP analysis was performed 1–4 h after micro-injection in cells where clustering of the Rab7-positive vesicles was apparent. The experiments were performed on multiple cells and at various days. Because the bleached vesicles were not completely stationary their positions were tracked by LysoTracker Red and corrected with a program written in Matlab (Mathworks).

Expression and purification of recombinant proteins. RILP and RILPsv were expressed in *Escherichia coli* strain Rosetta(DE3)pLysS (Novagen) at 20 °C overnight as hexahistidine-tagged (His_6-tagged) fusions using the pETM-11 expression vector (kind gift of Gunther Stier, EMBL, Heidelberg, Germany). After collection, bacteria were resuspended in buffer A (25 mM Hepes, pH 7.5, 300 mM NaCl, complete EDTA-free tablets (Roche), 1 mM PMSF, 5 mM β-mercaptoethanol, 10 mM imidazole, and 0.05% (v/v) Triton X-100) and lysed by sonication on ice. All subsequent steps were performed at 4 °C. Lysates were loaded onto pre-equilibrated BD Talon Metal Affinity (Clontech) resin and washed with buffer A containing 20 mM imidazole. The resin was then packed into a column and bound proteins were eluted with buffer A containing 400 mM imidazole. Eluted proteins were concentrated in storage buffer (25 mM Hepes, pH 7.5, 300 mM NaCl, and 10% (v/v) glycerol) using a Vivaspin-2 concentrator (Vivascience), shock-frozen, and stored at −80 °C.

Rab7 was cloned into pET-28a (Novagen) and expressed as His_6-tag fusion in *E. coli* strain BL21(DE3)pLysS. Recombinant His-Rab7 protein was purified under native conditions by affinity-chromatography using Ni^{2+} according to the manufacturers (Qiagen).

Rab7 and Rab5 were expressed in Rosetta(DE3)pLysS as GST fusions using the expression vector pRP261, a derivative of pGEX-3X (Amersham Biosciences). GST-fusions were affinity-purified using the glutathione–Sepharose 4B resin (Amersham Biosciences) as described by the manufacturer. Protein concentration was determined using the Bradford protein concentration assay (Bio-Rad) calibrated with bovine serum albumin standards.

Pull-down assays and immunoblot analysis. For the GST pull-down assay, 100 μg of GTPγS preloaded GST-Rab7 or GST-Rab5 immobilized on 20 μl of packed glutathione–Sepharose 4B (Amersham Biosciences)

resin was used per 5×10^6 Mel JuSo cells. For the His-tag pull-down assay, 20 µg of either His_6-RILP or His_6-RILPsv was immobilized on 10 µl of packed Talon resin.

Mel Juso cells were electroporated with either GFP-RILP or GFP-RILPsv. At 24–30 h after electroporation, cells were washed twice with PBS and lysed for 20 min on ice in binding buffer (20 mM Hepes, pH 7.5, 100 mM NaCl, 0.1% (v/v) Nonidet P-40, 5 mM EDTA, 10 mM $MgCl_2$, 1 mM DTT, and Complete EDTA-free protease inhibitor cocktail (Roche)). Total lysates were cleared by centrifugation at 12,000*g* for 10 min at 4 °C. Supernatants were incubated with immobilized GST-fusions or His_6-fusions for 2 h at 4 °C. Resin fractions were washed five times with 20 mM Hepes, pH 7.5, 150 mM NaCl, 0.1% (v/v) Nonidet P-40, 10 mM $MgCl_2$, and 1 mM DTT and resuspended in reducing Laemmli sample buffer. Protein samples were separated by SDS–PAGE, transferred onto PVDF membranes and probed with polyclonal anti-GFP before detection by ECL (Amersham).

In vitro GTPase assay. GTPase activity in solution was assayed by release of [^{32}P]Pi using a modified charcoal binding assay [26,27]. His_6-Rab7 (50 pmol) was preloaded with 4 µl of [γ-^{32}P]GTP (5000 Ci/mmol, Amersham Biosciences) in preload buffer (50 mM Tris/HCl, pH 7.5, 250 mM NaCl, 1 mM DTT, 5% (v/v) glycerol, and 0.5 mg/ml BSA) supplemented with 10 mM EDTA on ice for 2 h in 10 µl total volume. Preload reactions were diluted with 20 µl of preload buffer supplemented with 20 mM $MgCl_2$ prior to passage at 4 °C through a P-6 polyacrylamide Micro Bio-Spin column (Bio-Rad) pre-equilibrated with preload buffer supplemented with 10 mM $MgCl_2$.

The effect of RILP or RILPsv on the intrinsic GTP hydrolysis of Rab7 was analyzed by incubating preloaded His_6-Rab7 in reaction buffer (40 mM Tris/HCl, pH 8.0, 8 mM $MgCl_2$, 1 mM DTT, and 2 mM GTP) alone (intrinsic hydrolysis) or with 3 µM of His_6-RILP, His_6-RILPsv, or BSA. Reactions were performed for 5 h at 25 °C. Triplicate timed 50 µl aliquots were mixed with 1 ml of 7% activated charcoal (w/v) in 10 mM KH_2PO_4 on ice. The mixture was vortexted, and centrifuged at 3000*g* for 5 min at 4 °C, and the [^{32}P]Pi release in the pellet fraction was quantified by liquid scintillation counting.

Results

RILPsv, a natural occurring splice variant of the Rab7 effector RILP

Late endosomal and lysosomal transport is regulated by the small GTPase Rab7 and its effector RILP (Rab7-interacting lysosomal protein) [1,15]. Upon activation, Rab7 interacts with RILP, thereby recruiting the minus-end motor complex dynein–dynactin, which results in the accumulation of late endosomal/lysosomal compartments at the microtubule-organizing center (MTOC) [1].

Beside RILP, an alternatively spliced variant of RILP (RILPsv) was identified in the original yeast two-hybrid screen with Rab7. This variant lacks amino acids 315–342, encoded by exon VII, which represents a proline-rich region (Fig. 1A). RILPsv still contains the two coiled-coil regions and the spliced region partially overlaps with the area interacting with Rab7 and regulating clustering of late endosomes and lysosomes [19,20]. In the two-hybrid screen, the splice variant still interacted with Rab7, yet the preference for the GTP-bound form seemed less pronounced (Table S1).

Several human est sequences for RILP were found in the database that specifically lacks exon VII (data not shown). Moreover, RILPsv appeared to be present in different cell types and tissues, which is shown by RT-PCR (Fig. 1B). Two products corresponding to the expected sizes for, respectively, RILP and RILPsv appeared in the nested PCR using oligo's located in exon VI and VIII (Fig. 1B). As a positive control cDNA encoding RILP was used.

Ectopic expression of RILPsv causes clustering of late endocytic compartments

RILP induces clustering of late endosomal and lysosomal compartments tightly around the MTOC [1,15]. To compare the phenotypes of RILPsv and RILP, both proteins were expressed in Mel JuSo cells. Cells were fixed and stained for RILP (Fig. 2A, middle panels) and RILPsv (Fig. 2B, middle panels). The early endosomes and Golgi apparatus were identified by the markers EEA-1 (Figs. 2A and B, lower-left panel) and Golgin (Figs. 2A and B,

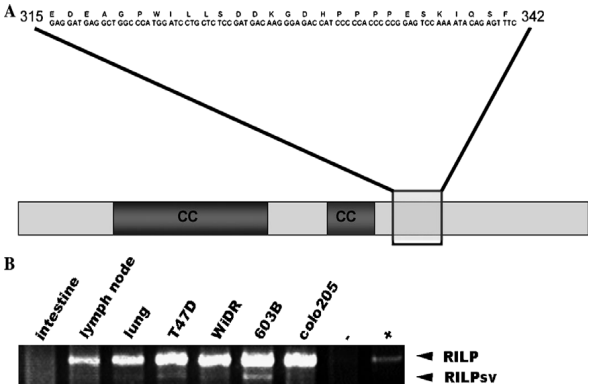

Fig. 1. A natural occurring splice variant of the Rab7 effector RILP. (A) Schematic representation of RILP (CC: represents the predicted coiled-coil region) and the amino acid sequence corresponding to exon VII, aa 315–342, absent in RILPsv is depicted by the gray box. (B) RNA isolated from indicated tissues and cell lines were analyzed by RT-PCR. PCR was performed with oligo's flanking exon VII and product sizes of both RILP and RILPsv are indicated.

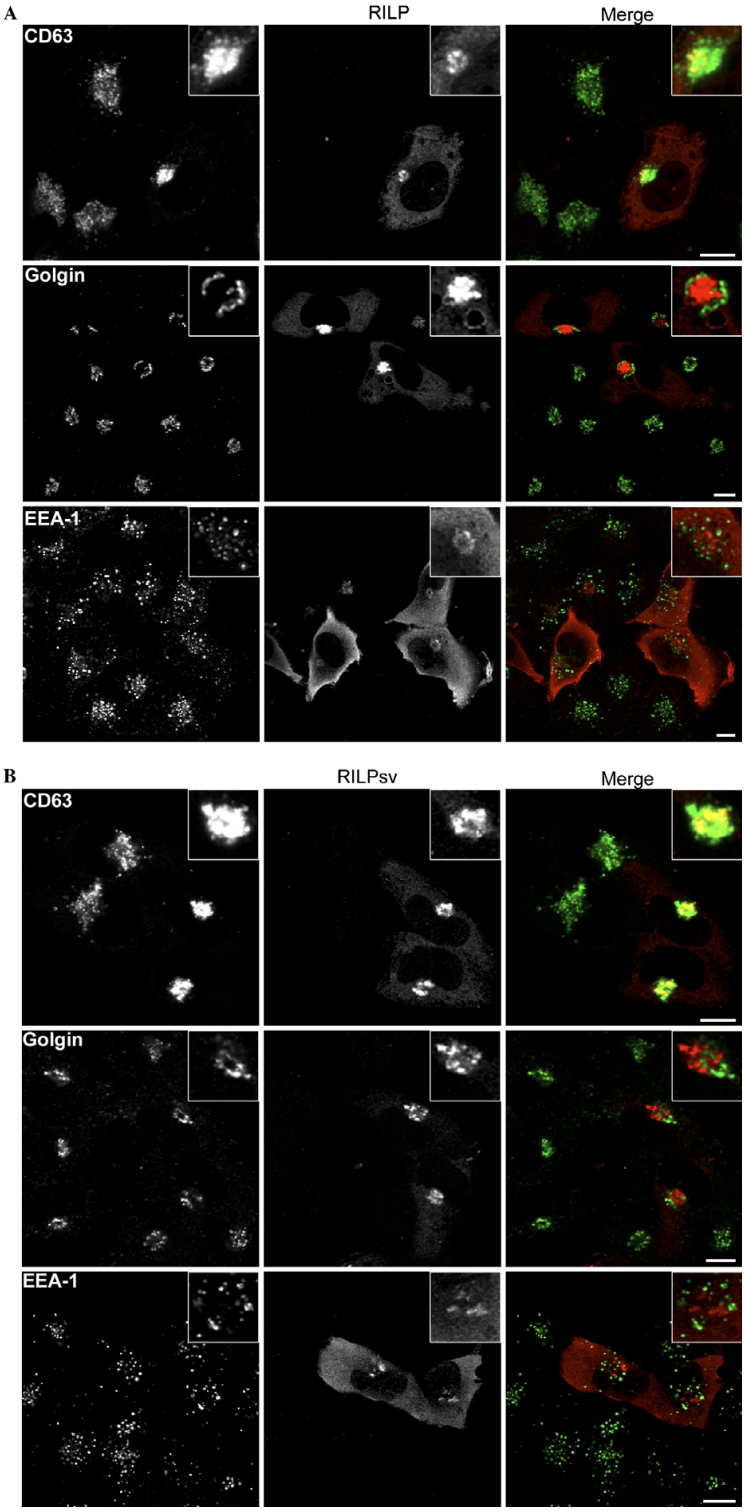
A
RILP
Merge
CD63
Golgin
EEA-1
B
RILPsv
Merge
CD63
Golgin
EEA-1

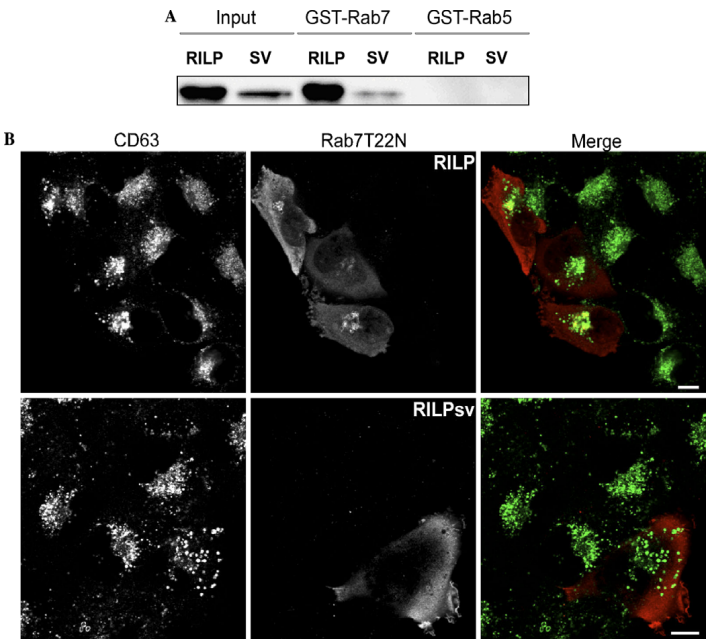

Fig. 3. Functional Rab7 is required for late endocytic clustering induced by RILPsv. (A) Equal amounts of GST-Rab7 or GST-Rab5 coupled to glutathione–Sepharose beads were incubated with cell lysates from Mel Juso cells expressing GFP-RILP or GFP-RILPsv. Proteins were transferred to PVDF and visualized by anti-GFP. RILP and RILPsv bind to GST-Rab7 (lanes 3 and 4), but not to GST-Rab5 (lanes 5 and 6). (B) Dominant-negative Rab7T22N was co-expressed in molar excess with RILP (upper panels) or RILPsv (lower panels) via micro-injection and immuno-labeled for CD63 (left panel) and RILP/RILPsv (middle panels). Co-expression of Rab7T22N (expression verified in single labeling; not shown) partially reversed the phenotypes of RILP and RILPsv (lower panels), shown by dispersed instead of clustered lysosomes (right panel). Bars equal 10 μm.

middle-left panel). RILPsv as well as RILP only affected the distribution of late endosomal and lysosomal compartments marked by CD63 (Figs. 2A and B, upper-left panel). The early endosomes were unaffected. It should be noted that the Golgi was still located perinuclearly, only the position of the late endosomes and lysosomes relative to the Golgi was affected. Whereas late endosomes and lysosomes in RILP-expressing cells moved inside the Golgi area, they remained clustered around or in-between the Golgi in RILPsv-expressing cells.

When the clusters were analyzed in more detail, we observed that the effect of RILP and RILPsv on late endosomal/lysosomal positioning was different. Whereas RILP induced a tight cluster of late endosomal/lysosomal compartments (Fig. 2A), RILPsv induced a less condensed, more dispersed cluster and often smaller separated clusters are observed (Fig. 2B). In HeLa cells, where late endosomes and lysosomes have a more dispersed localization, the difference between RILP and RILPsv is even more apparent (Figs. S1 and S2). These results indicate that exon VII affects clustering of late endosomes and lysosomes.

Functional Rab7 is necessary for late endosomal/lysosomal clustering induced by RILPsv

Both RILPsv and RILP interact with Rab7 in yeast two-hybrid assay. However, RILP induced a stronger transactivation, suggesting that it associates with Rab7 with a higher affinity (Table S1). To biochemically confirm that Rab7 interacts with both, RILP and RILPsv, Mel JuSo cells were transfected with cDNA encoding either EGFP-tagged RILP or RILPsv. Twenty-four hours after transfection, cells were lysed. Lysates were incubated with GST-Rab5wt or GST-Rab7wt immobilized on glutathione beads and

Fig. 2. RILPsv causes clustering of late endocytic compartments. (A) CLSM analyses of Mel Juso cells expressing either RILP or (B) RILPsv, immunolabeled with anti-CD63 (upper panel), anti-Golgin (middle panel) or anti-EEA-1 (lower panel). Both RILP and RILPsv only affect the localization of late endosomes and lysosomes as observed by clustering of CD63-positive compartments. Both EEA-1 and Golgi distribution are not affected, although the Golgi is partially repositioned when late endosomes and lysosomes occupy the space around the MTOC. Insets of the RILP clusters are shown in the upper right corner of the panel. Bars equal 10 μm.

bound proteins were detected by Western blotting with anti-GFP. Both EGFP-RILP and EGFP-RILPsv were pulled down only with GST-Rab7 and not with the related GST-Rab5 (Fig. 3A).

The involvement of Rab7 in the formation of the lysosomal clustering induced by RILPsv was studied in more detail by co-expression of a dominant-negative mutant of Rab7, Rab7T22N. High expression of Rab7T22N results in dispersion of the late endosomes and lysosomes. Upon co-expression with RILP, Rab7T22N can partially reverse RILP-induced clustering [1]. Cells were fixed and stained for CD63 (Fig. 3B, left panels), RILP or RILPsv (Fig. 3B, middle panels) 7 h after co-injection of cDNAs encoding, respectively, RILP or RILPsv and Rab7T22N. Clustering was reversed in a low percentage of the RILP-expressing cells, whereas almost all RILPsv-expressing cells showed a dispersed phenotype (Fig. 3B). Note the difference in distribution between RILP and RILPsv when co-expressed with Rab7T22N; RILPsv dissociated from the membrane, whereas RILP remained associated to the membrane. This again suggests that RILP interacts more strongly with endogenous Rab7 than RILPsv.

Binding of RILPsv to Rab7 prolongs its GTP-bound active state

Fluorescent recovery after photobleaching (FRAP) was successfully used to study the GTPase activation cycle of EGFP-tagged Rab7 [1,28]. After bleaching a portion of membrane-bound EGFP-Rab7, the recovery of fluorescence in the bleached spot was measured in time by CLSM. The recovery represents GTP hydrolysis and replacement of bleached membrane-bound EGFP-Rab7 with fluorescent EGFP-Rab7 from the cytosol, and thus represents the Rab7 activation cycle. Using this approach we showed that RILP locks Rab7 in the active, membrane-bound form [1].

To determine whether RILPsv has a similar effect on the Rab7 cycle, RILP or RILPsv was expressed in a Mel JuSo cell line stably expressing EGFP-Rab7. As shown before, in wild type EGFP-Rab7 expressing cells the mobile fraction (the percentage of maximal recovered EGFP-Rab7) is 64% (Figs. 4A and B) [1,28]. RILP expressing cells showed rapid clustering of the EGFP-Rab7 containing vesicles and a concomitant drop in the mobile fraction of EGFP-Rab7 to approximately 10% (Figs. 4A and B). Expression of RILPsv had a similar effect on recovery; after bleaching, only 20% of the EGFP-Rab7 was recovered (Figs. 4A and B). In both cases an accurate recovery time ($t_{1/2}$) could not be determined.

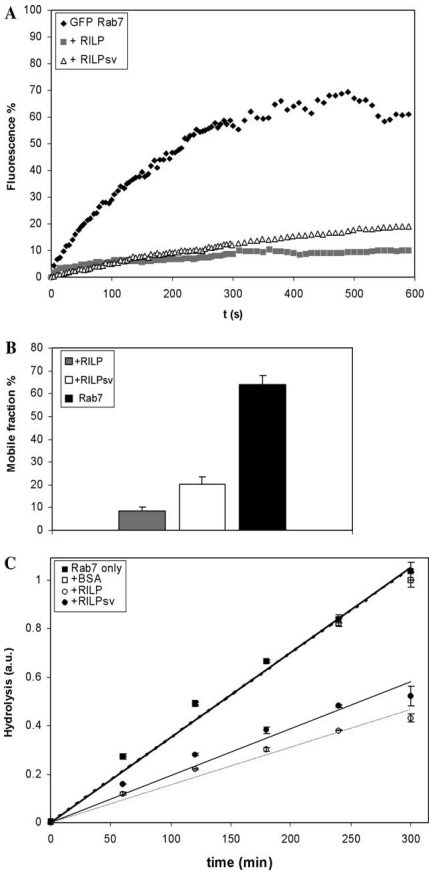

Fig. 4. RILPsv arrests Rab7 in the active state. (A) The Rab7 GTPase cycle was studied using FRAP. A portion of GFP-Rab7 compartments in control cells and cells expressing RILP or RILPsv were bleached and recovery of fluorescence in the bleached spot was plotted in a recovery curve. The fluorescence was related to the initial fluorescence set at 100%, $t = 0$ is the first measurement after the bleach. (B) Quantifications of the mobile fractions deduced from the recovery curves including SE are depicted ($n = 5$–10). (C) An in vitro assay was used to measure the GTPase cycle using [γ-^{32}P]GTP, in which the hydrolysis of GTP was followed in time by monitoring the release of [^{32}P]Pi. [^{32}P]Pi is slowly released from GTP-Rab7 (filled squares). Addition of His-RILP (open circles) and His-RILPsv (closed circles) significantly reduced the GTP hydrolysis rate of Rab7. BSA had no effect on the hydrolysis of Rab7 (open squares) and hydrolysis of Rab5 was not affected by the addition of His-RILP or His-RILPsv (data not shown).

Fig. 5. RILPsv fails to recruit dynein motors to late endocytic compartments. (A) CLSM analysis of Mel Juso cells ectopically expressing either RILP (upper panel) or RILPsv (middle and lower panels). RILP and RILPsv were labeled with anti-RILP (middle panels) and dynein–dynactin motors were visualized by anti-p150^{Glued} (left panels). (B) Motor recruitment in RILP and RILPsv expressing cells was quantified. Values are given as mean percentage of p150^{Glued} recruitment ± error bars indicating the standard deviation (>100 injected cells counted in two independent experiments). RILPsv shows a major reduction in dynein–dynactin motor recruitment. (C) Co-expression of RILP in RILPsv-expressing cells could restore the motor recruitment. RILP and RILPsv were expressed via micro-injection and labeled with anti-RILP (right panels) and dynein–dynactin motors were labeled by anti-p150^{Glued} (middle panels). Bars equal 10 μm.

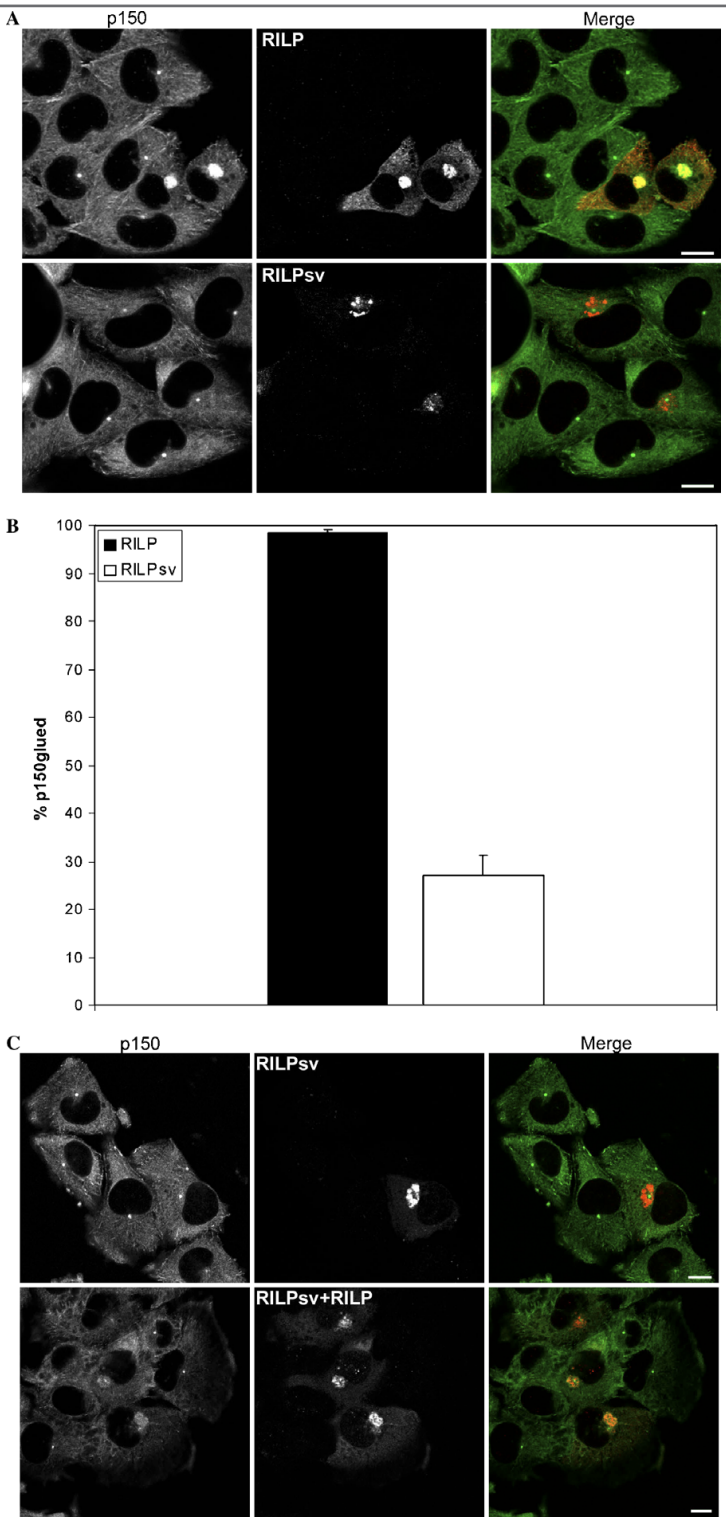
A
p150
Merge
RILP
RILPsv
B
RILP
RILPsv
% p150glued
100
90
80
70
60
50
40
30
20
10
0
C
p150
Merge
RILPsv
RILPsv+RILP

Beside the in vivo approach using FRAP, we used an in vitro approach using [γ-^{32}P]GTP to study the effect of His_6-RILP and His_6-RILPsv on the intrinsic GTPase activity of Rab7 [26,27]. Quantification of [^{32}P]Pi released from GTP-bound Rab7 showed that even after 5 h of hydrolysis saturation was not reached. This is consistent with the rather slow intrinsic GTPase activity of Rab7 [29] (Fig. 4C).

In order to test the effect of RILP and RILPsv on the hydrolysis rate of Rab7, His_6-RILP or His_6-RILPsv proteins were incubated with [γ-^{32}P]GTP loaded Rab7. Consistent with the FRAP data, addition of either His_6-RILP or His_6-RILPsv resulted in a significant decrease in GTP hydrolysis of Rab7 (Fig. 4C). Equimolar amounts of BSA had no effect on the GTP hydrolysis rate of Rab7 (Fig. 4C). Moreover, the addition of either His_6-RILP or His_6-RILPsv did not affect the hydrolysis rate of Rab5 (data not shown). Taken together, these data show that both RILP and RILPsv can strongly reduce Rab7 hydrolysis thereby keeping Rab7 in the active GTP-bound state.

Exon VII is critical for recruiting the minus-end dynein motor to late endocytic compartments

Although RILPsv like RILP interacts with Rab7, it results in a different phenotype upon ectopic expression. RILP has been shown to induce recruitment of the dynein–dynactin complex to late endosomal and lysosomal compartments [1]. To investigate whether RILPsv shares this ability with RILP, we injected cDNA encoding RILP or RILPsv in Mel Juso cells. After fixation, the p150^{Glued} subunit of the dynein–dynactin complex was detected. In RILP expressing cells, tight RILP-positive clusters were formed labeling for the p150^{Glued} subunit (Fig. 5A, upper panels). However, co-staining with p150^{Glued} was usually not observed in cells expressing RILPsv (Fig. 5A, lower panels). Quantification shows a significant decrease of approximately 70% in the recruitment of p150^{Glued} to the RILPsv-positive compartments (Fig. 5B). These findings indicate that exon VII is involved in the recruitment of the dynein–dynactin complex.

Interestingly, co-expression of RILP in RILPsv-expressing cells could restore motor recruitment (Fig. 5C), indicating that full-length RILP can compete with RILPsv for dynein recruitment to Rab7-positive compartments.

RILP and RILPsv both form hetero- and homo-dimers

Although RILPsv does not recruit the dynein–dynactin motor, it still induces clustering of late endocytic compartments. Other proteins have been described that cause clustering of late endosomal/lysosomal compartments independent of dynein–dynactin recruitment, such as mVPS18 and hVam6p [30,31]. These proteins are able to form homo-oligomers, which are critically involved in their ability to induce clustering. In addition, recent structural

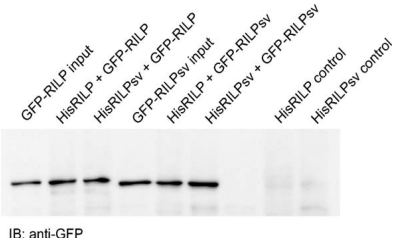

Fig. 6. RILP and RILPsv form hetero- and homo-dimers Mel Juso cells expressing GFP-RILP or GFP-RILPsv were lysed and incubated with either His-RILP or His-RILPsv coupled to Talon beads. Bound proteins were analyzed by immuno-blotting probed with anti-GFP antibodies. His-RILP and His-RILPsv can form both hetero- and homo-dimers with GFP-RILP and GFP-RILPsv. Non-transfected cells were used as a control.

data revealed that RILP acts as a dimer interacting with two Rab7 molecules [20]. To test the ability of RILP and RILPsv to form heterodimers, cells were electroporated with either EGFP-RILP or EGFP-RILPsv. Twenty-four hours after electroporation, cells were lysed and lysates were incubated with either His_6-RILP or His_6-RILPsv. Subsequently, lysates were run over a Ni^+ column to isolate the His-tagged proteins. Bound proteins were detected by Western blotting probed with anti-GFP (Fig. 6). His_6-RILP recruited both EGFP-RILP and EGFP-RILPsv. Moreover, His_6-RILPsv also interacted with EGFP-RILPsv. Thus, both RILP and RILPsv can form hetero- and homo-dimers, which might be responsible for the dynein-independent clustering of late endocytic structures in case of RILPsv.

Discussion

Late endosomal and lysosomal biogenesis is regulated by heterotypic and homotypic fusion, and bidirectional transport along microtubules to bring vesicles in close contact, for review see [4,6–8,32,33]. A key regulator in these processes is the small GTPase Rab7 [9–14]. Thus far, three Rab7 effectors have been described: Rabring7, RILP, and ORP1L [1,15–17]. All effectors induce lysosomal clustering. Additionally, ORP1L and RILP sequester dynein–dynactin motors onto lysosomal compartments resulting in a tight accumulation around the MTOC [1,17]. Here, we describe a natural occurring splice variant of RILP (RILPsv) lacking exon VII. Exon VII contains a proline-rich domain which is involved in protein–protein interactions. Like RILP, RILPsv also induces lysosomal clustering (albeit not as tight as RILP), but does not induce the recruitment of the dynein motor complex. This defines a proline-rich region of 27 amino acids, representing exon VII, involved in transferring a signal from Rab7 to the dynein motor complex.

Recently, Wang et al. [19] described two RILP-like proteins, RLP1 and RLP2, containing two highly conserved RILP homology domains. These proteins do not associate

with Rab7-positive compartments and do not affect the position of late endosomes and lysosomes. However, introduction of a 62 amino acid domain of RILP (274–333) could restore the ability of RLP1 to bind to Rab7 and to induce clustering of late endosomes and lysosomes.

RILPsv lacks amino acid 315–342, but still interacted with Rab7. This is in accordance with the observations by Wu et al. [20] that amino acids 241–320 of RILP are required for Rab7 binding, of which the main part is contained within RILPsv. Moreover, like RILP, RILPsv can lock Rab7 in the active, membrane-bound state as is shown by both the FRAP analyses and the GTPase assay. This is supported by the recently published crystal structure of Rab7 and RILP showing that RILP is a dimer surrounded by two GTP-loaded Rab7 proteins. The regions in RILP that contact the switch and interswitch regions of Rab7 are still present in RILPsv [20]. Interestingly, expression of RILPsv results in a different phenotype compared to that induced by RILP. This difference is more evident in HeLa cells, which have a less pronounced perinuclear localization of late endosomes and lysosomes compared to the melanoma-cell line Mel JuSo. We showed that the ability of RILPsv to induce recruitment of the minus-end dynein–dynactin motor complex is largely reduced, implicating exon VII in motor recruitment. Previously, we have shown that a deletion mutant of RILP lacking the N-terminal half (RILP-ΔN), still containing exon VII, fails to recruit the dynein motor as well [1]. Thus information in both the N-terminus and exon VII of RILP is required for dynein motor recruitment. Moreover, we show that RILP can compete with RILPsv for Rab7 binding, thereby inducing dynein motor recruitment. Thus, two products from the same gene can induce different effects in terms of motor protein recruitment, but compete for the same binding site: Rab7-GTP.

Although RILPsv cannot efficiently recruit the minus-end dynein motor, it induces late endosomal clustering. Two other late endosomal/lysosomal-associated proteins cause similar clustering without inducing dynein motor recruitment, mVPS18 and hvam6p [30,31]. These proteins are mammalian homologues of subunits of the yeast homotypic fusion complex, HOPS, which is involved in vacuolar fusion [34–42]. A common feature of mVPS18 and hvam6p is their CLH (clathrin homology) domain, which is essential for clustering of late endosomes and lysosomes. In addition, this domain appeared to be involved in homo-oligomerization and interaction with other components of the HOPS complex [30,31,43,44].

RILP has no CLH domain, but both RILP and RILPsv are able to hetero- and homo-dimerize. This might explain the observed phenotype for RILPsv. No dynein motor is recruited, but the hetero- or homo-dimerization of RILPsv with itself or endogenous RILP still results in clustering of lysosomal compartments, comparable to mVps18 and hvam6p. Yet, only full-length RILP induces dynein–dynactin motor recruitment resulting in a compact lysosomal cluster.

Our data describe a natural occurring splice variant of the Rab7 effector RILP lacking only 27 amino acids encoded in exon VII. This 27 amino acid, proline-rich stretch is critical for dynein-motor recruitment to Rab7-positive compartments and transport of these compartments to the microtubule minus-end. We show an example of a splice variant of an effector protein that adds an additional layer of complexity to the regulation of vesicle fusion and transport by Rab proteins.

Acknowledgments

We thank M. vd Vijver and D. Atsma for providing RNA isolated from different human tissues, members of the Neefixlab, A. Griekspoor and M. Voorhoeve for helpful discussions, and Lauran Oomen and Lenny Brocks for assistance with CLSM. This work was supported by grants from The Netherlands Cancer Society KWF and NWO (Zon MW PGS 912-03-026). N. Rocha is supported by a FCT/FSE PhD scholarship, within the Third Framework Program.

Appendix A. Supplementary data

Supplementary data associated with this article can be found, in the online version, at doi:10.1016/j.bbrc.2006.03.178.

References

[1] I. Jordens, M. Fernandez-Borja, M. Marsman, S. Dusseljee, L. Janssen, J. Calafat, H. Janssen, R. Wubbolts, J. Neefjes, The Rab7 effector protein RILP controls lysosomal transport by inducing the recruitment of dynein-dynactin motors, Curr. Biol. (2001) 1680–1685.
[2] E. Nielsen, F. Severin, J.M. Backer, A.A. Hyman, M. Zerial, Rab5 regulates motility of early endosomes on microtubules, Nat. Cell Biol. 1 (1999) 376–382.
[3] B. Short, C. Preisinger, J. Schaletzky, R. Kopajtich, F.A. Barr, The Rab6 GTPase regulates recruitment of the dynactin complex to Golgi membranes, Curr. Biol. 12 (2002) 1792–1795.
[4] I. Jordens, M. Marsman, C. Kuijl, J. Neefjes, Rab proteins, connecting transport and vesicle fusion, Traffic 6 (2005) 1070–1077.
[5] J.A. Hammer 3rd, X.S. Wu, Rabs grab motors: defining the connections between Rab GTPases and motor proteins, Curr. Opin. Cell Biol. 14 (2002) 69–75.
[6] M.C. Seabra, C. Wasmeier, Controlling the location and activation of Rab GTPases, Curr. Opin. Cell Biol. 16 (2004) 451–457.
[7] H. Stenmark, V.M. Olkkonen, The Rab GTPase family, Genome Biol. 2 (2001), REVIEWS3007.
[8] M. Zerial, H. McBride, Rab proteins as membrane organizers, Nat. Rev. Mol. Cell Biol. 2 (2001) 107–117.
[9] C. Bucci, P. Thomsen, P. Nicoziani, J. McCarthy, B. van Deurs, Rab7: a key to lysosome biogenesis, Mol. Biol. Cell 11 (2000) 467–480.
[10] Y. Feng, B. Press, A. Wandinger-Ness, Rab 7: an important regulator of late endocytic membrane traffic, J. Cell Biol. 131 (1995) 1435–1452.
[11] S. Meresse, J.P. Gorvel, P. Chavrier, The rab7 GTPase resides on a vesicular compartment connected to lysosomes, J. Cell Sci. 108 (Pt. 11) (1995) 3349–3358.
[12] B. Press, Y. Feng, B. Hoflack, A. Wandinger-Ness, Mutant Rab7 causes the accumulation of cathepsin D and cation-independent mannose 6-phosphate receptor in an early endocytic compartment, J. Cell Biol. 140 (1998) 1075–1089.

[13] F. Schimmoller, H. Riezman, Involvement of Ypt7p, a small GTPase, in traffic from late endosome to the vacuole in yeast, J. Cell Sci. 106 (Pt. 3) (1993) 823–830.
[14] H. Wichmann, L. Hengst, D. Gallwitz, Endocytosis in yeast: evidence for the involvement of a small GTP-binding protein (Ypt7p), Cell 71 (1992) 1131–1142.
[15] G. Cantalupo, P. Alifano, V. Roberti, C.B. Bruni, C. Bucci, Rab-interacting lysosomal protein (RILP): the Rab7 effector required for transport to lysosomes, EMBO J. 20 (2001) 683–693.
[16] K. Mizuno, A. Kitamura, T. Sasaki, Rabring7, a novel Rab7 target protein with a RING finger motif, Mol. Biol. Cell 14 (2003) 3741–3752.
[17] M. Johansson, M. Lehto, K. Tanhuanpaa, T.L. Cover, V.M. Olkkonen, The oxysterol-binding protein homologue ORP1L interacts with Rab7 and alters functional properties of late endocytic compartments, Mol. Biol. Cell 16 (2005) 5480–5492.
[18] T. Wang, W. Hong, Interorganellar regulation of lysosome positioning by the Golgi apparatus through Rab34 interaction with Rab-interacting lysosomal protein, Mol. Biol. Cell 13 (2002) 4317–4332.
[19] T. Wang, K.K. Wong, W. Hong, A unique region of RILP distinguishes it from its related proteins in its regulation of lysosomal morphology and interaction with Rab7 and Rab34, Mol. Biol. Cell 15 (2004) 815–826.
[20] M. Wu, T. Wang, E. Loh, W. Hong, H. Song, Structural basis for recruitment of RILP by small GTPase Rab7, EMBO J. 24 (2005) 1491–1501.
[21] S. Meresse, O. Steele-Mortimer, B.B. Finlay, J.P. Gorvel, The rab7 GTPase controls the maturation of Salmonella typhimurium-containing vacuoles in HeLa cells, EMBO J. 18 (1999) 4394–4403.
[22] H. Stenmark, R.G. Parton, O. Steele-Mortimer, A. Lutcke, J. Gruenberg, M. Zerial, Inhibition of rab5 GTPase activity stimulates membrane fusion in endocytosis, EMBO J. 13 (1994) 1287–1296.
[23] J.P. Gorvel, P. Chavrier, M. Zerial, J. Gruenberg, rab5 controls early endosome fusion in vitro, Cell 64 (1991) 915–925.
[24] C. Vennegoor, J. Calafat, P. Hageman, F. van Buitenen, H. Janssen, A. Kolk, P. Rumke, Biochemical characterization and cellular localization of a formalin-resistant melanoma-associated antigen reacting with monoclonal antibody NKI/C-3, Int. J. Cancer 35 (1985) 287–295.
[25] E.A. Reits, J.C. Vos, M. Gromme, J. Neefjes, The major substrates for TAP in vivo are derived from newly synthesized proteins, Nature 404 (2000) 774–778.
[26] D.R. Brandt, T. Asano, S.E. Pedersen, E.M. Ross, Reconstitution of catecholamine-stimulated guanosinetriphosphatase activity, Biochemistry 22 (1983) 4357–4362.
[27] T. Higashijima, K.M. Ferguson, P.C. Sternweis, E.M. Ross, M.D. Smigel, A.G. Gilman, The effect of activating ligands on the intrinsic fluorescence of guanine nucleotide-binding regulatory proteins, J. Biol. Chem. 262 (1987) 752–756.
[28] M. Marsman, I. Jordens, C. Kuijl, L. Janssen, J. Neefjes, Dynein-mediated vesicle transport controls intracellular Salmonella replication, Mol. Biol. Cell 15 (2004) 2954–2964.
[29] A.D. Shapiro, M.A. Riederer, S.R. Pfeffer, Biochemical analysis of rab9, a ras-like GTPase involved in protein transport from late endosomes to the trans Golgi network, J. Biol. Chem. 268 (1993) 6925–6931.
[30] S. Caplan, L.M. Hartnell, R.C. Aguilar, N. Naslavsky, J.S. Bonifacino, Human Vam6p promotes lysosome clustering and fusion in vivo, J. Cell Biol. 154 (2001) 109–122.
[31] V. Poupon, A. Stewart, S.R. Gray, R.C. Piper, J.P. Luzio, The role of mVps18p in clustering, fusion, and intracellular localization of late endocytic organelles, Mol. Biol. Cell 14 (2003) 4015–4027.
[32] P. Novick, M. Zerial, The diversity of Rab proteins in vesicle transport, Curr. Opin. Cell Biol. 9 (1997) 496–504.
[33] J. Somsel Rodman, A. Wandinger-Ness, Rab GTPases coordinate endocytosis, J. Cell Sci. 113 (Pt. 2) (2000) 183–192.
[34] M. Huizing, A. Didier, J. Walenta, Y. Anikster, W.A. Gahl, H. Kramer, Molecular cloning and characterization of human VPS18, VPS 11, VPS16, and VPS33, Gene 264 (2001) 241–247.
[35] B.Y. Kim, H. Kramer, A. Yamamoto, E. Kominami, S. Kohsaka, C. Akazawa, Molecular characterization of mammalian homologues of class C Vps proteins that interact with syntaxin-7, J. Biol. Chem. 276 (2001) 29393–29402.
[36] N. Nakamura, A. Hirata, Y. Ohsumi, Y. Wada, Vam2/Vps41p and Vam6/Vps39p are components of a protein complex on the vacuolar membranes and involved in the vacuolar assembly in the yeast Saccharomyces cerevisiae, J. Biol. Chem. 272 (1997) 11344–11349.
[37] A. Price, W. Wickner, C. Ungermann, Proteins needed for vesicle budding from the Golgi complex are also required for the docking step of homotypic vacuole fusion, J. Cell Biol. 148 (2000) 1223–1229.
[38] S.C. Richardson, S.C. Winistorfer, V. Poupon, J.P. Luzio, R.C. Piper, Mammalian late vacuole protein sorting orthologues participate in early endosomal fusion and interact with the cytoskeleton, Mol. Biol. Cell 15 (2004) 1197–1210.
[39] S.E. Rieder, S.D. Emr, A novel RING finger protein complex essential for a late step in protein transport to the yeast vacuole, Mol. Biol. Cell 8 (1997) 2307–2327.
[40] T.K. Sato, P. Rehling, M.R. Peterson, S.D. Emr, Class C Vps protein complex regulates vacuolar SNARE pairing and is required for vesicle docking/fusion, Mol. Cell 6 (2000) 661–671.
[41] D.F. Seals, G. Eitzen, N. Margolis, W.T. Wickner, A. Price, A Ypt/Rab effector complex containing the Sec1 homolog Vps33p is required for homotypic vacuole fusion, Proc. Natl. Acad. Sci. USA 97 (2000) 9402–9407.
[42] A.E. Wurmser, T.K. Sato, S.D. Emr, New component of the vacuolar class C-Vps complex couples nucleotide exchange on the Ypt7 GTPase to SNARE-dependent docking and fusion, J. Cell Biol. 151 (2000) 551–562.
[43] T. Darsow, D.J. Katzmann, C.R. Cowles, S.D. Emr, Vps41p function in the alkaline phosphatase pathway requires homo-oligomerization and interaction with AP-3 through two distinct domains, Mol. Biol. Cell 12 (2001) 37–51.
[44] J.A. Ybe, F.M. Brodsky, K. Hofmann, K. Lin, S.H. Liu, L. Chen, T.N. Earnest, R.J. Fletterick, P.K. Hwang, Clathrin self-assembly is mediated by a tandemly repeated superhelix, Nature 399 (1999) 371–375.

Chapter 5

Rab7-RILP-ORP1L receptors couple late endosomal transport and fusion
In preparation

Rab7-RILP-ORP1L receptors couple late endosomal transport and fusion

Nuno Rocha, Marije Marsman, Coenraad Kuijl, Rik van der Kant, Wilbert Zwart, Ingrid Jordens, Lennert Janssen, and Jacques Neefjes

Division of Tumor Biology, The Netherlands Cancer Institute, Amsterdam, The Netherlands

Fusion between late endosomal compartments is crucial for degradation of endocytosed material. Motor-based vesicular transport brings late endosomal membranes into close proximity prior to their tethering/docking and fusion. We propose that the control of these two consecutive processes is combined in one single tripartite complex on late endosomal membranes, the Rab7-RILP-ORP1L complex. RILP establishes the molecular link between Rab7 and the dynein-dynactin microtubule motor for centripetal vesicular transport. ORP1L, a second Rab7 effector, controls the interaction of RILP with p150^{Glued}, a subunit of dynactin. In addition, Rab7 has also been implicated in tethering/docking and fusion of late endosomal compartments, but how this is regulated is unclear. We show that Vam6p, a specific tethering/docking factor that promotes fusion of late endosomal compartments, is also recruited to Rab7 on late endosomal membranes in a RILP-dependent manner. Furthermore, we show that ORP1L governs this, suggesting a common regulatory mechanism for late endosomal transport and tethering/docking and fusion. This would provide coordinated spatio-temporal control and continuity for these two consecutive steps within the late endocytic route.

INTRODUCTION

Rab GTPases are targeted to specific subcellular compartments and orchestrate the spatio-temporal regulation of intracellular endomembrane trafficking by regulating vesicular transport, docking/tethering of organelle bilayers, and ultimately their fusion (Jordens et al., 2005; Somsel Rodman and Wandinger-Ness, 2000).

Examples of Rab GTPases implicated in recruiting (directly or through effector molecules) motor proteins to specific membranes for vesicular transport include (Jordens et al., 2005): Rab4, Rab5, and Rab6, which recruit members of the kinesin superfamily of motor proteins; Rab8, Rab11, and Rab27a, recruit myosin motor proteins; and Rab6 and Rab7, support the recruitment of the minus end-directed motor dynein. Rab7 associates to membranes of late endosomal structures (Jordens et al., 2001; Meresse et al., 1995), including late endosomes, lysosomes, major histocompatibility class II-containing

* Corresponding author: Division of Tumor Biology, The Netherlands Cancer Institute, Plesmanlaan 121, Amsterdam 1066 CX, The Netherlands. Tel.: + 31 20 5122012; Fax: + 31 20 5122029; E-mail: J.NEEFJES@NKI.NL

compartments (MIICs) (Jordens et al., 2001), phagosomes (Harrison et al., 2004; Marsman et al., 2004), early melanosomes (Jordens et al., 2006), and cytolytic granules (Stinchcombe et al., 2006). The Rab7 effector Rab7-interacting lysosomal protein (RILP) interacts with $p150^{Glued}$, a subunit of dynactin, to recruit the dynein-dynactin motor to late endosomal membranes. The Rab7-RILP complex thus acts as a specific receptor for the minus-end dynein motor. After dynein recruitment to late endosomal membranes, active centripetal transport of late endosomal compartments still requires the concerted activities of two other proteins: an additional Rab7 effector, oxysterol-binding protein (OSBP)-related protein 1L (ORP1L), which is part of the tripartite complex Rab7-RILP-ORP1L; and βIII spectrin, which acts as a second receptor for dynein-dynactin on late endosomal membranes. ORP1L is thought to target the Rab7-RILP-$p150^{Glued}$-dynein complex to βIII spectrin on late endosomal membranes leading to full activation of minus-end directed transport (Johansson et al., 2007). In addition, ORP1L responds to changes in late endosomal cholesterol content with variations in its conformational state, thereby controlling access of dynein-dynactin to its receptor Rab7-RILP (Chapter 3 of this thesis).

Rab GTPases and their effectors are also implicated in orchestrating the assembly of complexes that regulate tethering/docking and fusion of vesicular membranes (Cai et al., 2007; Grosshans et al., 2006). For example, the early endosomal Rab GTPase-effector complex, Rab5-EEA1, interacts with syntaxin-13, a t-SNARE required for early endosomal homotypic fusion. Rab7/Ypt7p is involved in tethering/docking and fusion of late endosomal compartments. The homotypic fusion and vacuole protein sorting (HOPS) complex is recruited to Rab7/Ypt7p-bearing membranes to assemble soluble N-ethylmaleimide-sensitive factor attachment protein receptor (SNARE) complexes (Luzio et al., 2007), an event that leads to bilayer fusion (Sollner et al., 1993). However, it is not clear how this is regulated. In addition, the HOPS complex appears to act as an effector of Rab5 and a guanine nucleotide exchange factor (GEF) for Rab7 in the process of Rab5-Rab7 conversion for early-to-late endosome maturation (Rink et al., 2005).

The HOPS complex is a conserved large multisubunit complex that comprises four class C VPS proteins Vam1p/Vps11p, Vam9p/Vps16p, Vam6p/Vps39p, and the Sec1/Munc-like protein Vam5p/Vps33p, as well as two class B VPS proteins, Vam6p/Vps39p and Vam2p/Vps41p, and likely plays a range of roles in intracellular trafficking, including tethering/docking and fusion of late endosomal bilayers (Caplan et al., 2001; Poupon et al., 2003; Ungermann et al., 2000; Wurmser et al., 2000). In yeast, the class C VPS/HOPS complex functions as an effector of the Rab GTPase Ypt7p/Rab7 and interacts with unpaired SNAREs required for vacuole fusion (Collins et al., 2005).

In mammalian cells, overexpression of Vam6p, a subunit of the HOPS complex, resulted in tethering/docking and fusion of late endosomal compartments (Caplan et al., 2001). It was proposed that Vam6p exerts its function either downstream of, or in parallel to, Rab7, but the precise mechanism remains unclear (Caplan et al., 2001). Moreover, Vam6p was also found associated with microtubules and fusion of EEA-1-positive early endosomes, suggesting a connection between SNARE-dependent fusion and the microtubule cytoskeletal network in the endocytic route (Richardson et al., 2004).

Here, we show that recruitment of Vam6p to late endosomal membranes is RILP-dependent, possibly through a direct RILP-Vam6p interaction. Furthermore, we show that ORP1L governs this interaction, suggesting a common regulatory mechanism for late endosomal transport, docking/tethering, and fusion. This points to a model where the tripartite Rab7-RILP-ORP1L complex orchestrates the control of both late endosomal transport and

fusion, thereby providing spatio-temporal coordination for these two consecutive processes.

RESULTS

RILP-dependent dynamic recruitment of Vam6p to late endosomal membranes

Overexpression of Vam6p has been reported to induce tethering/docking and fusion of late endosomal membranes (Caplan et al., 2001). However, the mechanism by which Vam6p, and possibly other subunits of the HOPS complex, are recruited to late endosomal membranes remains unresolved. To test whether RILP, which establishes the molecular bridge between Rab7 and the dynein-dynactin motor for microtubular transport, could also be involved in the recruitment of Vam6p, we co-transfected MelJuSo cells with Vam6p and RILP or ΔN-RILP, a truncated mutant of RILP that binds to GTP-Rab7 but fails to recruit the dynein motor (Jordens et al., 2001; Wu et al., 2005) and analyzed the intracellular distribution of Vam6p by confocal laser-scanning microscopy. Ectopically expressed Vam6p is predominantly cytosolic and does not significantly localize to CD63-positive compartments. However, upon RILP co-expression, but not ΔN-RILP or ORP1L, Vam6p is found associated to lysosomal membranes and extensively co-localizing with RILP on compact perinuclear organelle clusters (Figure 1). This suggests that RILP is crucial for the recruitment of Vam6p to late endosomal membranes.

To determine whether Vam6p and RILP may be part of a common physical complex, MelJuSo cells were transfected with mRFP-tagged Vam6p and GFP-tagged RILP or ΔN-RILP and subjected to immunoprecipitation with the anti-GFP antibody or an irrelevant rabbit IgG. Immunoblotting of the isolates with the anti-mRFP antibody revealed co-immunoprecipitation of mRFP-Vam6p

1

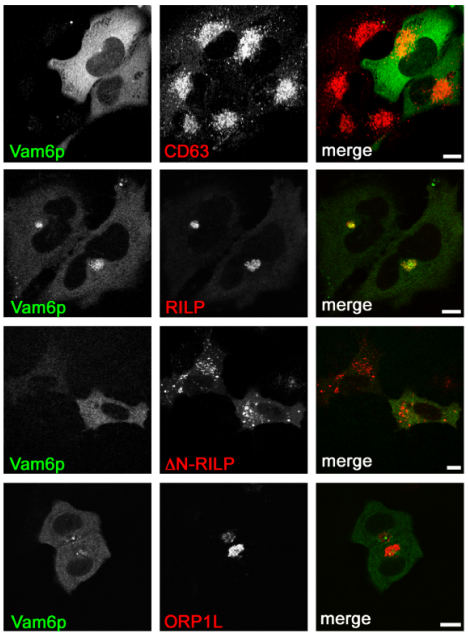

Figure 1. RILP-mediated recruitment of Vam6p to late endosomal membranes. MelJuSo cells were co-transfected with mRFP-Vam6p and GFP-RILP, GFP-ΔN-RILP, or GFP-ORP1L, as indicated, prior to confocal microscopy. Immunofluorescence confocal microscopy for the first row of the panel was done using anti-CD63 antibodies. n>100 for each condition. Scale bars, 10μm.

with GFP-RILP (Figure 2A). The Vam6p-RILP interaction was further confirmed by incubating immobilized recombinant His-RILP on a metal affinity resin with lysates from MelJuSo cells overexpressing GFP-Vam6p. Immunoblotting analysis with the anti-GFP antibody revealed that GFP-Vam6p interacted *in vitro* with purified His-RILP (Figure 2B). These data suggest that RILP and Vam6p not only co-localize on late endosomal membranes but are also part of a common physical complex.

RILP interacts directly with the C-terminal region of $p150^{Glued}$ of dynactin to recruit dynein-dynactin for centripetal microtubular transport. An analogous scenario could be envisaged

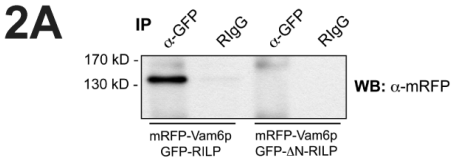

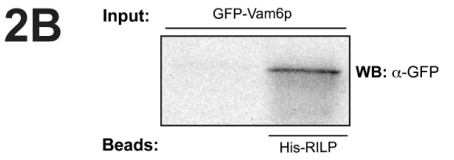

Figure 2. Vam6p co-isolates with RILP. (A) Immunoprecipitated proteins were isolated from lysates of MelJuSo cells transfected with mRFP-Vam6p and GFP-RILP or GFP-ΔN-RILP using anti-GFP antibodies (a-GFP) or irrelevant rabbit IgG (RIgG), and immunobloted using anti-mRFP antibodies (a-mRFP), as indicated. (B) Metal affinity beads or purified His-RILP immobilized on metal affinity beads (indicated as Beads:) were used to pull-down GFP-Vam6p from MelJuSo cell lysates (indicated as Input:). Anti-GFP antibodies (α-GFP) were used for immunoblotting.

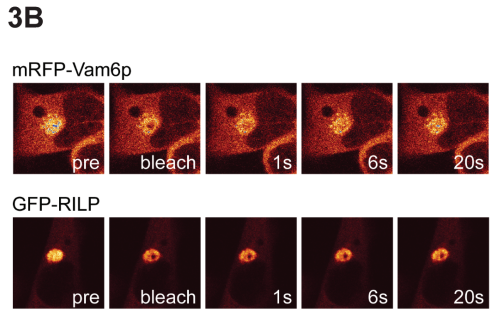

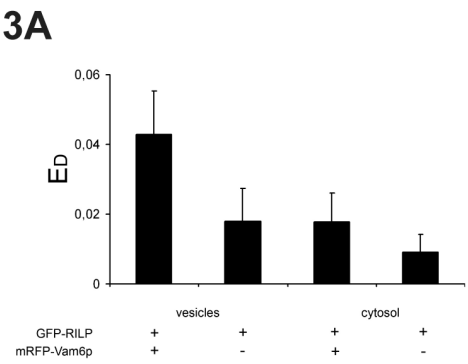

Figure 3. Dynamic interaction of Vam6p with RILP on late endosomal membranes. (A) FRET between GFP-RILP and mRFP-Vam6p. MelJuSo cells were transfected with GFP-RILP or co-transfected GFP-RILP and mRFP-Vam6p, as indicated. These cells were co-cultured with MelJuSo cells stably expressing H2B-GFP as a reference marker with a lifetime of 2.6 ns. The fluorescence lifetime of GFP was determined on GFP-RILP-bearing vesicles that were immotile during data acquisition or on cytosolic GFP-RILP, as indicated. The donor FRET efficiencies (E_D) between GFP- and mRFP-tagged proteins were plotted in the bar chart. Means + SD are shown. (B) Dynamics of Vam6p and RILP on late endosomal membranes analyzed by FRAP. pre: before photobleaching; bleach: immediately after photobleaching; 1s, 6s, and 20s, indicate time elapsed (in seconds) since photobleaching. Quantification of recovery time ($T_{1/2}$, in seconds) and immobile fraction calculated from the recovery curves.

for the recruitment of the HOPS complex for docking/tethering of late endosomal membranes, with Vam6p establishing a direct interaction with RILP. Given that Vam6p was precipitated on immobilized purified His-RILP from cell lysates, we cannot exclude the possibility that other factors present in the reaction mixture were present at the RILP-Vam6p interface.

The RILP-Vam6p interaction was further analyzed using FRET (fluorescence resonance energy transfer) in living MelJuSo cells expressing GFP-RILP and mRFP-Vam6p. FRET can occur when fluorophores with spectral overlap are in close proximity (<8 nm) (Förster, 1948). We measured FRET by FLIM (fluorescence lifetime imaging microscopy. FLIM allows the detection of the time between

photon absorbance by the donor fluorophore and emission. This decreases when energy transfer to the acceptor fluorophore occurs. Consistent with our previous conclusions, the calculated donor FRET efficiencies (E_D) between GFP-RILP and mRFP-Vam6p indicate that the two molecules are in close proximity on vesicular membranes (Figure 3A).

We next analyzed the relative dynamics of Vam6p and RILP on late endosomal membranes using FRAP (fluorescence recovery after photobleaching). We bleached a portion of membrane-associated mRFP-Vam6p in living MelJuSo cells expressing also HA-tagged RILP. Next, we measured in time the recovery of fluorescence in the bleached spot. The recovery relates to the dynamic equilibrium responsible for the replacement of non-fluorescent/bleached mRP-Vam6p in the spot for fluorescent mRFP-Vam6p from the cytosolic pool and, possibly, membrane-associated pool from the surroundings of the spot. This provides information on the dynamics of Vam6p presence on RILP-harboring membranes. The same method was applied to study to the dynamics of RILP presence on membranes of cells expressing GFP-RILP. We observed that the immobile fraction (calculated from the recovery curves) was ~20% and ~65% for mRFP-Vam6p and GFP-RILP, respectively, and that mRFP-Vam6p cycled faster than mRFP-Vam6p, as reflected by the determined $T_{1/2}$ (Figure 3B).

Taken together these data indicate that Vam6p is recruited dynamically to late endosomal membranes in a RILP-dependent manner.

RILP is required for Vam6p-induced clustering and tethering/docking of late endosomal bilayers

To examine the effect of Vam6p recruitment to RILP-bearing late endosomal membranes in more detail, we performed ultrastructural analyses on MelJuSo cells co-expressing HA-tagged RILP or ΔN-RILP and GFP-tagged Vam6p. Immunoelectron microscopy on cryosections revealed that Vam6p is found predominantly associated to late endosomal membranes in cells co-expressing RILP (Figure 4a). In contrast, in cells co-expressing the truncated mutant ΔN-RILP, Vam6p association to membranes is dramatically reduced (Figure 4b). Furthermore, co-expression of RILP, but not ΔN-RILP, and Vam6p induces massive clustering of late endosomal compartments with their bilayers appearing tethered/docked (Figures 4a, 4c, and 4d).

ORP1L controls the recruitment of Vam6p to RILP-bearing late endosomal membranes

We have recently shown that ORP1L controls $p150^{Glued}$ binding to the Rab-RILP receptor and thus late endosomal transport and positioning (Chapter 3 of this thesis). Co-expression of RILP with a truncated mutant of ORP1L lacking the C-terminal OSBP-related domain (ΔORD) prevented recruitment of $p150^{Glued}$ by RILP and resulted in centrifugal relocation of RILP-positive compartments within the cell. In contrast, we have previously observed that this phenotype could be rescued if the OSBP-related domain (ORD) in ORP1L was exchanged for a tandem of ORP1L pleckstrin-homology (PH) domains. This chimera possibly mimics the ORD of ORP1L in a membrane-associated state (Chapter 3 of this thesis). To test whether ORP1L is also involved in the control of Vam6p recruitment to RILP-positive membranes, we transfected MelJuSo cells with GFP-Vam6p and mRFP-ΔORD, or mRFP-ORP1L and HA-RILP, or mRFP-ΔORD and HA-RILP, or mRFP-ΔORDPHDPHD and HA-RILP, prior to fixation and analyses by immunofluorescence confocal microscopy with anti-HA antibodies (Figure 5). Vam6p, RILP, and ORP1L, extensively co-localized

4

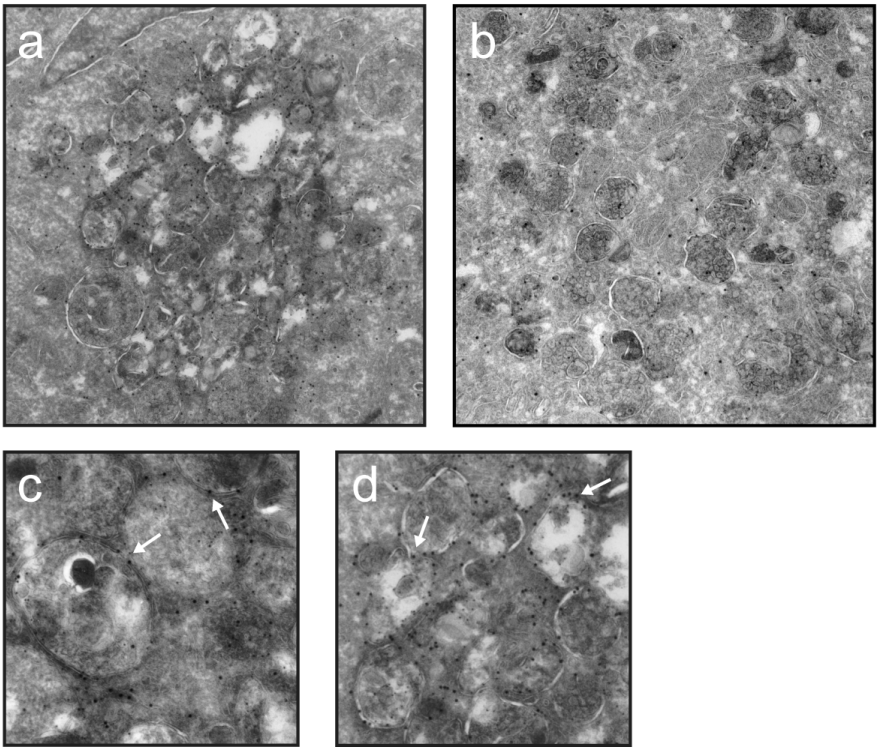

Figure 4. Vam6p is recruited to late endosomal RILP-positive membranes and induces their docking/tethering. Immunoelectron microscopy analyses on cryosections from MelJuSo cells expressing GFP-Vam6p and (a) HA-RILP or (b) ΔN-RILP. Gold particles label anti-GFP antibodies. Successful expression of RILP or ΔN-RILP was judged based on the characteristic distinct phenotypes. (c) and (d) show magnifications of representative micrographs from cells expressing GFP-Vam6p and HA-RILP showing tethering/docking of Vam6p-positive bilayers (indicated by arrows).

on juxtanuclear clusters of late endosomal organelles. Conversely, co-expression of Vam6p, RILP, and ΔORD, caused the relocation of late endosomal compartments to the periphery of the cell, as expected. Moreover, despite RILP overexpression, ΔORD excluded Vam6p from late endosomal membranes rendering it predominantly cytosolic. Vam6p recruitment to late endosomal membranes, as well as their clustering at the minus end of microtubules, could be rescued by expression of the ΔORDPHDPHD chimera (Figure 5). Taken together these data suggest that ORP1L controls Vam6p recruitment to RILP-positive membranes.

RILP couples late endosomal transport to tethering/docking of late endosomal bilayers

RILP overexpression induces minus end-directed transport by recruiting the dynein-dynactin motor and results in dense clustering of late endosomal compartments in the juxtanuclear area (Jordens et al., 2001). Concomitantly, RILP induces recruitment of

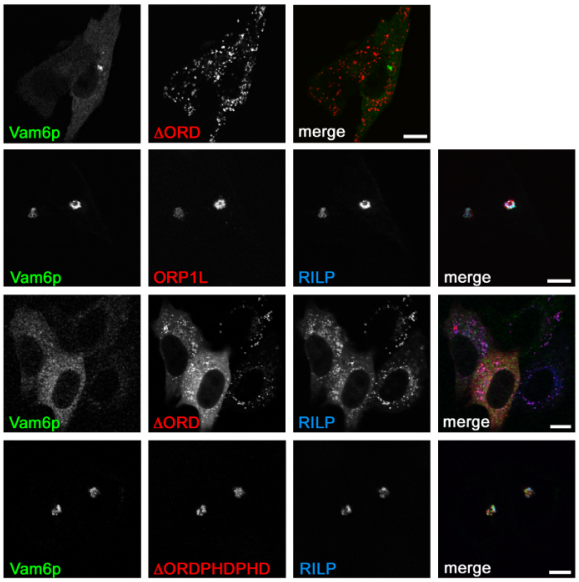

Figure 5. ORP1L controls recruitment of Vam6p to the Rab7-RILP receptor on late endosomal membranes. MelJuSo cells were co-transfected with GFP-Vam6p and mRFP-ΔORD, GFP-Vam6p and HA-RILP and mRFP-ORP1L, GFP-Vam6p and HA-RILP and mRFP-ΔORD, or GFP-Vam6p and GFP-RILP and mRFP-ΔORDPHDPHD, as indicated, prior to immunofluorescence confocal microscopy using anti-HA antibodies. n>100 for each condition. Scale bars, 10μm.

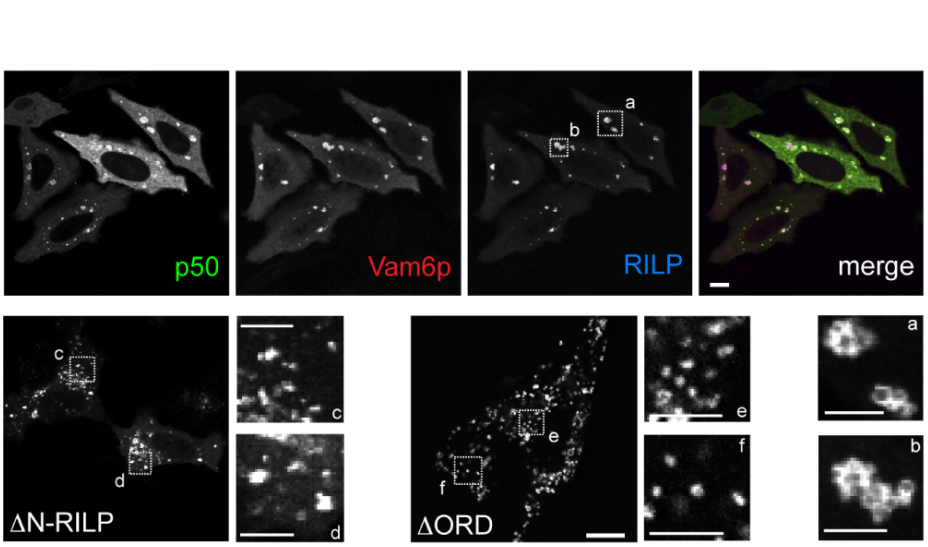

Figure 6. Uncoupling of late endosomal transport and fusion by p50^{dynamitin} overexpression. MelJuSo cells were co-transfected with GFP-p50^{dynamitin}, mRFP-Vam6p and HA-RILP, as indicated. (a) and (b): Magnification of clusters of RILP-positive vesicles. (c) and (d): Magnification of ΔN-RILP-positive vesicles from MelJuSo cells expressing mRFP-Vam6p and GFP-ΔN-RILP. (e) and (f): Magnification of ΔORD-positive vesicles from MelJuSo cells expressing mRFP-Vam6p and GFP-ΔORD. n>100 for each condition. Scale bars, 10μm.

Vam6p to late endosomal membranes and induces their tethering/docking (Figures 1 and 4). It is thought that late endosomal transport brings bilayers into close proximity to affect the efficiency of trafficking steps such as tethering/docking and fusion (Caviston and Holzbaur, 2006; Jordens et al., 2005). We tested whether selective abrogation of centripetal dynein-based transport of late endosomal organelles was accompanied by an absence of tethering/docking of bilayers. We made use of $p50^{dynamitin}$ overexpression, which inactivates dynein transport by disassembling dynein's adaptor dynactin (Burkhardt et al., 1997; Johansson et al., 2007). We then tested whether Vam6p is still able to induce tethering/docking. GFP-$p50^{dynamitin}$ and mRFP-Vam6p were overexpressed in MelJuSo cells with HA-RILP, to induce recruitment of Vam6p. Cells were fixed and analyzed by immunofluorescence confocal microscopy with anti-HA antibodies. Vam6p and RILP extensively co-localized on vesicle clusters. However, given that the dynein-dynactin motor was inhibited by GFP-$p50^{dynamitin}$ overexpression, these clusters were no longer present in the juxtanuclear area but dispersed throughout the cell (Figure 6, top panel). A closer examination of the RILP/Vam6p-positive clusters (Figure 6a and 6b) reveals that these appear to comprise a higher number of vesicles than those of MelJuSo cells expressing ΔN-RILP or ΔORD, truncation mutants that prevent the recruitment of Vam6p to late endosomal membranes (Figures 6c–f). Furthermore, the diameter of each individual vesicle appears to be larger in cells where Vam6p was efficiently recruited to late endosomal membranes (Figures 6a–f), suggesting that Vam6p could have promoted vesicular fusion and thus an increase in vesicle size.

DISCUSSION

Rab GTPases are key elements of the vesicular transport and endomembrane trafficking machineries (Caviston and Holzbaur, 2006; Jordens et al., 2005; Pfeffer, 2001; Zerial and McBride, 2001). They are of strategic importance in determining organelle identity by associating to specific organelle membranes. This is a dynamic association dependent on the ability of Rab GTPases to cycle between an active GTP-bound state and an inactive GDP-bound state. Thus, Rab GTPases, either directly or by organizing the recruitment of soluble effector molecules, bring spatial and temporal resolution to intracellular membrane trafficking reactions.

Motor-dependent vesicular transport is thought to facilitate membrane tethering/docking upstream of SNARE-dependent fusion by bringing vesicular membranes into close contact (Jordens et al., 2005; Somsel Rodman and Wandinger-Ness, 2000). In principle, a single RabGTPase could orchestrate the recruitment of both the transport and tethering/docking machineries to a specific organelle. This would provide concerted control for two consecutive steps in the course of intracellular vesicle trafficking.

We show here how the recruitment of subunits of macromolecular complexes involved in late endosomal transport and tethering/docking is regulated by single tripartite receptor—Rab7-RILP-ORP1L—whose assembly on late endosomal membranes is dictated by the small GTPase Rab7. The dynein-dynactin motor is recruited to Rab7 membranes in a RILP-dependent manner (Johansson et al., 2007). This is further controlled by ORP1L which regulates access of the motor complex to RILP (Chapter 3 of this thesis). Our data point to an analogous regulatory mechanism operating in the recruitment of the tethering/docking machinery upstream of bilayer fusion. We show that Vam6p, a subunit of the HOPS complex required for SNARE assembly, also depends on RILP for its recruitment to Rab7 late endosomal membranes. It is likely that RILP and Vam6p

establish a direct interaction, although binding studies using purified recombinant proteins have to be performed to define the binding interface between RILP and Vam6p. In addition, we show that ORP1L is able to control the access of Vam6p to RILP. Furthermore, given that $p50^{dynamitin}$ overexpression inhibited centripetal transport but not tethering/docking of vesicles, the RILP-dependent recruitment of Vam6p appears to be independent of dynein's function. This obviously does not exclude that dynein-based transport influences the efficiency of membrane tethering/docking events.

The cholesterol sensor ORP1L responds with conformational changes to variations in late endosomal content thereby acting as a switch that controls access of dynein to the Rab7-RILP receptor (Chapter 3 of this thesis). Whether ORP1L is also responding to cholesterol content variations to control the access of Vam6p/HOPS complex to its receptor Rab7-RILP remains to be tested. However, this appears to be likely since the ΔORDPHDPHD chimera, which mimics the high-cholesterol content conformational state of ORP1L, rescues the recruitment of Vam6p to the Rab7-RILP which is disrupted by ΔORD expression.

The existence of a common regulatory mechanism for sequential reactions, such as transport and tethering/docking, is consistent with the recently proposed models for Rab conversion/cascades and organelle maturation (Caviston and Holzbaur, 2006; Grosshans et al., 2006; Markgraf et al., 2007) where RabGTPases and their effectors coordinate consecutive reactions along the endocytic route and may provide an integrated system for the spatial and temporal specificity in intracellular trafficking.

EXPERIMENTAL PROCEDURES

REAGENTS

Rabbit anti-GFP and rabbit anti-mRFP antibodies were generated using purified His-mRFP or His-GFP recombinant proteins as immunogens, respectively. Cross-reactivity was excluded by Western blot analyses with various mRFP- or GFP-labelled fusion proteins. Rabbit polyclonal anti-CD63 was described elsewhere (Vennegoor et al., 1985). Rabbit polyclonal anti-HA antibody (Y11:sc-805) was from Santa Cruz Biotechnology.

cDNA CONSTRUCTS AND VECTORS

Human Vam6p was a kind gift of J. Bonifacino (Caplan et al., 2001) and was subcloned into a pEGFP-C1 (BD Biosciences Clonetech, USA) and a custom made pmRFP-C1 (Johansson et al., 2007) vectors, for N-terminal GFP and mRFP tagging, respectively. Rab7, RILP, ORP1L, and $p50^{dynamitin}$ cDNA constructs have been described previously (Johansson et al., 2005; Johansson et al., 2007; Jordens et al., 2001; Marsman et al., 2004).

CELL CULTURE

Monolayers of MelJuSo cells were maintained in Iscoves Modified Dulbecco's Medium (IMDM) medium (Gibco) supplemented with 5% FCS, in 5% CO_2 at 37°C.

CONFOCAL MICROSCOPY ON FIXED SAMPLES

Transfected cells were fixed at 48 hr post-transfection with 4% formaldehyde in PBS for 30 min and permeabilized for 5 min with 0.05% Triton X-100 in PBS, at room temperature. Nonspecific binding of antibodies was blocked by 0.5% BSA/PBS for 40 min, after which cells were incubated with a primary antibody in 0.5% BSA/PBS for 1 hr at room temperature. Bound primary antibodies were visualized with Alexa Fluor secondary antibody conjugates (Invitrogen). Cells were mounted in Vectashield mounting medium (Vector Laboratories, USA). The specimens were analyzed with confocal laser scanning microscopes (TCS-SP1, -SP2 or AOBS) equipped with HCX PL APO 63x/NA 1.32 and HCX PL APO lbd.bl 63×/NA 1.4

oil-corrected objective lenses (all from Leica, Mannheim, Germany). The acquisition software used was Leica LCS.

FRAP and FLIM

FRAP experiments were performed as described previously (Jordens et al., 2001; Reits et al., 2000).

FLIM experiments were performed with MelJuSo cells stably expressing GFP-ORP1L-mRFP cultured on Delta T dishes (Bioptechs). Prior to measurements, cells were mounted in bicarbonate-buffered saline medium (140 mM NaCl, 5 mM KCl, 2 mM $MgCl_2$, 1 mM $CaCl_2$, 23 mM $NaHCO_3$, 10 mM [D-]glucose, and 10 mM Hepes, pH 7.3) and analyzed at 37°C in a 5% CO_2 culture hood surrounding the objective stage of the microscope. Images were taken on a Leica inverted DM-IRE2 microscope with a HCX PL APO 63x/NA 1.35 glycerol corrected objective lens equipped with a Lambert Instruments (LI) frequency domain lifetime attachment (Leutingewolde, The Netherlands), controlled by the manufacturer's LI FLIM software. GFP was excited with ~4 mW of 488 nm light from a LED modulated at 40 MHz, and emission was collected at 490–550 nm using an intensified charge-coupled device camera (CoolSNAP HQ; Roper Scientific). To calculate the GFP lifetime, the intensities from 12 phase-shifted images (modulation depth ~70%) were fitted with a sinus function, and lifetimes were derived from the phase shift between excitation and emission. For internal controls, cells were co-cultured with MelJuSo cells expressing H2B–GFP only. Lifetimes were referenced to a 1 μM solution of rhodamine-G6 in saline that was set at a 4.11 ns lifetime. The donor FRET efficiency E_D was calculated as $E_D = 1 -$ (measured lifetime/GFP lifetime in control cells) (Zwart et al., 2005).

ELECTRONMICROSCOPY

MelJuSo cells were fixed in a mixture of 4% formaldehyde (w/v) and 0.1% (v/v) gluteraldehyde in 0.1 M phosphate buffer, pH 7.2. Ultra-thin cryosections were incubated with the anti-GFP antisera. Secondary antibodies were coupled to gold. Images were made using a Philips CM 10 electron microscope.

PROTEIN IMMUNOPRECIPITATION AND PULL-DOWN

MelJuSo cells transfected with mRFP-Vam6p were washed with ice-cold PBS and scraped into 400 μL of cell lysis buffer (20 mM Hepes, 150 mM NaCl, 2 mM $MgCl_2$, 0.5% Triton X-100, pH 7.5) supplemented with Complete EDTA-free Protease Inhibitor Cocktail. Cell lysates were obtained by incubation on ice for 10 min followed by centrifugation for clearing. The supernatants were then incubated for 25 min on protein G-Sepharose 4 FF resin (Amersham Biosciences) followed by incubation with anti-GFP antisera or an irrelevant rabbit IgG as control for 2 hr. The antibody complexes were then precipitated with protein G-Sepharose 4 FF resin and washed extensively with the cell lysis buffer. The immunoprecipitates were subjected to immunoblotting with anti-mRFP antibodies.

For the pull-down of GFP-Vam6p on immobilized purified His-RILP, MelJuSo cells were transfected with GFP-Vam6p and lysates were obtained as described above. Cleared lysates were then incubated either with empty Talon Co^{2+}-affinity resin or with His-RILP immobilized on the same type of resin. After recovery of the resins by centrifugation and extensive washing with lysis buffer, the precipitated proteins were analyzed by immunoblotting with anti-GFP antisera. His-RILP production and purification was described before (Johansson et al., 2007).

ACKNOWLEDGEMENTS

Nuno Rocha was supported by a grant from the Portuguese Foundation for Science and Technology FCT/ FSE/ POCI 2010. This work

was supported by grants from the Dutch Cancer Society KWF and the Chemical Sciences Section of NWO. We thank Helen Pickersgill for critically reading the manuscript.

REFERENCES

Burkhardt, J.K., Echeverri, C.J., Nilsson, T., and Vallee, R.B. (1997). Overexpression of the dynamitin (p50) subunit of the dynactin complex disrupts dynein-dependent maintenance of membrane organelle distribution. The Journal of cell biology 139, 469-484.

Cai, H., Reinisch, K., and Ferro-Novick, S. (2007). Coats, tethers, Rabs, and SNAREs work together to mediate the intracellular destination of a transport vesicle. Developmental cell 12, 671-682.

Caplan, S., Hartnell, L.M., Aguilar, R.C., Naslavsky, N., and Bonifacino, J.S. (2001). Human Vam6p promotes lysosome clustering and fusion in vivo. The Journal of cell biology 154, 109-122.

Caviston, J.P., and Holzbaur, E.L. (2006). Microtubule motors at the intersection of trafficking and transport. Trends in cell biology 16, 530-537.

Collins, K.M., Thorngren, N.L., Fratti, R.A., and Wickner, W.T. (2005). Sec17p and HOPS, in distinct SNARE complexes, mediate SNARE complex disruption or assembly for fusion. The EMBO journal 24, 1775-1786.

Förster, T. (1948). Zwischenmolekulare energiewandering und fluoreszenz. . Annalen Physik 6, 55–75.

Grosshans, B.L., Ortiz, D., and Novick, P. (2006). Rabs and their effectors: achieving specificity in membrane traffic. Proceedings of the National Academy of Sciences of the United States of America 103, 11821-11827.

Harrison, R.E., Brumell, J.H., Khandani, A., Bucci, C., Scott, C.C., Jiang, X., Finlay, B.B., and Grinstein, S. (2004). Salmonella impairs RILP recruitment to Rab7 during maturation of invasion vacuoles. Molecular biology of the cell 15, 3146-3154.

Johansson, M., Lehto, M., Tanhuanpää, K., Cover, T.L., and Olkkonen, V.M. (2005). The oxysterol-binding protein homologue ORP1L interacts with Rab7 and alters functional properties of late endocytic compartments. Molecular biology of the cell 16, 5480-5492.

Johansson, M., Rocha, N., Zwart, W., Jordens, I., Janssen, L., Kuijl, C., Olkkonen, V.M., and Neefjes, J. (2007). Activation of endosomal dynein motors by stepwise assembly of Rab7-RILP-p150Glued, ORP1L, and the receptor betalll spectrin. The Journal of cell biology 176, 459-471.

Jordens, I., Fernandez-Borja, M., Marsman, M., Dusseljee, S., Janssen, L., Calafat, J., Janssen, H., Wubbolts, R., and Neefjes, J. (2001). The Rab7 effector protein RILP controls lysosomal transport by inducing the recruitment of dynein-dynactin motors. Curr Biol 11, 1680-1685.

Jordens, I., Marsman, M., Kuijl, C., and Neefjes, J. (2005). Rab proteins, connecting transport and vesicle fusion. Traffic 6, 1070-1077.

Jordens, I., Westbroek, W., Marsman, M., Rocha, N., Mommaas, M., Huizing, M., Lambert, J., Naeyaert, J.M., and Neefjes, J. (2006). Rab7 and Rab27a control two motor protein activities involved in melanosomal transport. Pigment Cell Res 19, 412-423.

Luzio, J.P., Pryor, P.R., and Bright, N.A. (2007). Lysosomes: fusion and function. Nature reviews 8, 622-632.

Markgraf, D.F., Peplowska, K., and Ungermann, C. (2007). Rab cascades and tethering factors in the endomembrane system. FEBS letters 581, 2125-2130.

Marsman, M., Jordens, I., Kuijl, C., Janssen, L., and Neefjes, J. (2004). Dynein-mediated vesicle transport controls intracellular Salmonella replication. Molecular biology of the cell 15, 2954-2964.

Meresse, S., Gorvel, J.P., and Chavrier, P. (1995). The rab7 GTPase resides on a vesicular

compartment connected to lysosomes. Journal of cell science 108 (Pt 11), 3349-3358.

Pfeffer, S.R. (2001). Rab GTPases: specifying and deciphering organelle identity and function. Trends in cell biology 11, 487-491.

Poupon, V., Stewart, A., Gray, S.R., Piper, R.C., and Luzio, J.P. (2003). The role of mVps18p in clustering, fusion, and intracellular localization of late endocytic organelles. Molecular biology of the cell 14, 4015-4027.

Reits, E.A., Vos, J.C., Gromme, M., and Neefjes, J. (2000). The major substrates for TAP in vivo are derived from newly synthesized proteins. Nature 404, 774-778.

Richardson, S.C., Winistorfer, S.C., Poupon, V., Luzio, J.P., and Piper, R.C. (2004). Mammalian late vacuole protein sorting orthologues participate in early endosomal fusion and interact with the cytoskeleton. Molecular biology of the cell 15, 1197-1210.

Rink, J., Ghigo, E., Kalaidzidis, Y., and Zerial, M. (2005). Rab conversion as a mechanism of progression from early to late endosomes. Cell 122, 735-749.

Sollner, T., Whiteheart, S.W., Brunner, M., Erdjument-Bromage, H., Geromanos, S., Tempst, P., and Rothman, J.E. (1993). SNAP receptors implicated in vesicle targeting and fusion. Nature 362, 318-324.

Somsel Rodman, J., and Wandinger-Ness, A. (2000). Rab GTPases coordinate endocytosis. Journal of cell science 113 Pt 2, 183-192.

Stinchcombe, J.C., Majorovits, E., Bossi, G., Fuller, S., and Griffiths, G.M. (2006). Centrosome polarization delivers secretory granules to the immunological synapse. Nature 443, 462-465.

Ungermann, C., Price, A., and Wickner, W. (2000). A new role for a SNARE protein as a regulator of the Ypt7/Rab-dependent stage of docking. Proceedings of the National Academy of Sciences of the United States of America 97, 8889-8891.

Vennegoor, C., Calafat, J., Hageman, P., van Buitenen, F., Janssen, H., Kolk, A., and Rumke, P. (1985). Biochemical characterization and cellular localization of a formalin-resistant melanoma-associated antigen reacting with monoclonal antibody NKI/C-3. International journal of cancer 35, 287-295.

Wu, M., Wang, T., Loh, E., Hong, W., and Song, H. (2005). Structural basis for recruitment of RILP by small GTPase Rab7. The EMBO journal 24, 1491-1501.

Wurmser, A.E., Sato, T.K., and Emr, S.D. (2000). New component of the vacuolar class C-Vps complex couples nucleotide exchange on the Ypt7 GTPase to SNARE-dependent docking and fusion. The Journal of cell biology 151, 551-562.

Zerial, M., and McBride, H. (2001). Rab proteins as membrane organizers. Nature reviews 2, 107-117.

Zwart, W., Griekspoor, A., Kuijl, C., Marsman, M., van Rheenen, J., Janssen, H., Calafat, J., van Ham, M., Janssen, L., van Lith, M., et al. (2005). Spatial separation of HLA-DM/HLA-DR interactions within MIIC and phagosome-induced immune escape. Immunity 22, 221-233.

Chapter 6

Summary and Discussion

Summary and Discussion

Late endosomal compartments have been in the past dismissively regarded as mere sinks where degradative processes occur. Emerging evidence points to crucial specialized roles played by these organelles in a wide range of cellular processes that go well beyond their conventional role in degradation, including cell signaling transduction and termination, and control of innate and adaptive immunity. Late endosomal compartments include late endosomes, lysosomes and the functionally specialized lysosomal-related organelles (LROs) cytolitic granules, phagosomes, and major histocompatibility complex class II (MHC II)-containing/-enriched compartments (MIICs) among others (reviewed in [1]) .

MHC II antigen presentation (reviewed in Chapter 1) is a prime example of how compartmentalization and functional specialization of the late endosomal route are exploited in complex cellular processes. MHC II molecules are assembled from α and β subunits in the endoplasmic reticulum (ER) to constitute a peptide-binding cleft. They are then chaperoned through the *trans* Golgi network and enter the endocytic pathway, thus gaining access to exogenous antigenic peptides there generated. Facilitated binding of ligand peptides to the peptide-binding groove of MHC II molecules occurs in subdomains of the highly specialized lysosomal organelle best-known as MIIC. Resultant MHC II-peptide complexes are ultimately transported to the plasma membrane for display at the cell surface. The MIICs use the microtubule cytoskeleton and motor proteins of opposite polarities for their intracellular transport. MHC II-peptide complexes that reach the cell surface can be recognized by $CD4^+$ T cells for immune responses to pathogens and tumors.

Most of the research conducted in the field of MHC II antigen presentation has focused on the events leading to the formation of MHC II-peptide complexes inside the specialized MIIC. Consistently, considerable effort has been geared toward the development of strategies to manipulate the generation of MHC II-peptide complexes. Although this has undoubtedly yielded significant results, extending our focus to include other aspects of the cell biology of antigen presentation, such as intracellular transport and trafficking of MHC II molecules, will almost certainly increase the spectrum of targets for therapeutic intervention in autoimmunity or manipulation of presentation of vaccine antigens, as well as the development of innovative modes to manipulate immunity against invasive pathogens and tumors.

The studies described in this thesis aimed at gaining a more advanced level of understanding of the molecular mechanisms that govern the intracellular transport of MIICs and LROs. Furthermore, the finding that cholesterol is, surprisingly, a messenger involved in this, provides a mechanistic explanation for the characteristic phenotypes observed in some lipid storage diseases (reviewed in [2]) like Niemann-Pick type C disease.

Here, a novel molecular mechanism, based on the studies presented in Chapters 2 and 3 of this thesis, is postulated and aims at explaining the complex pattern of intracellular motility exhibited by MIICs. We visualized already in 1996, by time-lapse imaging microscopy, the movement of MIICs carrying GFP-tagged MHC II molecules. These compartments exhibit microtubule-based movement from the Golgi area around the microtubule-organizing center (MTOC) toward the plasma membrane and move characteristically in a so-called bidirectional manner and in a stop-and-go fashion [3]. This is mediated by the alternate activities of the oppositely directed microtubule-based motor proteins dynein (powers microtubule-based

minus end-directed centripetal transport to the MTOC) and kinesins (power microtubule-based plus end-directed centrifugal transport to the plasma membrane) [4]. How the activities of the molecular motors are spatially and temporally coordinated is a long-standing question since.

We propose here that a signaling cascade initiated by the activation of the small GTPase Rab7 is responsible for the control of MIIC intracellular transport. Rab7 activation renders this small GTPase membrane-associated to specify the site for the recruitment of two of its soluble effectors—RILP and ORP1L. We show that the assembled tripartite Rab7-RILP-ORP1L complex is then responsible for governing the activity of the dynein-dynactin motor for centripetal microtubule transport. RILP not only establishes a positive feedback loop by lengthening the presence of Rab7 (and of its own, consequently) on late endosomal membranes through inhibition of the GTPase cycle of Rab7 but also interacts directly with the $p150^{Glued}$ subunit of dynein's adaptor dynactin to recruit this molecular motor to late endosomal membranes. For full activation of transport toward the minus end of microtubules, a second receptor on the surface of late endosomal membranes—βIII spectrin—is required. In an ORP1L-dependent mechanism, the Rab7-RILP-$p150^{Glued}$-dynein complex is targeted to βIII spectrin and centripetal transport ensues. Swift switching of transport direction by polarized motors (dynein and kinesins) is controlled by late endosomal cholesterol content which determines the conformational state of ORP1L. Notably, the conformation of ORP1L dictates the accumulation of ER integral membrane proteins—VAP-A and VAP-B—in late endosomal membranes to control the access of dynein-dynactin to the Rab7-RILP receptor and thus transport and intracellular positioning of MIICs and other LROs.

This model is consistent with the concept of Rab GTPases functioning as key regulators of transport of subcellular compartments by organizing the recruitment of soluble effector molecules, scaffolding proteins, and adaptor proteins to create tightly localized domains on specific membranes, a concept which is emerging as a common theme in the field (reviewed in [5], [6], [7]).

Another emerging paradigm in the field pertains to the role played by GTPases in orchestrating the coupling of each reaction with the next along the endocytic route (reviewed in [6], [8], [9]) in order to maintain directionality and organelle identity in the pathway. In Chapter 5, we propose that the Rab7-RILP-ORP1L complex operating in late endosomal transport also plays a regulatory role in tethering/docking and fusion of late endosomal bilayers downstream of motor-driven transport. We show that Vam6p, a specific tethering/docking factor that promotes fusion of late endosomal organelles [10], is recruited to Rab7-bearing membranes in a RILP-dependent manner. ORP1L controls this, thus influencing fusion of late endosomal compartments. Whether cholesterol and VAPs are also implicated in this mechanism remains to be determined.

Taken together these data suggest that a single RabGTPase-effectors complex—the Rab7-RILP-ORP1L complex—regulates both transport and fusion, thereby conveying spatiotemporal specificity to two consecutive processes in late endosomal trafficking.

While the findings described in this thesis provide novel insights into the regulation of intracellular trafficking of MIICs and LROs, they also raise a series of intriguing questions. This is particularly true for those pertaining to the fine-tuning of these seemingly robust regulatory mechanisms. The findings described in Chapter 4 could serve to illustrate this. We identified and characterized a naturally occurring splice variant of RILP (RILPsv) that competes with RILP for Rab7 but fails to recruit efficiently the dynein-dynactin motor and thus may provide an extra dimension to the control of trafficking. Furthermore, what is the physiological relevance of a

molecule such as cholesterol acting in the control of late endosomal trafficking? The implication of the ER membrane proteins VAP-A and VAP-B in the control of late endosomal cholesterol-dependent processes could hint at a role played by the Rab7-RILP-ORP1L in intercompartmental communication between late endosomal compartments and the ER and thus a possible function in integrating late endosomal trafficking and cellular cholesterol homeostasis (reviewed in [11]). In the ER, cholesterol is enzymatically processed to generate a variety of oxygenated derivatives known as oxysterols. Furthermore, what is the relevance of particular oxysterols, if any, as signaling molecules in the endocytic pathway?

Future studies will certainly address these and other questions and may reveal novel targets for therapeutic intervention in pathologies ascribed to malfunctioning of the endolysosomal system which can include immunity- and pigmentation-related syndromes (reviewed in [1]), as well as those associated to dysfunctions in cholesterol or oxysterol homeostasis (reviewed in [2] and [12]).

1. Raposo, G., et al., Lysosome-related organelles: a view from immunity and pigmentation. Cell Struct Funct, 2002. 27(6): p. 443-56.

2. Maxfield, F.R. and I. Tabas, Role of cholesterol and lipid organization in disease. Nature, 2005. 438(7068): p. 612-21.

3. Wubbolts, R., et al., Direct vesicular transport of MHC class II molecules from lysosomal structures to the cell surface. J Cell Biol, 1996. 135(3): p. 611-22.

4. Wubbolts, R., et al., Opposing motor activities of dynein and kinesin determine retention and transport of MHC class II-containing compartments. J Cell Sci, 1999. 112 (Pt 6): p. 785-95.

5. Caviston, J.P. and E.L. Holzbaur, Microtubule motors at the intersection of trafficking and transport. Trends Cell Biol, 2006. 16(10): p. 530-7.

6. Grosshans, B.L., D. Ortiz, and P. Novick, Rabs and their effectors: achieving specificity in membrane traffic. Proc Natl Acad Sci U S A, 2006. 103(32): p. 11821-7.

7. Pfeffer, S.R., Rab GTPases: specifying and deciphering organelle identity and function. Trends Cell Biol, 2001. 11(12): p. 487-91.

8. Jordens, I., et al., Rab proteins, connecting transport and vesicle fusion. Traffic, 2005. 6(12): p. 1070-7.

9. Cai, H., K. Reinisch, and S. Ferro-Novick, Coats, tethers, Rabs, and SNAREs work together to mediate the intracellular destination of a transport vesicle. Dev Cell, 2007. 12(5): p. 671-82.

10. Caplan, S., et al., Human Vam6p promotes lysosome clustering and fusion in vivo. J Cell Biol, 2001. 154(1): p. 109-22.

11. Ikonen, E., Cellular cholesterol trafficking and compartmentalization. Nat Rev Mol Cell Biol, 2008. 9(2): p. 125-38.

12. Björkhem, I. and U. Diczfalusy, Oxysterols: friends, foes, or just fellow passengers? Arterioscler Thromb Vasc Biol, 2002. 22(5): p. 734-42.

Nederlandse samenvatting

Summary in Dutch

Nederlandse samenvatting

Het afweersysteem is ontwikkeld om invasieve ziektemakers maar ook andere afwijkingen het hoofd te bieden. Meer precies zijn dit virussen, bacteriën en andere micro-organismen, maar ook kanker en zelfs voedsel- en omgevingsfactoren kunnen door het afweersysteem 'gezien' worden. Deze factoren heten 'antigenen'. Het afweersysteem kent twee defensielijnen: één is een minder specifieke maar wel snellere eerste lijn verdediging, genaamd de 'aangeboren afweer', en de ander een meer specifieke maar tragere 'aangepaste afweer'. Dit laatste is sterk afhankelijk van het presenteren aan de oppervlakte van cellen van antigenen die dan weer herkend worden door andere cellen van het afweersysteem. Dit wordt 'antigen presentatie' genoemd en kan door drie leden van één eiwitfamilie gedaan worden: door CD1 eiwitten en door MHC klasse I en MHC klasse II eiwitten. CD1 eiwitten presenteren niet eiwit materiaal en meestal vetzuurachtige stoffen terwijl MHC klasse I en II eiwitten fragmenten van eiwitten presenteren die peptiden genoemd worden. MHC klasse I eiwitten presenteren aan het afweersysteem peptiden welke in de cel normaliter door proteasomen gemaakt worden. MHC klasse II doet dit normaliter van eiwitten die door de cel opgenomen zijn en afgebroken zijn in de endosomale route door lysosomale proteasen. Om een fragment (peptide) van zo'n eiwit te krijgen gaan MHC klasse II eiwitten dan ook endosomen in en ze ontmoeten het peptide dan op een plek dat dan weer MIIC (voor MHC klasse II compartiment) genoemd wordt. Uiteindelijk worden MHC klasse II eiwitten dan uit het MIIC getransporteerd om aan het oppervlak te komen. Hier kunnen afweercellen (zoals CD4+T cellen) het MHC klasse II-peptide complex herkennen en hierop reageren door allerlei stoffen uit te scheiden zodat andere afweer cellen (zoals de antilichaamuitscheidende B cel) hun werk gaan doen. Daarnaast zijn MHC klasse II eiwitten ook belangrijk voor de controle van cytotoxische T cellen, om auto-immuun ziekten te voorkomen en om goed te reageren op pathogenen en stoffen uit de omgeving. MHC klasse II is dus een centrale regulator van afweer reacties in het lichaam. Ondanks ons gedetailleerd begrip van het mechanisme van antigen presentatie door MHC klasse II eiwitten, is van een aantal stappen in dit proces nagenoeg niets bekend. Het bestuderen en begrijpen van de celbiologie van antigen presentatie is van belang omdat dit handvaten kan geven om het afweersysteem te manipuleren zoals bij auto-immuun ziekten maar ook bij onvoldoende afweer bij infectieziekten en kanker. De focus in 'het veld' is het proces dat leidt tot binding van peptiden door MHC klasse II eiwitten. In dit proefschrift beschrijf ik een aantal studies naar het mechanisme dat transport van de MIICs controleert. MIICs worden in de cel nogal vreemd heen-en-weer getransporteerd door de alterende activiteiten van moleculaire motoren. De dyneine motor brengt MIIC naar binnen en kinesine motoren brengen deze weer naar buiten en beide zijn ze verantwoordelijk voor dit bizarre gedrag. Maar hoe deze motor eiwitten weer in tijd-en-ruimte gecontroleerd worden, is onduidelijk. Op grond van onze proeven stellen wij een nieuw model voor dat de controle van transport van MHC klasse II moleculen verklaart. We beschrijven inhoofdstuk 2 hoe de dyneine motor op MIIC gereguleerd wordt door het kleine GTPase Rab7. Rab7 wordt geactiveerd op het membraan van MIIC en rekruteert dan zijn effector eiwit Rab7-Interacting Lysosomal Protein (RILP) en OSBP-Related Protein 1L (ORP1L) om het RILP-Rab7-ORP1L complex te vormen. Dit complex functioneert als de receptor van de dyneine motor op het buitenmembraan van het MIIC. Wij tonen aan dat dit gebeurt omdat RILP de verbinding vormt

tussen Rab7 en de p150^{Glued} subunit van de dyneine motor. Dit is echter niet voldoende en het ORP1L eiwit vormt een schakel met een meer algemene receptor voor de dyneine motor, βIII spectrine. Deze receptor bindt met de Arp1 subunit van de dyneine motor. Hoewel dit model verklaart hoe Rab7 naar binnen gericht transport van MIC door de dyneine motor controleert, verklaart het niet de omkeer in richting noch de beëindiging van naar binnen gericht transport. Inhoofdstuk 3 laten we zien hoe cholesterol in MIICs bepaalt dat de dyneine motor aan MIIC bindt. Cholesterol bepaalt de conformatie van ORP1L en daarmee toegang van de dyneine motor op zijn receptor Rab7-RILP. Vervolgens wordt de positie van late endosomes en lysosomen als MIIC bepaald. Deze regulatie is verloren in bepaalde neuronale opstapeling ziekten als Niemann-Pick type C, die gekarakteriseerd worden door abnormale clustering van deze structuren. Op deze wijze bepaalt Rab7 transport van MIICs door oplosbare effector eiwitten te rekruteren. Deze binden weer andere eiwitten om lokale moleculaire machines aan het werk te zetten zodat transport en fusie processen van start gaan. Dit laatste laten we zien inhoofdstuk 5. We stellen dat Rab7 samen met RILP en ORP1L membraanbinding en fusie controleren. Dit proces is gekoppeld aan membraan transport. Transport en fusie van MIICs door Rab7 met zijn effector eiwitten RILP en ORP1L laten zien hoe deze processen in tijd en ruimte plaats vinden. Daarnaast laat het zien dat naar binnen gericht transport en organel fusie twee opeenvolgende processen zijn. Inhoofdstuk 4 beschrijven we de identificatie en karakterisatie van een splice variant van RILP (genaamd RILPsv). Dit eiwit mist 27 aminozuren, kan Rab7 binden maar niet de dyneine motor. We veronderstellen dat RILPsv betrokken kan zijn bij de fijn-regulatie van dyneine motor transport zoals gecontroleerd door de Rab7-RILP receptor.

Het werk dat in dit proefschrift gepresenteerd wordt geeft aldus een moleculaire verklaring van transportdoor motoreiwitten van compartimenten in een cel. Dit is een essentiële stap in de uitvoering van antigen presentatie door MHC klasse II eiwitten. Daarnaast verklaren we hoe cholesterol immuun responsen kanbeïnvloeden en het cellulaire fenotype van bepaalde ziekten zoals Niemann-Pick type C disease.

Curriculum Vitae

Nuno Rocha

Curriculum Vitae

Nuno Rocha was born in Lisbon, Portugal, on February 18, 1976. In 1994, he completed successfully secondary studies at the Antonio Nobre high school in Porto, Portugal. In the same year, he started his MSc in Biochemistry at the Faculty of Sciences from the University of Porto, Portugal. From November 1998 to February 1999, he joined the group of Cell and Applied Microbiology of Prof. Dr. P. Moradas-Ferreira at the Institute for Molecular and Cell Biology in Porto for his first practical internship. He was then awarded an Erasmus grant and he moved to Denmark to join the group of Protein Crystallography of Dr. J. Nyborg at Aarhus University, until September 1999. There he was involved in the production of crystals of mutants of *Thermus aquaticus* Elongation Factor-Tu as well as in data collection, interpretation of electron densities and model building. In 2000, he graduated in Biochemistry (option "Applied Biochemistry") with distinction from the University of Porto. In March 2001, he joined the group of Protein Crystallography of Dr. A. Perrakis at the Netherlands Cancer Institute, Amsterdam, The Netherlands. He was then granted a personal doctoral fellowship from the Portuguese Foundation for Science and Technology. In the winter of 2003, he started preparing the work presented in this thesis at the group of Prof. Dr. J.J. Neefjes at the Division of Tumor Biology of the Netherlands Cancer Institute Amsterdam.

Appendices

Appendix A
Color Figures

Figures 1 and **2** from **Chapter 1** &
Figures 2, **3**, **5**, and **6** from **Chapter 2**

Figure 1 from **Chapter 1** (page 18)

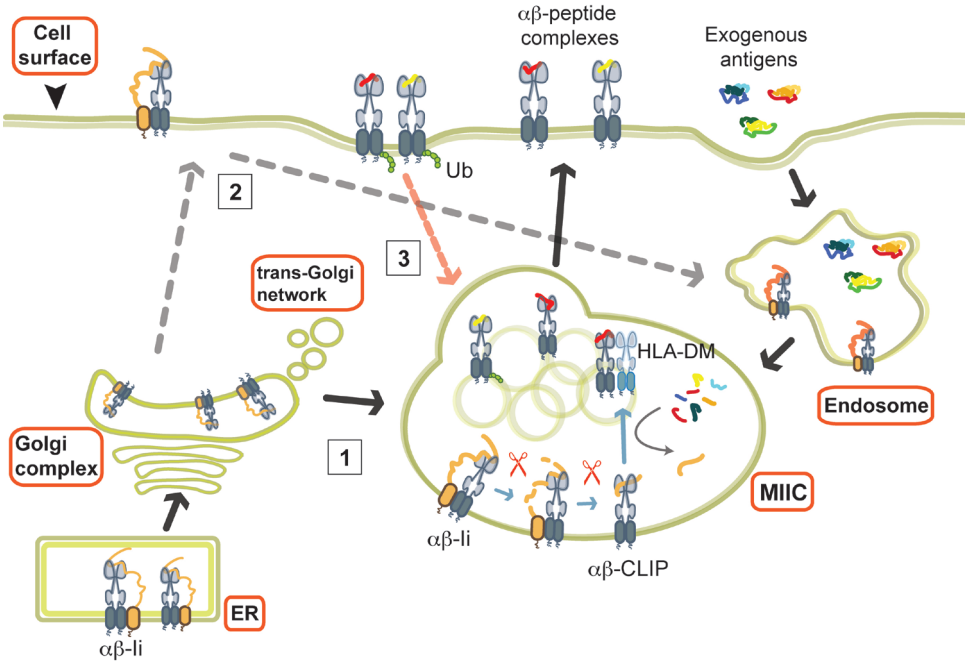

Figure 2 from **Chapter 1** (page 20)

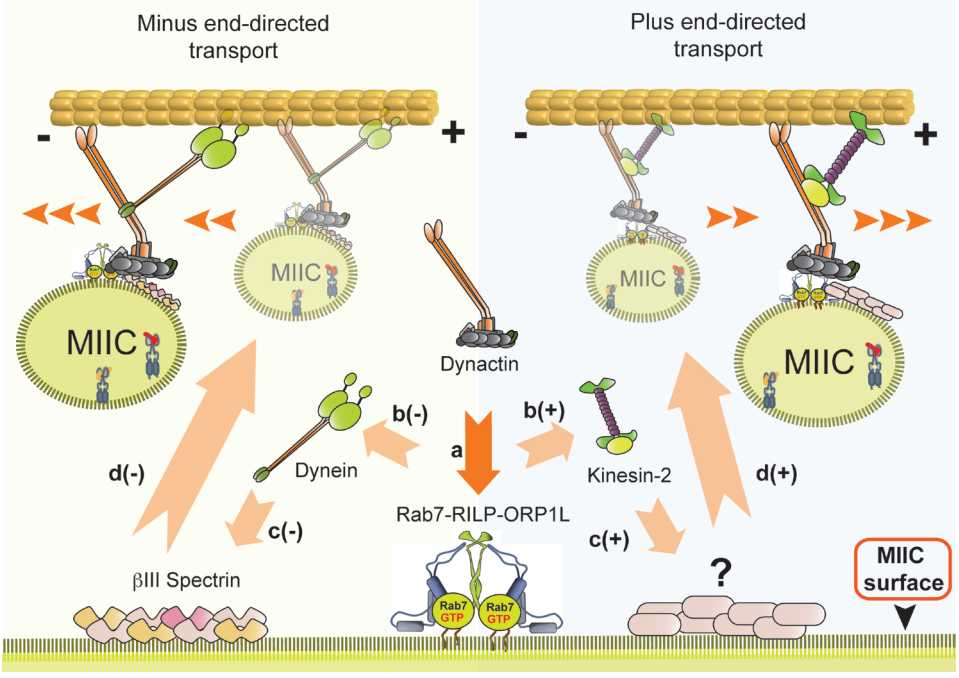

Figure 2 from **Chapter 2** (page 31)

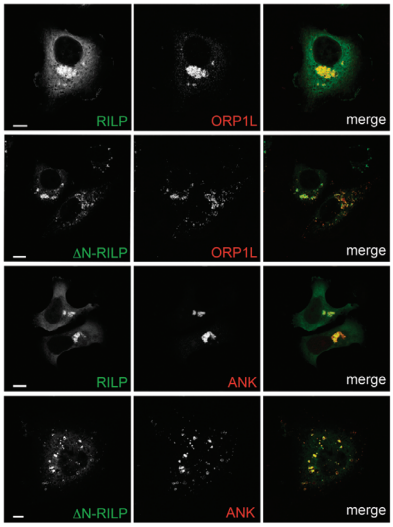

Figure 3 from **Chapter 2** (page 32)

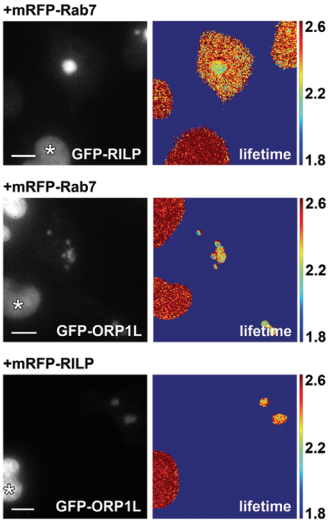

Figure 5 from **Chapter 2** (page 34)

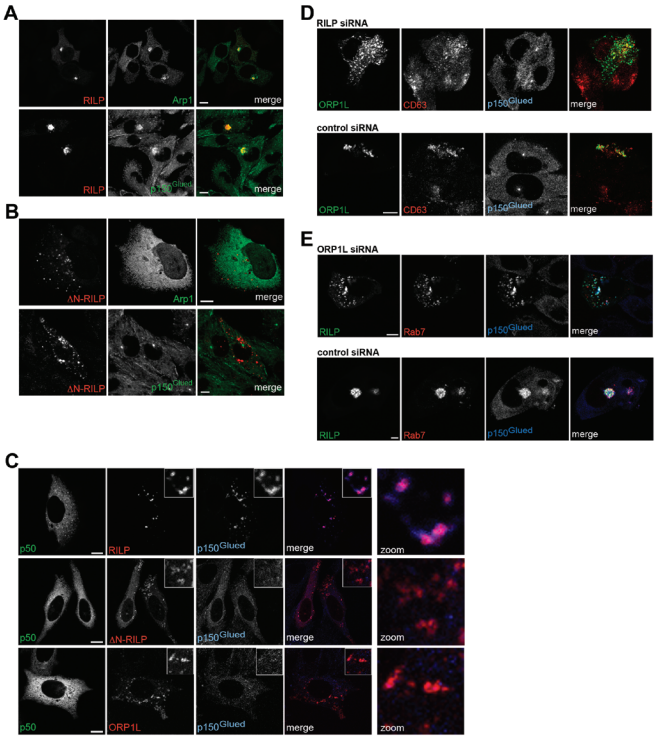

Figure 6 from **Chapter 2** (page 35)

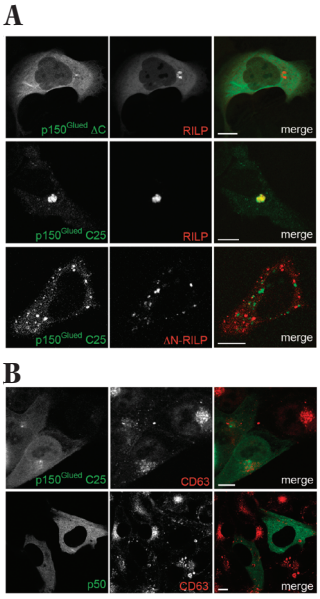

Figures 7 and **8** from **Chapter 2** &
Figures 1, **3**, and **4** from **Chapter 3**

Figure 7 from **Chapter 2** (page 36)

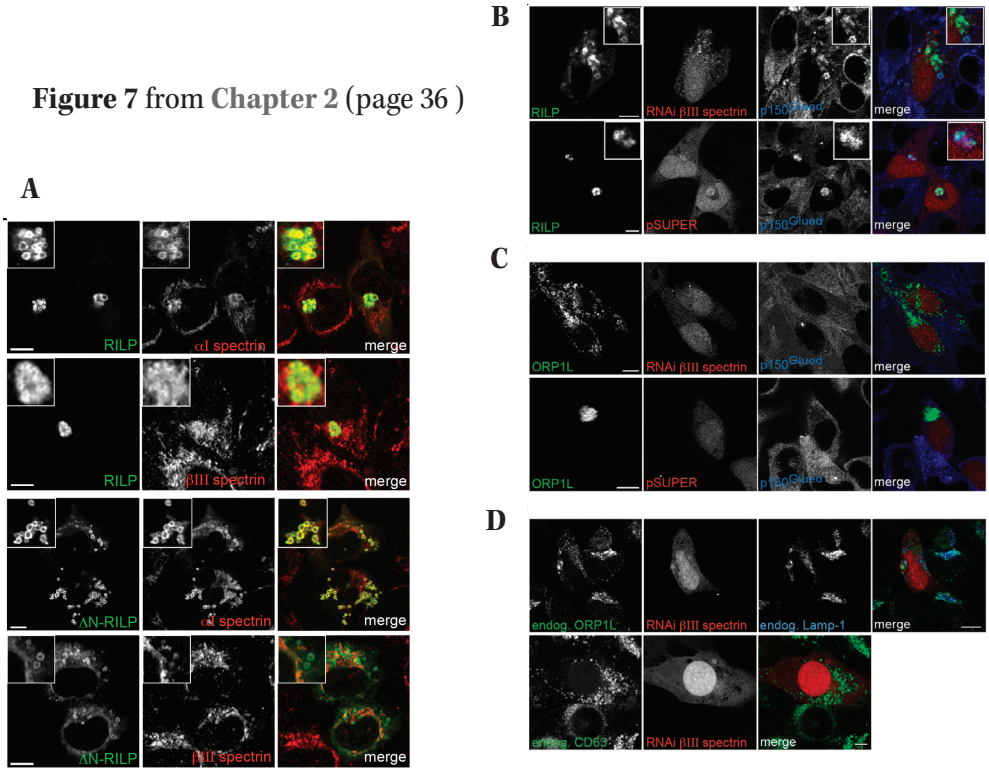

Figure 8 from **Chapter 2** (page 38)

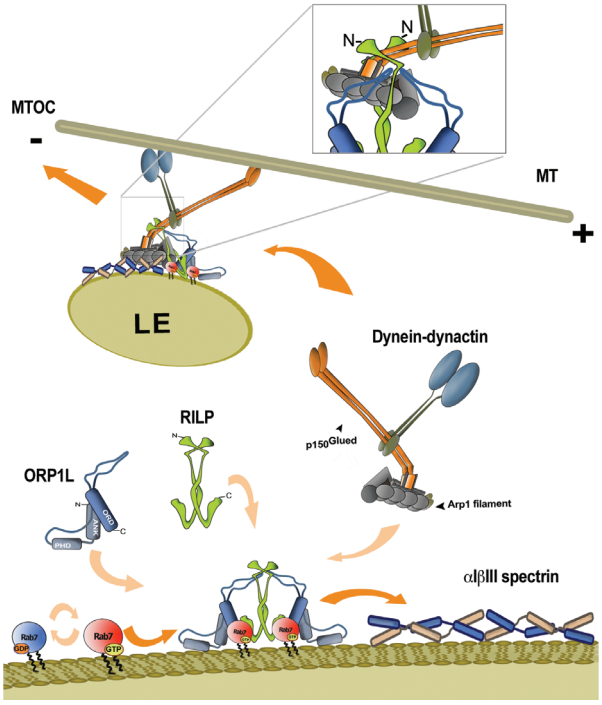

Figure 1 from **Chapter 3** (page 48)

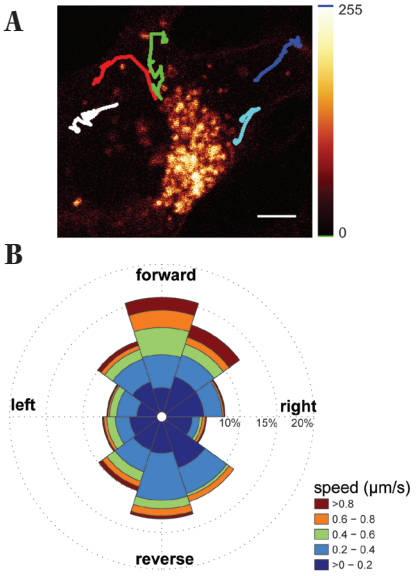

Figure 3 from **Chapter 3** (page 51)

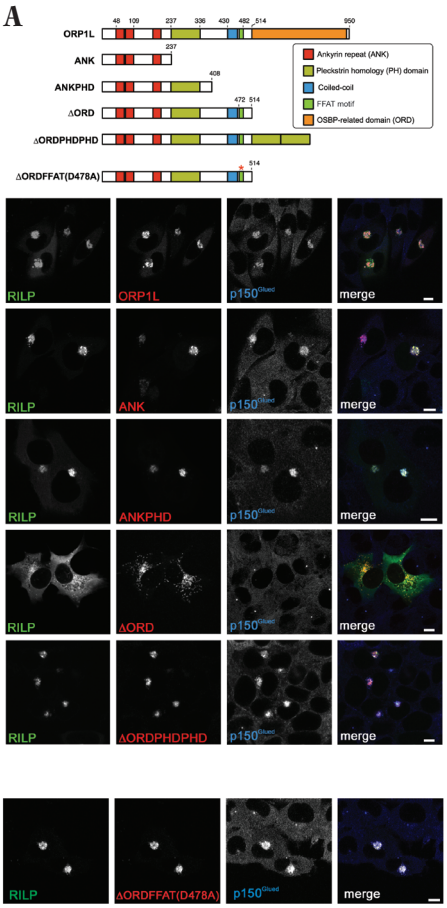

Figure 4 from **Chapter 3** (page 53)

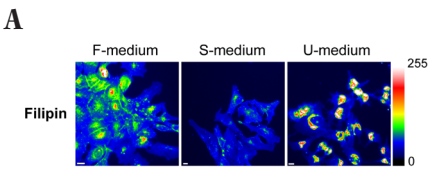

Figure 4 from **Chapter 3** (page 53)

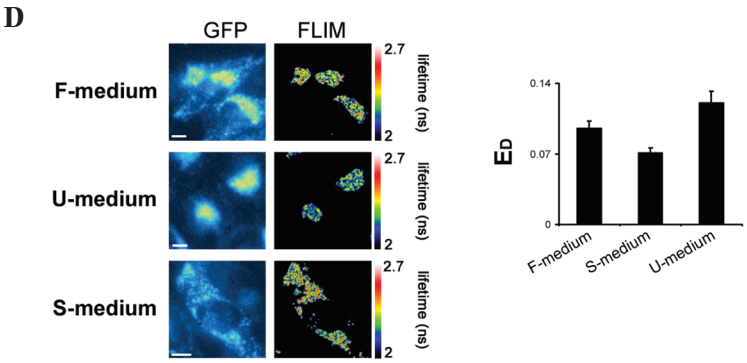

Figures 5, **6**, **7**, and **S2** from **Chapter 3**

Figure 5 from **Chapter 3** (pages 56 and 57)

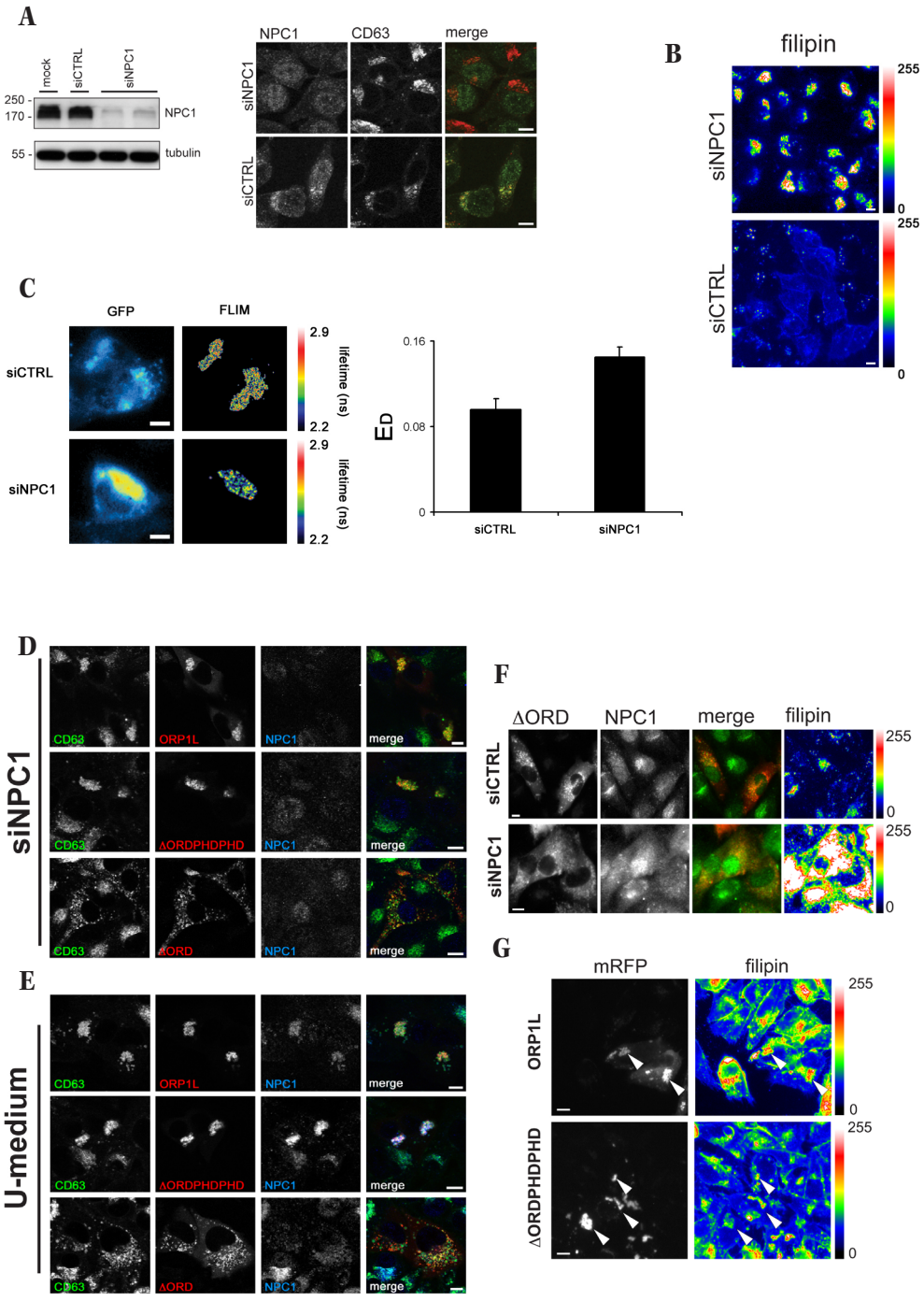

Figure 6 from **Chapter 3** (page 59)

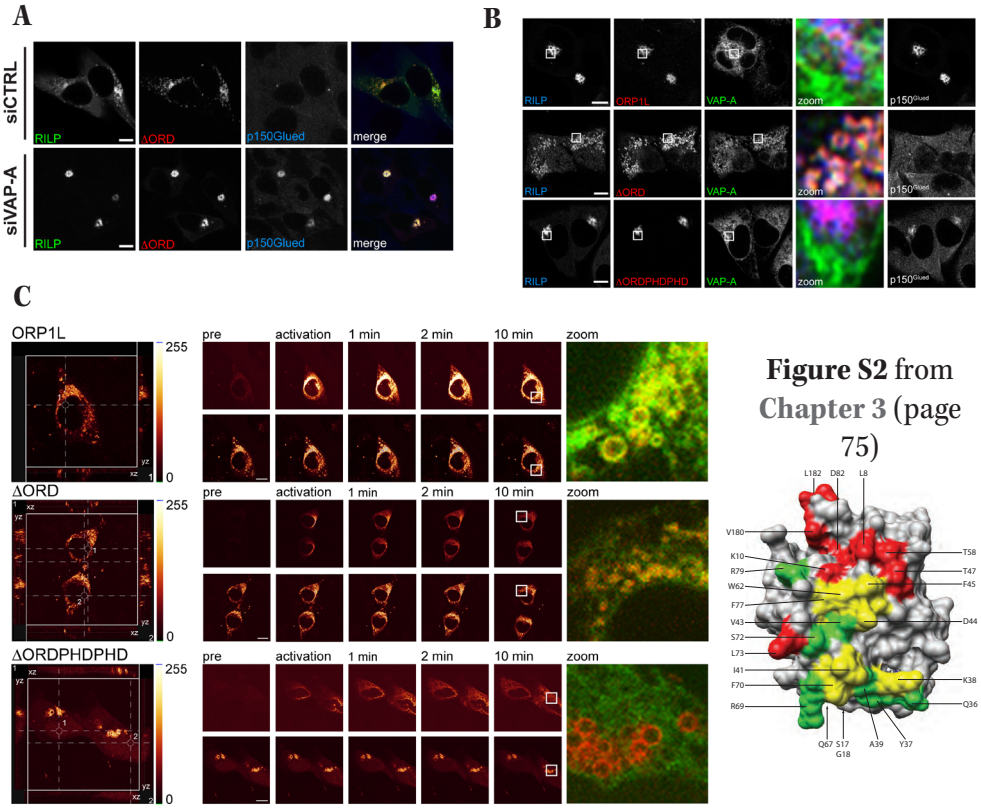

Figure S2 from **Chapter 3** (page 75)

Figure 7 from **Chapter 3** (page 61)

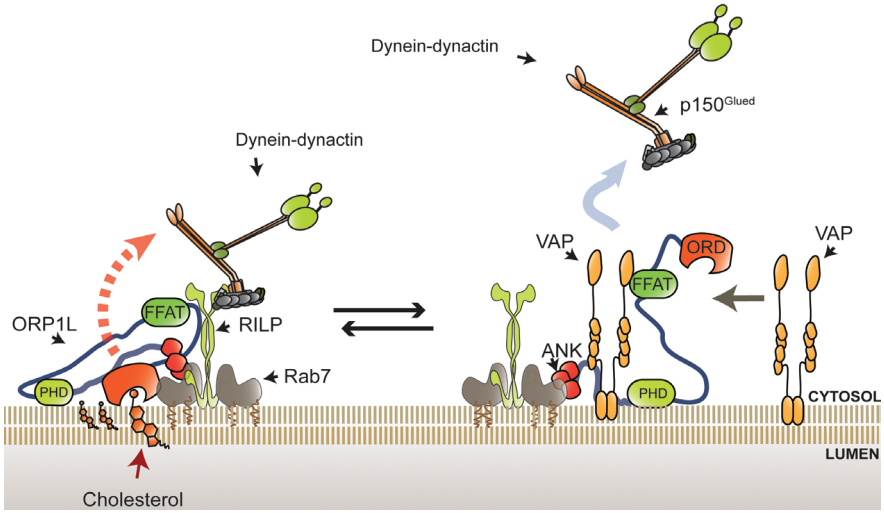

Figures 2, **3**, and **5** from **Chapter 4** &
Figures 1, **5**, and **6** from **Chapter 5**

Figure 2 from **Chapter 4** (page 82)

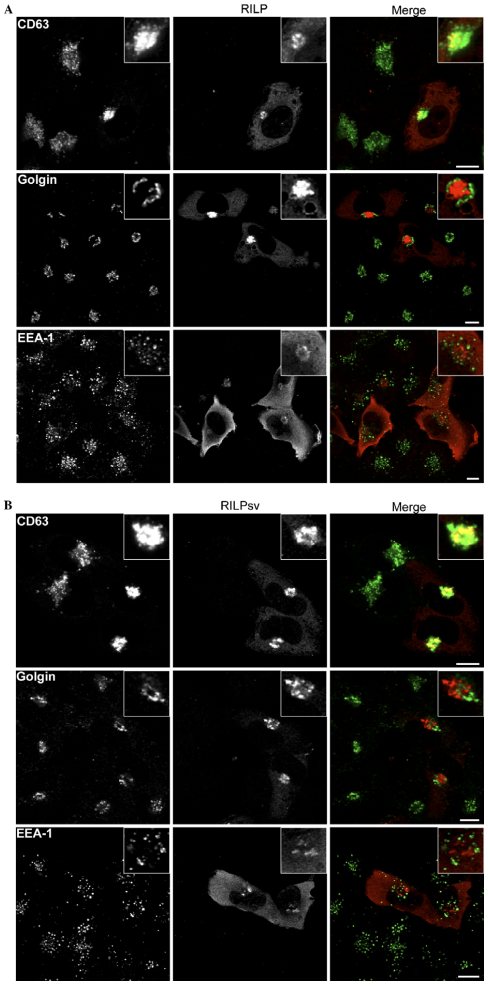

Figure 5 from **Chapter 4** (page 85)

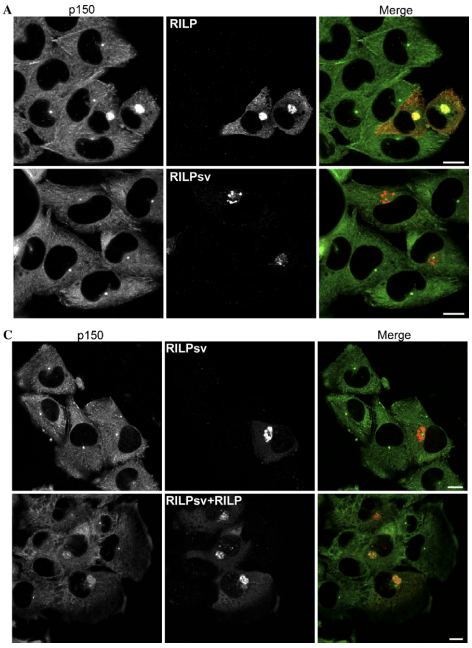

Figure 3 from **Chapter 4** (page 83)

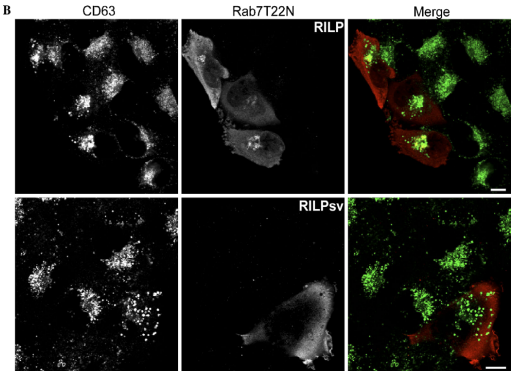

Figure 1 from **Chapter 5** (page 95)

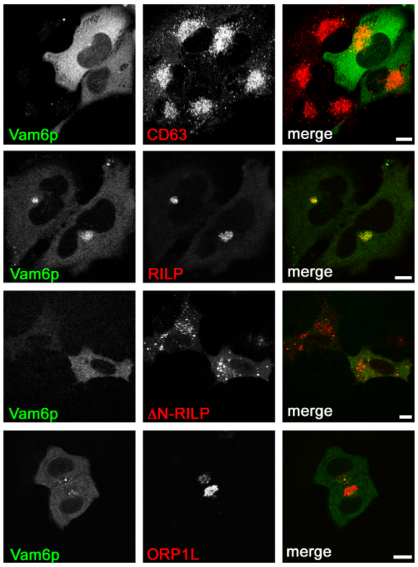

Figure 5 from **Chapter 5** (page 99)

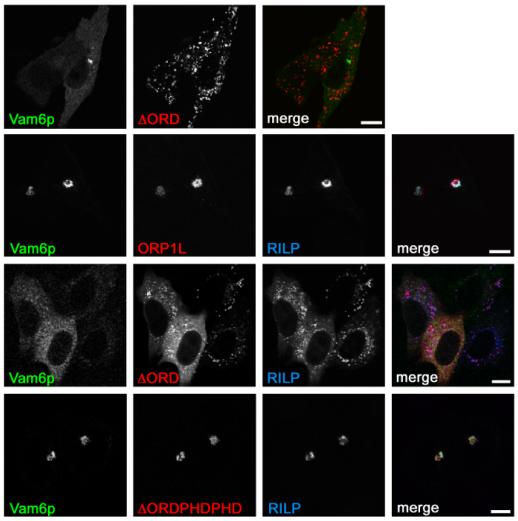

Figure 6 from **Chapter 5** (page 99)